NANSEN-TUTU CENTRE
MARINE ENVIRONMENTAL RESEARCH

Three oceans symposium: Marine science and services in the greater Agulhas region

PROCEEDINGS OF THE NANSEN-TUTU CENTRE SYMPOSIUM IN MEMORY OF THE LATE PROF. MATHIEU ROUAULT

6-7th November 2023, Cape Town, South Africa

Introduction

Prof. Mathieu Rouault studied fluid mechanics at the Aix-Marseille Université where he graduated in 1989, together with his friend Bertrand Chapron. Mathieu's initial research focused on ocean and atmosphere interactions. In 1990, he completed a PhD at the Risø National Laboratory (Denmark) and this research led to a seminal paper on the impact of sea-spray on heat fluxes which has been cited 345 times. Between 1990 and 1992, he undertook a post-doc at the Naval Graduate School in Monterey (USA), where his passion for surfing grew. He was therefore enthusiastic in accepting a position in the Department of Oceanography at UCT in 1992 which would allow him to surf along the African shores. At UCT, he became a research officer and later professor and the chairholder of the South African Research Chairs Initiative (SARChI) for Ocean and Atmospheric Modelling in the Department of Oceanography. He also served as the co-director of the Nansen Tutu Centre for Marine Environmental Research.

He was a distinguished oceanographer and climatologist interested in all aspects of ocean and atmosphere interactions, from creating numerical models to experimental work at sea, from turbulent to global scale. One of his proudest achievements was the instrumental role he played in the deployment of the PIRATA South East Extension Atlas mooring (Kizomba), in the tropical Atlantic. The PIRATA buoy deployment for Mathieu marked the return of Southern Africa in the international arena of global climate observation. Other highlights include his research on El Niño-Southern Oscillation (ENSO), Benguela Niños, Agulhas Current variability and rainfall variability in Southern Africa, and the discovery of two currents in the Indian Ocean. His findings have contributed to better predictions of climate events like droughts and floods, which are crucial for effective climate adaptation and mitigation strategies. His legacy continues to inspire and influence the field of marine and climate sciences.

Prof. Mathieu Rouault was a passionate advocate for African students, especially in ocean and climate sciences. As Director of the Nansen-Tutu Centre at the University of Cape Town, he provided invaluable mentorship, supervision, and financial support to students from the honours to the postdoctoral levels. He mentored and promoted young scientists from all over Africa. Through initiatives like SOMISANA, he promoted sustainable ocean modeling and fostered scientific growth on the continent. He encouraged critical thinking and collaboration, building a supportive national and international community that empowered young African researchers. His dedication significantly advanced marine and climate research and helped shape the next generation of African scientists. Thereby, he helped to strengthen the foundation for future research on climate change and its impacts in Africa. He also enjoyed treating the students, postdocs and research associates of the Nansen Tutu to lunch at the UCT club.

Mathieu deeply loved and cared for his wife, Marjolaine, and their three sons. At home he was also a good gardener. His passion for surfing was well known and far ahead of most, and he was highly respected by the big wave surfer community in Hout Bay. He transmitted his passion and respect for the ocean and waves to his sons, who all learned to surf and also qualified as lifeguards in their hometown Fish Hoek.

Mathieu loved going to Madagascar to surf and meet his friend Gigi in Lavanono at the very remote southern tip of Madagascar where he was maintaining a weather station. Mathieu's legacy was honoured by the local fishing community of Lavanono who held a traditional funeral ceremony for him, usually only reserved for Malagasy people. Friendship and respect were highly valued by Mathieu´s. He was always keen to invite research colleagues and students home for a "braai" and enjoying the mix of discussion being around science or the Cape Peninsula living conditions.

Tragically, Prof. Rouault passed away unexpectedly on January 17, 2023, shortly after returning from the training course during the One Ocean Expedition sail voyage onboard St. Lehmkuhl from Maputo to Cape Town. During this leg the topics in focus included regional characteristics of upper ocean dynamics, air-sea interaction and biogeochemistry and marine biology. Mathieu coordinated the training and data collection of the air-sea interaction group along the Agulhas Current and in the adjacent shelf seas.

The three oceans symposium in memory of Prof. Rouault included 32 participants from France, Norway, South Africa and other countries around southern Africa. It was held over two days at the Breakwater Lodge in Cape Town, the same venue that gathered 80 participants to celebrate the 10-year anniversary of the Nansen Tutu Centre in 2020. The symposium, focused on showcasing student research in marine science and services. It featured an excellent array of young and more mature scientists demonstrating the diversity and quality of the science that is currently being undertaken in this dynamic and fascinating oceanic region.

The proceedings are grouped into the following sections.

- Ocean processes and dynamics from mesoscale to large scale: The Agulhas Region
- Ocean processes and dynamics from mesoscale to large scale: The Benguela Region
- Air-sea interactions and influences on climate on land
- Marine heat waves and ocean warming
- Southern Ocean

We wish you happy reading!

Organizing Committee

Dr. Annette Samuelsen, NERSC, NTC
Prof. Isabelle Ansorge, UCT, NTC
Prof. Johnny Johannessen, NERSC, NTC
Dr. Cristo Whittle, CSIR, NTC

Proceeding Review and Editing Committee

Dr. Annette Samuelsen, NERSC, NTC
Prof. Babatunde Abiodun
Prof. Johnny Johannessen, NERSC, NTC

A warm thanks to all Nansen Tutu Research Associates who helped review the extended abstracts and to Dr. Marjolaine Krug and Dr. Fabrice Collard for their contributions to the introduction.

Table of Contents

Ocean processes and dynamics from mesoscale to large scale: The Agulhas Region

Ocean processes and dynamics from mesoscale to large scale: Benguela region

Air-sea interactions and influences on climate on land

Marine heat waves and ocean warming

Southern ocean

Revisiting Mesoscale Variability in the Agulhas System: A Decade Later

P Penven[1], B Backeberg[2,3], L Braby[4], I. Halo[3,5], J. Hermes[4], M. Krug[3,5]

[1]University Brest, CNRS, IRD, Ifremer, Laboratoire d'Oeéanographie Physique et Spatiale (LOPS), IUEM, Brest, France.

[2]Deltares, Netherlands

[3]Nansen Tutu Center for Marine Environmental Research, Department of Oceanography, University of Cape, Town, Rondebosh, Cape Town, 7700, Western Cape, South Africa

[4]Egagasini Node, South African Environmental Observation Network, Cape Town, South Africa,

[5]Department of Forestry, Fisheries and the Environment, Oceans and Coasts Research, Cape Town, South Africa

Abstract: Surface mean and eddy kinetic energy, derived from a 25-year CROCO simulation (1993-2018), unveil seasonal dynamics and decadal trends in the Western Indian Ocean. Seasonal energy exhibits a coastal propagation along Madagascar and Southern Africa, while trends confirm Backeberg et al. (2012) findings of a sustained gyre strengthening over the long term.

1. Introduction

An admirable trait of our late dear friend and colleague, Professor M. Rouault, was his skill in fostering collaboration among researchers. One such collaboration led to the finding, as highlighted by Backeberg et al. (2012), that mesoscale variability within the Agulhas system intensified between 1993 and 2009. This intensification was particularly notable in the Mozambique Channel and south of Madagascar, attributed to the strengthening of the Indian Ocean's subtropical gyre due to increased trade winds (Backeberg et al., 2012).

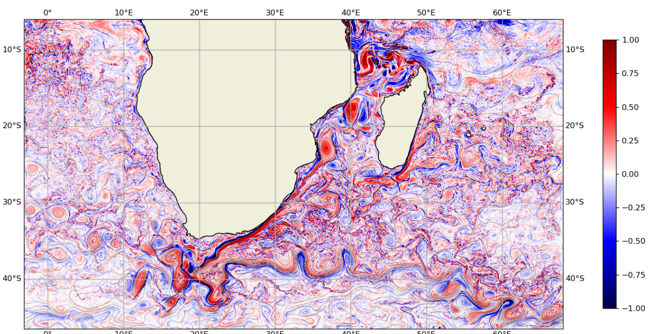

Figure 1: Example of surface vorticity divided by the Coriolis parameter (f) from the 1/36° resolution South West Indian Subtropical Gyre (SWAG36) simulation.

Given that the greater Agulhas system exhibits exceptionally high mesoscale variability (Lutjeharms, 2006), it serves as an ideal testbed for high-resolution model simulations. Recent experiments employing high-resolution models, specifically focusing on simulating the western subtropical gyre of the Indian Ocean for extended periods, provide an excellent opportunity to reassess these processes.

Here we show that the trends are still robust for the lower latitudes, around Madagascar and the Mozambique Channel with an agreement between the numerical model simulation and satellite altimetry. This is, however, less true for the Agulhas Current core and the Agulhas Retroflection region.

2. Data and method

CROCO (Coastal and Regional Ocean Community model) stands out as a versatile ocean model, known for its adaptability to various oceanic and coastal environments (Auclair et al., 2022). Evolving from the ROMS ocean model (Shcheptkin and McWilliams, 2005), CROCO employs hydrostatic primitive equations, utilizing topographic-following vertical coordinate and higher order numerical schemes. It has demonstrated capabilities for simulating a wide range of ocean processes, from large-scale oceanic circulations to fine-scale coastal dynamics.

The South West Indian Subtropical Gyre (SWAG) simulations are designed to investigate oceanic processes surrounding southern Africa, particularly focusing on the western portion of the Indian Ocean's subtropical gyre and the southeastern Atlantic. Building upon prior research, these simulations utilize recent datasets and incorporate the latest advancements in CROCO to execute high-resolution, long-term oceanic simulations spanning from 1993 to 2018. The SWAG experiments systematically address diverse dynamic processes governing the gyre, spanning the entire western region of the South West Indian Ocean subtropical gyre and the eastern sector of the South Atlantic subtropical gyre (see Figure 1). This domain encompasses key features such as Madagascar, the Mozambique Channel, the Agulhas Current, and the Benguela Current, with a specific focus on elucidating the interconnections between the Mozambique Channel and the Agulhas Current, where energy transfers between eddies and mean currents remain incompletely understood.

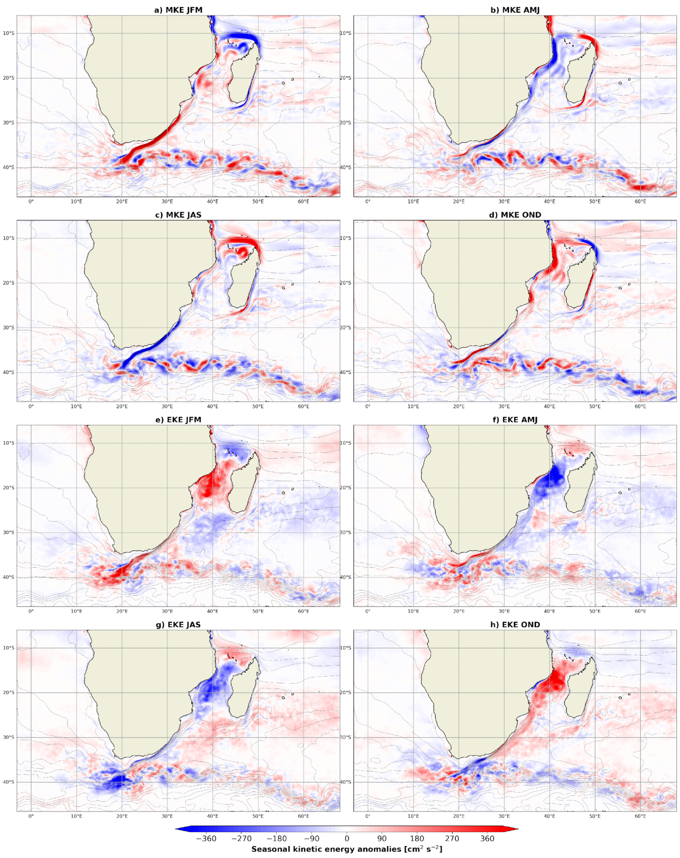

Figure 2: Seasonal climatology of surface geostrophic monthly MKE (panels a to d) and EKE (panels e to h) derived from SWAG36.

We utilize daily GLORYS 1/12° reanalysis (Lellouche et al., 2021) to establish the lateral open boundaries for the SWAG simulations. Additionally, hourly ERA5 atmospheric reanalysis (Hersbach et al., 2020) is employed to drive surface bulk parameterization. Our model integrates bottom topography data from GEBCO2020 (Weatherall et al., 2020). Daily river discharge data for the region's 56 most significant rivers are sourced from a global streamflow reanalysis (GLOFAS 3.1, Alfieri et al., 2020). Particular emphasis is placed on understanding the behavior of the Agulhas Current and its retroflection, which remain acknowledged challenges in ocean modeling (Penven et al., 2011). To tackle this, meticulous attention is given to the treatment of topography. Ensuring that the slope parameter ($r=\nabla(h)/h$, where h represents bottom topography) remains consistently below 0.25 and coastal waters (points at the land mask) never exceed 80 meters, facilitates a suitable slope for the Agulhas Current to adjust. We employ the current-wind feedback parameterization (Renault et al., 2020), known for its significant impact on the Agulhas Retroflection (Renault et al., 2017). Horizontal viscosity parameterization (Smagorinsky, 1963) is utilized to selectively dampen instabilities in the Agulhas Current. Several simulations are conducted with increasing resolutions: 1/4° (SWAG4), 1/12° (SWAG12), and 1/36° (SWAG36), corresponding to approximately 2.7 kilometers for SWAG36, with a grid size of 2560 X 1680 X 75 points. As such SWAG36 adequately resolves small-scale structures in the region as depicted in Figure 1.

Following the approach outlined by Backeberg et al. (2012), we address changes in surface ocean dynamics in the region by examining the variability in mean kinetic energy (MKE representing the mean flow) and eddy kinetic energy (EKE representing mesoscale variability) derived from surface geostrophic velocities (facilitating comparison with altimetry). To ensure a robust separation between the mean and the mesoscale variability, mean monthly values of MKE and EKE are derived using the following expressions:

$$MKE = 0.5 < <u>^2 + <v>^2 > \quad \text{and}$$

$$EKE = 0.5 < u'^2 + v'^2 >,$$

where u and v are surface geostrophic velocities, <> denotes a 3 months block average centered over each month and the primes (') the anomalies around these averages. This ensures the absence of cross terms when summing EKE and MKE to obtain the monthly total kinetic energy.

3. Results

Figure 2 illustrates a seasonal climatology of surface geostrophic monthly MKE (Figures 2a to 2d) and EKE (Figures 2e to 2h) based on 25 years of simulation (1993-2018). Focusing on the area north of Madagascar, we observe the North Madagascar Current (NMC) accelerating in fall (April-May-June; Figure 2b). This acceleration propagates toward the African continent in the following season, winter (July-August-September; Figure 2c). By spring (October-November-December; Figure 2d), the enhanced MKE reaches the Mozambican coast and the Mozambique Channel, accompanied by a substantial increase in EKE in the central Mozambique Channel (Figure 2h). As summer arrives (January-February-March;

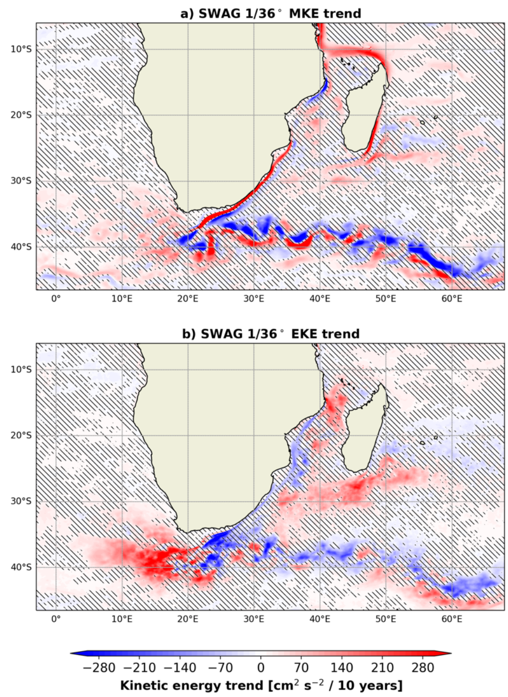

Figure 3: Linear decadal trends in MKE (panel a) and EKE (panel b) for SWAG36. Regions where the trends are not significant at 95% are hashed.

Figure 2a), this enhanced energy propagation extends into the Agulhas Current, resulting in increased eddy variability in the Agulhas Retroflection (Figure 2e). During the same period, north of Madagascar, the previously observed acceleration in MKE is now replaced by a deceleration (indicated by the blue pattern in Figure 2a). Similar to the observed acceleration, this deceleration also propagates down the Mozambique Channel, toward the Agulhas Current in the following seasons. It i s noteworthy that these climatologies in EKE and MKE align well with AVISO altimetry (not shown).

Figure 3 illustrates the linear decadal trends in MKE and EKE for SWAG36 spanning the years 1993 to 2018. While hashed regions indicate where trends are not significant at the 95% confidence level, significant signals are still discernible, particularly along the major currents in the region. The major boundary currents (such as the North Madagascar Current, East Madagascar Current, and Agulhas Current) all exhibit a notable increase, reaching up to 300 $cm^2 s^{-2}$ per decade in certain areas (Figure 3a). A significant rise in EKE is evident in the central/northern Mozambique Channel and south of Madagascar, as well as in the Cape Cauldron (Figure 3b). An alternative positive/negative pattern is observed for both EKE and MKE in the Agulhas Return Current. Trends in EKE and MKE for SWAG36 are generally consistent with AVISO data for the regions around Madagascar. However, there are discrepancies for the Agulhas Current and retroflection, where the increase is more pronounced for EKE (accompanied by a decrease in MKE) according to altimetry data.

4. Discussion

Utilizing a new 1/36° CROCO simulation spanning the years 1993-2018, we have successfully captured the long-term variability in surface geostrophic MKE and EKE. The model demonstrates agreement with altimetry data regarding the annual cycle, depicting a propagation pattern that is initiated in the fall north of Madagascar and then extended southward throughout the year towards the Agulhas Current. This observed pattern could be attributed to different Rossby wave propagation speeds at different latitudes, which directly influence the seasonal cycle (Hutchinson et al., 2018). SWAG36 reveals a strengthened Agulhas Current during the austral summer, consistent with findings by Krug and Tournadre (2012) and Hutchinson et al. (2018). This seasonality is indicative of a large-scale propagating signal in both mean and eddy flows around the western side of the Subtropical gyre, aligning closely with altimetry observations.

Regarding linear trends, the findings of Backeberg et al. (2012) remain relevant for the region encompassing Madagascar and the Mozambique Channel, indicating a general intensification of the subtropical gyre evident in both mean and eddy flows. However, trends are less distinct in the southern region, with the model indicating a mean increase in the Agulhas Current, while observations suggest a rise in mesoscale variability (eddies/meanders), as documented by Beal and Elipot (2016) and Backeberg et al. (2012).

References

Alfieri, L. et al. (2020), A global streamflow reanalysis for 1980-2018, Journal of Hydrology X, 6, 100049.

Auclair, F. et al. (2022), Coastal and Regional Ocean COmmunity model (1.3), Zenodo. https://doi.org/10.5281/zenodo.7415343

Backeberg, B. C., P. Penven and M. Rouault (2012), Impact of intensified Indian Ocean winds on the mesoscale variability of the Agulhas system, 2012, Nature Climate Change, 2, 608-612.

Beal, L. M. and S. Elipot (2016), Broadening not strengthening of the Agulhas Current since the early 1990s. Nature, 540, 570.

Hersbach, H. et al. (2020), The ERA5 global reanalysis, Q J R Meteorol Soc., 146, 1999-2049.

Hutchinson, K. et al. (2018), Seasonal phasing of Agulhas Current transport tied to a baroclinic adjustment of near-field winds, J. Geophys. Res., 123, 2018JC014319.

Krug, M. and J. Tournadre (2012), Satellite observations of an annual cycle in the Agulhas Current. Geophysical Research Letters, 39, L15607.

Lellouche, J. M. et al. (2021) The Copernicus Global 1/12° Oceanic and Sea Ice GLORYS12 Reanalysis, Front. Earth Sci. 9, 698876.

Lutjeharms, J. R. E. (2006), The Agulhas Current, Springer-Verlag.

Penven, P., S. Herbette and M. Rouault (2011), Ocean modelling in the Agulhas Current system, Proceedings of the Joint Nansen-Tutu Scientific Opening Symposium and OceansAfrica Meeting, Nansen-Tutu Centre for Marine Environmental Research, December 7-9 2010, 17-21.

Renault, L., J. C. McWilliams and P. Penven (2017). Modulation of the Agulhas Current retroflection and leakage by oceanic current interaction with the atmosphere in coupled simulations. Journal of Physical Oceanography, 47(8), 2077-2100. h

Renault, L. et al. (2020). Recipes for how to force oceanic model dynamics. Journal of Advances in Modeling Earth Systems, 12, e2019MS001715..

Shchepetkin, A. F. and J. C. McWilliams (2005), The regional oceanic modeling system (ROMS): a split-explicit, free-surface, topography-following-coordinate oceanic model, Ocean Model., 9, 347-404.

Smagorinsky, J. (1963), General circulation experiments with primitive equations, Mon. Weather Rev., 91, 99-164.

Weatherall, P. et al. (2020), The GEBCO_2020 Grid - a continuous terrain model of the global oceans and land, British Oceanographic Data Centre, National Oceanography Centre, NERC, UK, doi:10.5285/a29c5465-b138-234d-e053-6c86abc040b9.

Two Drifters: An Unexpected Journey

M.G. Hart-Davis[1,5], B.C. Backeberg[2,3,5], J.A. Johannessen[3,4], O. Breivik[4]

[1] Deutsches Geodätisches Forschungsinstitut, Technische Universität München (DGFI-TUM)

[2] Deltares, Delft, Netherlands

[3] Nansen Environmental and Remote Sensing Center, Bergen, Norway

[4] Geophysical Institute, University of Bergen, Bergen, Norway

[5] Nansen-Tutu Centre, Department of Oceanography, University of Cape Town, South Africa

Abstract: A surface drifter-pair was deployed on the 11th of April 2015 in the core of the Agulhas Current. The drifters remained in close proximity to each other while following the core of the Agulhas Current and Retroflection over a three-week period. As the drifters approached the Agulhas Plateau in the Agulhas Return Current, they began to separate 22 days after their deployment. One drifter was ejected from the Agulhas Return Current while the other remained in its core. The unexpected near-identical trajectories of the two drifters and their eventual separation provide an interesting case study for divergence and convergence processes in western boundary currents and their inertial overshoots, including challenges today's state-of-the-art observing systems face in diagnosing high-resolution, submesoscale, dynamical processes governing the drifter trajectories. This study aims to use the available observations, including along-track satellite altimetry, satellite-derived surface currents and sea surface temperature products as well as global reanalysis data and the latest products from the ESA World Ocean Circulation project to understand the pathways of these drifters both prior to their separation and particularly during their separation. Here, preliminary analyses of the drifter trajectories and the SST field are presented as a starting point to better understand divergence and convergence processes along the pathways of the drifters. Future work will include expanding this analysis to include observations from other measurement platforms.

1. Introduction

In-situ observations such as surface drifters, moorings, gliders, Argo floats and shipboard measurements have been extensively used to study the Agulhas Current (Lutjeharms & Ansorge, 2001; Boebel et al., 2003; Krug et al., 2017). Surface drifters have been used for a wide range of purposes, including mapping large-scale ocean currents and tracking oil spills (Lumpkin et al., 2017). Additionally, the trajectories of surface drifter-pairs deployed at the same location has elucidated regions of strong submesoscale variability, advancing our understanding of ocean surface dynamics (Lumpkin & Elipot, 2010; van Sebille et al., 2015; Dora et al., 2020). It is not common for surface drifter-pairs to be deployed at the same locations (pers. comm. Rick Lumpkin).

However, the information provided by paired drifter deployments can significantly advance our quantitative understanding of mixing and dispersion processes in the ocean (van Sebille et al., 2015). The information provided by the drifter-pair deployed in the Agulhas Current on 11 April 2015 and other examples analysed in Lumpkin and Elipot (2010) highlights the value of drifter-pair deployments in advancing our quantitative understanding of submesoscale upper ocean dynamics.

In this study, the trajectory of a surface drifter-pair deployed in the Agulhas Current over a 40-day period is analysed together with satellite sea surface temperature (SST) observations with the aim to gain a preliminary understanding of the dynamics affecting the trajectories of the two surface drifters and their eventual separation. In doing so, this study also assesses the appropriateness of state-of-the-art satellite derived SST measurements in monitoring submesoscale processes. Future work will include expanding the analysis to include observations from other measurement platforms.

2. Data and method

In this study, the trajectories of a drifter-pair deployed in the Agulhas Current are studied (Figure 1). Location and velocity data from both drifters interpolated to 6-hourly intervals are analysed. Both drifters were drogued at 15 m depths for the duration of the study.

The Group for High-Resolution Sea Surface Temperature (GHRSST) provides daily global SST data at a 0.01° spatial resolution (https://doi.org/10.5067/GHG1S-4FP01). The high spatial and temporal resolution G1SST product is used to examine the surface expressions of the upper ocean mesoscale features (Figures 2 and 3).

To analyse the role that SST fronts might play in governing the trajectories of the drifters, we first locate the position of the largest SST front to the left and right of the daily drifter location perpendicular to its trajectory. From this, we calculate the distance between those two points (Figure 3a) and plot its width against drifter velocities (Figure 3b) and the distance between the two drifters (Drifter Separation; Figure 3c). Satellite-derived surface current data is obtained from the World Ocean Circulation (WOC) project. The objectives of this ESA-funded WOC project are to develop and validate innovative methodologies allowing for the optimisation of the synergetic capacity offered by satellite data, in situ measurements, and numerical

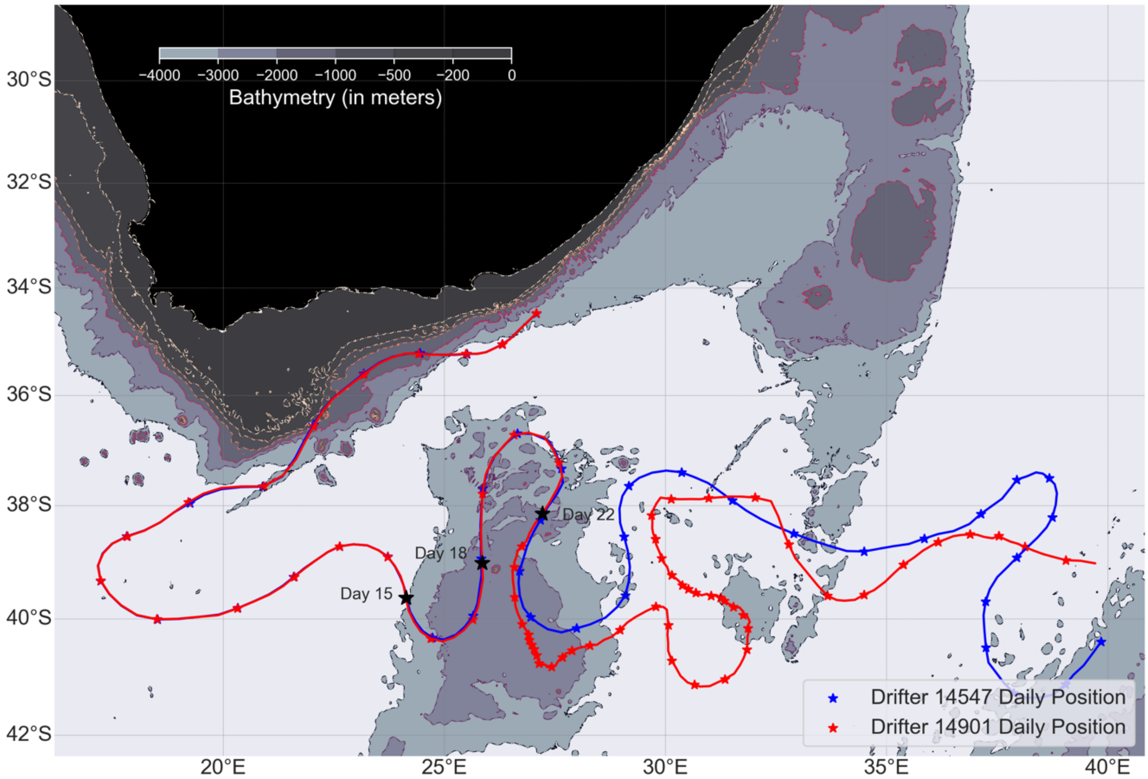

Figure 1. The pathway of a drifter-pair (red and blue lines) deployed in the Agulhas Current on the 11th of April 2015 for the first 40 days after deployment.

models for improving the quantitative estimates of upper-layer ocean circulation**.** The WOC data are openly and freely available at https://www.worldoceancirculation.org/Products.

3. Results and Discussion

Drifters 14901 and 14547 were deployed at the same location in the core of the Agulhas Current at 33.903°S and 27.753°E on 11 April 2015 (Morris et al., 2015). The weekly mean G1SST and WOC geostrophic currents are overlaid and compared to the drifter trajectories (Figure 2). The SST fields and meandering pattern of geostrophic currents show that both drifter pathways tend to follow the core of the Agulhas Current quite well. When the drifters reach the Agulhas Retroflection (week two), they follow the anticyclonic pathway connected with the retroflection of the current.

In week three, the drifters begin to show slight variations, with drifter 14901 beginning to trail behind drifter 14547 (seen in Figure 2) although the drifters still follow the trajectory of the core of the Agulhas Return Current. In week four, drifter 14547 follows the U-shape of the current remarkably well; however, drifter 14901 begins to deviate from the core current path and separates from drifter 14547. Additionally, an anticyclonic eddy is evident in both the SST field and WOC velocity fields near 25°E and 40.5°S, which may influence the variability of the region and, hence, the drifter trajectories and separations.

Figure 3 shows the distance between the largest SST front to the left and the largest SST front to the right of each drifter trajectory against the drifter distance travelled (Figure 3a), the daily drifter velocities (Figure 3b), and the separation distance between the two drifters (Figure 2c). It confirms that the two drifters remained in very close proximity to each other (< 4 km) during the first ~1800 km (3 weeks) of their journey along the Agulhas Current, Retroflection and Agulhas Return Current. Additionally, their daily velocities were nearly the same (Figure 3b) until ~1800 km (day 21). After that, as the two drifters meander around the northern reaches of the Agulhas Plateau (week 4, Figure 2), their separation distance continues to increase, with drifter 14901 beginning to trail slightly behind drifter 14547 (Figure 3b, c).

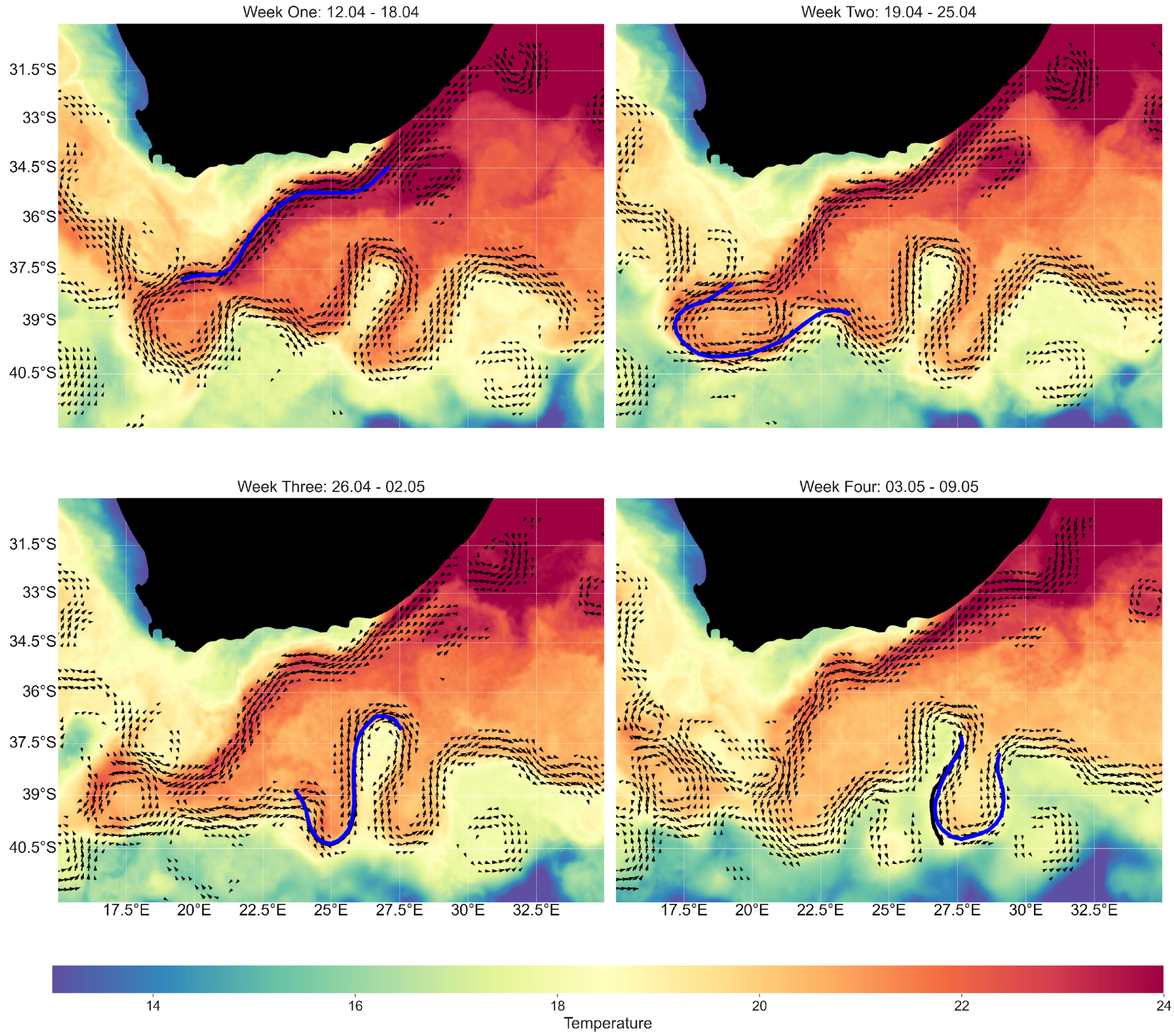

Figure 2. The drifter trajectories overlaid onto the weekly averaged SST (◦C) fields extracted from the satellite-derived G1SST Level 4 dataset and the weekly averaged WOC total velocity streamplots (only showing velocities exceeding 0.5 m.s-1) for the first four weeks of the drifters' lifespan.

At ~1600 km distance travelled (day 14), the separation distance between the two drifters gradually increases until ~2400 km distance travelled (day 23), when a drastic increase in their separation distance occurs (>15km). This may suggest that the drifters became exposed to different upper ocean dynamics, forcing them apart. Following this separation, drifter 14547 continues to follow the core of the Agulhas Return Current, while drifter 14901 moves more slowly along the outer edge of the Agulhas Return Current (week 4, Figure 2).

There does not appear to be a consistent relationship between the drifter separation (Figure 3c) and the distance between the strongest SST fronts to the left and right of each drifter trajectory (Figure 3a). There appear to be four events where the distance between SST fronts is notably different between the two drifters: (i) between 550 and 800km, (ii) between 1350 and 1600km, (iii) between 1725 and 1900km, and (iv) between 2050 and 2450km. These events are marked by the gray boxes in Figure 3. Interestingly it appears that

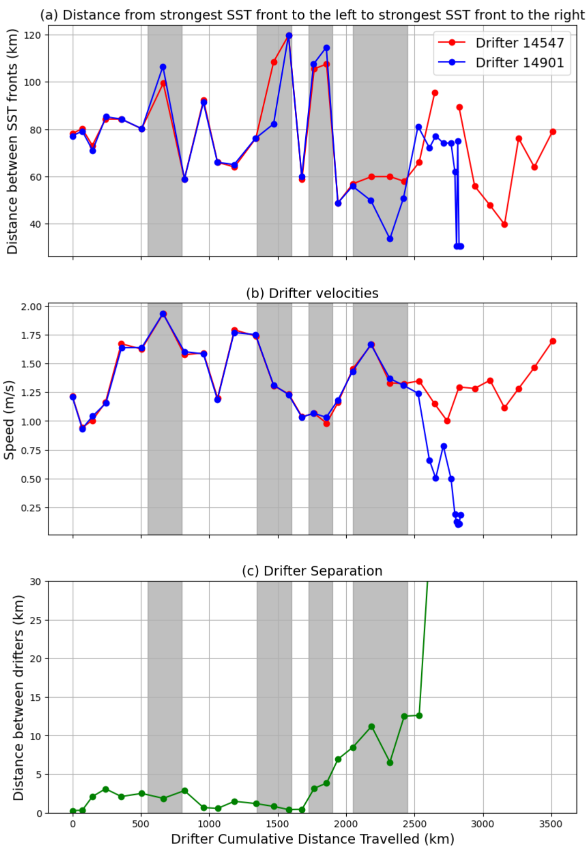

Figure 3. (a) The distance between the strongestSST front to the left and the strongest SST front to the right of each drifter trajectory against drifter distance travelled. (b) The velocity (m.s-1) of drifter 14547 (red) and drifter 14901 (blue) against drifter distance travelled. (c) Separation distance (in km) between drifter 14901 and drifter 14547 against distance travelled.

if the distance between fronts is narrower for one or the other drifter, their separation distance reduces or increases less rapidly. Notably, between 2000 and 2500km the distance between SST fronts is significantly different for a prolonged period, and following that event, the two drifters begin to separate completely.

This analysis suggests that during the last event, the two drifter trajectories are governed by different currents or current regimes. It remains unclear what the driving processes are that determine the drifter separation. It may be hypothesised that the drifters are impacted by different dynamical ocean processes or atmospheric frontal systems, causing the drifters to diverge from their parallel paths.

4. Conclusions

This preliminary study of the trajectories of a drifter pair deployed in the Agulhas Current suggests that the distance of the largest SST front from the drifter trajectory (left or right) contributes to the eventual drifter's separation. It is hypothesised that during such events, the two drifters are impacted by different dynamical ocean processes, causing them to diverge from their parallel paths.

However, this study is limited by the spatio-temporal resolution of the satellite-derived SST data. Additional analyses are needed to confirm which ocean processes are responsible for the drifters' parallel trajectories and eventual separation.

Future work will expand on the preliminary results of the SST front analysis presented here (Figure 3) to analyses of Lagrangian structures from Finite Size Lyapunov Exponents, running particle trajectory modelling experiments and assessing their skill scores. This, in turn, will be combined with observations from other measurement platforms, including, for example, total currents, geostrophic currents, Stokes drift, Ekman currents at the surface and 15m depth, and significant wave height, period, direction, and wind stress.

References

Boebel, O., Rossby, T., Lutjeharms, J., Zenk, W., & Barron, C. (2003). Path and variability of the Agulhas Return Current. Deep Sea Research Part II: Topical Studies in Oceanography, 50 (1), 35–56.

Dora, S., Khedekar, R., & Aparna, S. (2020). Trajectories of three drifters deployed simultaneously in the north eastern Arabian sea. Journal of Earth System Science, 129 (1), 1–8.

Krug, M., Swart, S., & Gula, J. (2017). Submesoscale cyclones in the Agulhas Current. Geophysical Research Letters, 44 (1), 346–354.

Lumpkin, R., & Elipot, S. (2010). Surface drifter pair spreading in the North Atlantic. Journal of Geophysical Research: Oceans, 115 (C12).

Lutjeharms, J., & Ansorge, I. (2001). The Agulhas Return Current. Journal of Marine Systems, 30 (1-2), 115–138.

Morris, T., Brummer, G.-J., & Louw, G. (2015). Cruise Report Agulhas System Climate Array (ASCA) Cruise. SAEON, 1–73.

van Sebille, E., Waterman, S., Barthel, A., Lumpkin, R., Keating, S. R., Fogwill, C., & Turney, C. (2015). Pairwise surface drifter separation in the western Pacific sector of the Southern Ocean. Journal of Geophysical Research: Oceans, 120 (10), 6769–6781.

Origin of the 2023 early retroflection in the Agulhas Current: Satellite-based evidence

J. A. Johannessen[1], F. Collard[2], B. Chapron[3], T. Lamont[4,5,6], C. Russo[4], B. Backeberg[7], M. Hart-Davis[8]

[1] Nansen Environmental and Remote Sensing Research Center, Bergen, Norway,

[2] OceanDataLab, Plouzane, France,

[3] Ifremer, Plouzane, France,

[4] Oceans & Coasts Research, Department of Forestry, Fisheries and the Environment, Cape Town, South Africa

[5]Bayworld Centre for Research and Education, Cape Town, South Africa

[6]Department of Oceanography, University of Cape Town, South Africa

[7] Deltares, The Netherlands

[8] TUM, Germany

Abstract: Retroflection describes the ability of the Agulhas Current to loop backward on itself at the southern tip of Africa to become the Agulhas Return Current (Bang, 1970; Lutjeharms, 1981). While the retroflection is usually located at about 18-20° E, early retroflections have been encountered as far east as 26° E (Rouault et al., 2003; Lutjeharms, 2006; Dencausse et al., 2010; van Aiken et al., 2013). In this proceedings paper we use the data visualisation portal (SynTool) to investigate the spatial and temporal evolution of an early retroflection of the Agulhas Current encountered in May-July 2023. In agreement with Johannessen et al. (2020), the analysis provides evidence that the early retroflection is triggered by the north-to-south co-alignment of a cyclonic eddy inshore of the Agulhas Current core with a large meander in the Agulhas Return Current located at about 24-26° E.

1. Introduction

The greater Agulhas Current system is energetic with complex and intense upper ocean dynamics expressed by distinct collocated gradients in sea surface temperature (SST), chlorophyll *a*, sea surface height (SSH) and surface current. This is evidenced in the mean dynamic topography (MDT) shown in Figure 1 after Rio et al., (2014), expressing strong gradients in the SSH related to the poleward flowing Agulhas Current core, the retroflection and the eastward flowing meandering Agulhas Return Current. Maximum mean surface geostrophic currents of about 1.5 m/s are encountered in the current core (Rouault et al., 2010). Extending to more than 1000 m depth, the corresponding mean volume transport is reported to range from 70-90 Sv (Bryden et al., 2005; Gordon et al., 1987). It is estimated that 80 - 90% of the transport in the core is returned to the Indian Ocean by the Agulhas Return Current. The remaining water is transported into the South Atlantic by filaments and eddy shedding. These eddies, often named "Agulhas rings", can reach 200-300 km in diameter, and transport large amounts of heat and salt from the Indian to the South Atlantic Ocean (e.g. Lutjeharms, 2006).

The ability of the Agulhas Current to curve backward on itself at the southern tip of Africa to become the Agulhas Return Current is maintained through conservation of vorticity (Bang, 1970; Lutjeharms, 1981). Infrequent episodes of early retroflection of the Agulhas

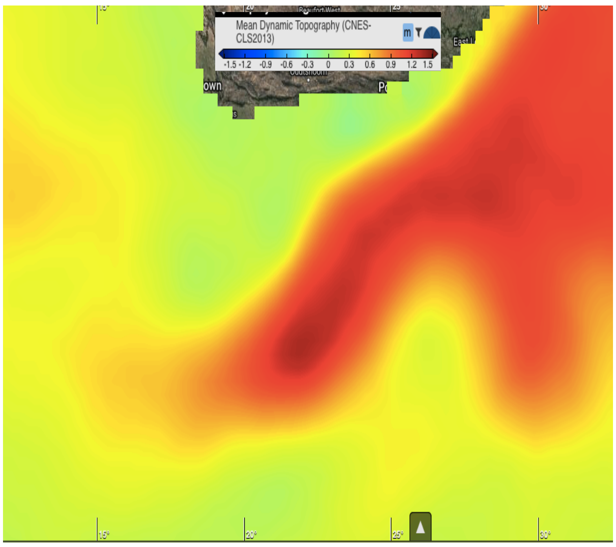

Figure 1. Mean dynamic topography of the greater Agulhas Current (Rio et al., 2014). The inserted color scale marks the elevation range from -1.5 m to + 1.5 m.

Current have been reported to last from weeks to months (e.g. Lutjeharms, 2006; van Aiken et al., 2013; Dencausse et al., 2010). The dynamics of these early retroflections may significantly change the eddy shedding and the south-westward heat, salt and volume transports.

Using the altimeter-based Location of the Agulhas Current Core and Edges (LACCE) method, Russo et al. (2020) identified a total of seven early retroflection events between 1993 and 2019. Four of these events (in 1999, 2000-2001, 2008, and 2019) reached easternmost longitudes exceeding 24 °E. In comparison, the remaining three events (in 2013, 2014, and 2018) were much less extreme, with easternmost longitudes between 22 and 23 °E, and more closely resembled Agulhas ring shedding events, as opposed to early retroflection events (Russo et al., 2020). The early retroflection events have a broad range of durations; while the reported 2000-2001 case lasted for 5-6 months, the 2019 retroflection event was only evident for close to two weeks. Moreover, while two of the seven events took place during winter, the remaining events occurred in summer and spring.

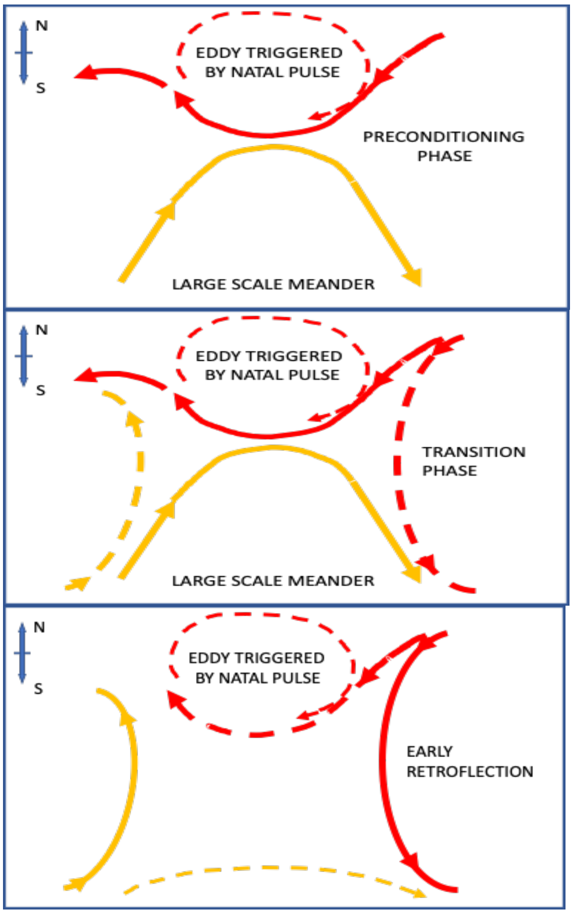

Figure 2. Schematic illustration of the evolution towards early retroflection. (upper) Preconditioning phase ensured by co-aligned eddy inshore of the Agulhas Current core (red curving-arrows) and larger semi-stationary meander in the Agulhas Return Current (light brown curving-arrows). (middle) Emerging of the transition phase. (lower) Formation of the early retroflection.

In this proceedings paper we investigate an early retroflection event in the Agulhas Current system encountered in May-July 2023. Using the SynTool visualization portal applied to the GlobCurrent-based satellite data (Johannessen et al., 2018; Chapron et al., 2019) we follow the stepwise evolution of this early retroflection event following the conceptual approach (illustrated in Figure 2) proposed by Johannessen et al., (2020), notably:

(i) A Natal pulse forms and starts to propagate south-westward as a cyclonic eddy (~60-100 km diameter) along the inshore edge of the Agulhas Current core.
(ii) The distinct semi-permanent large bell-shaped topographically steered clockwise curving meander (~300 - 400 km) in the Agulhas Return Current is centered over the Agulhas Plateau at about 38° S and 25° E.
(iii) The cyclonic eddy aligns with the large meander in a north-south direction and the surface current patterns gradually merge to set-up the transition phase to form an early retroflection.

In section 2 the data and analyses are presented, followed by discussion of results in section 3. The summary and outlook are then addressed in section 4.

2. Data and analyses

Benefitting from satellite sensor synergy one can derive daily to weekly maps of SST, near surface wind fields and upper layer velocity fields. Hence the temporal and spatial evolution of these fields can be regularly monitored as demonstrated in the GlobCurrent project (http://globcurrent.ifremer.fr). The data are interpolated to a 25 km^2 grid with a temporal resolution of three hours for the Ekman components and daily for the geostrophic current and SST fields (Rio et al., 2014; Johannessen et al., 2018; Chapron et al., 2019).

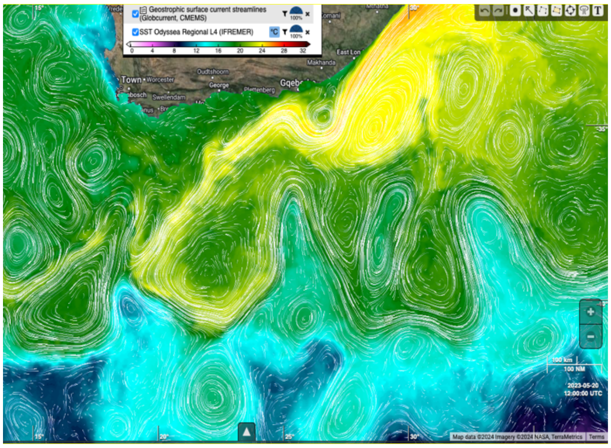

Figure 3. Fields of SST (color) and surface geostrophic current (white lines) for 20 May 2023. The inserted SST color scale ranges from around 8° to 25° C.

The OceanDataLab developed SynTool visualization portal (https://ovl.oceandatalab.com) is then used to collocate and display the gridded fields, both in near real- time and offline modes as shown in Figure 3. The SST fields reveal gradual transition to colder water in the Agulhas Current core from 27° C in the northeast to 15° C in the retroflection area in the southwest. Strong SST and surface current gradients are noted along the boundary in the core while they are less pronounced in the Agulhas Return Current. Moreover, the mesoscale variability depicts evidence of a Natal pulse at the inshore edge of the Agulhas Current east of Gqeberha (formerly Port Elizabeth), while significant structures and mesoscale variability including eddy shedding are evidenced in the retroflection region. In comparison, larger semi-permanent meandering patterns are present in the Agulhas Return Current (consistent with MDT, Figure 1).

As suggested by Johannessen et al., (2020) and schematically illustrated in Figure 2 the hypothesis is that an upstream meander of the Agulhas Current core south of Durban triggers the poleward advection of a 100 km diameter cyclonic eddy (Natal Pulse) along the inshore edge of the Agulhas Current core. At around 24-26° E the eddy becomes co-aligned with a semi-stationary anticyclonic meander in the Agulhas Return Current with a dimension of 300 – 400 km. The gradual evolution to this north-to-south co-alignment is considered to represent the preconditioning phase that subsequently triggers the transition to an early retroflection event. This is further discussed below according to the early retroflection encountered from 20 May to 20 July 2023.

3. Discussion of results

The temporal evolution of the SST field overlaid on the surface geostrophic current from 30 May are shown in Figure 4 at time steps 5 June, 10 June and 2 July to 15 July 2023. Between 20 May and 30 May (see Figure 3 and Figure 4a) a south-westward propagating cyclonic eddy inshore of the Agulhas Current core (a remnant of a Natal pulse) is seen to co-align in a north-south direction with the meander in the Agulhas Return Current centred around 24-26° E. The preconditioning has thus been established, and the transition into an early retroflection is reached on 10 June 2023, consistent with the hypothesis schematically shown in Figure 2.

The early retroflection persists until around 5 July 2023. During this 30-day period the lateral heat, salt and volume transports to the southwest will be reduced (see Figure 4c). In turn, the regional weather, precipitation patterns, wave-current refraction and marine ecosystem might also be impacted. Moreover, a filament of cold water from the Antarctic Circumpolar Current (ACC) is seen to protrude northwards towards the coastal area south of Gqeberha. The early retroflection gradually starts to break down after 2 July (Figure 4d) and is seen to return to a more typical longitude of retroflection by 15 July 2023 (Figure 4e). This event was also identified by Russo & Lamont (2024), who used the LACCE method to show that it was the third longest early retroflection since 1993, with only the 2000-2001 and 2008 events lasting longer (142 and 42 days, respectively). The break-down of the early retroflection appears to result from a gradual weakening and disappearance of the north-south directed alignment of the inshore cyclonic eddy along the Agulhas Current core and the big meander in the return current around 24-26° E.

As the satellite-based SST and surface current fields are assimilated it is expected that operational ocean models and marine services provide proper simulations of the evolution of the early retroflection. This is confirmed by inspection of the SST and surface current fields delivered by the Copernicus Marine Environment Monitoring Service (CMEMS) in the period from 20 May to 15 July 2023 (https://marine.copernicus.eu). Leveraging on

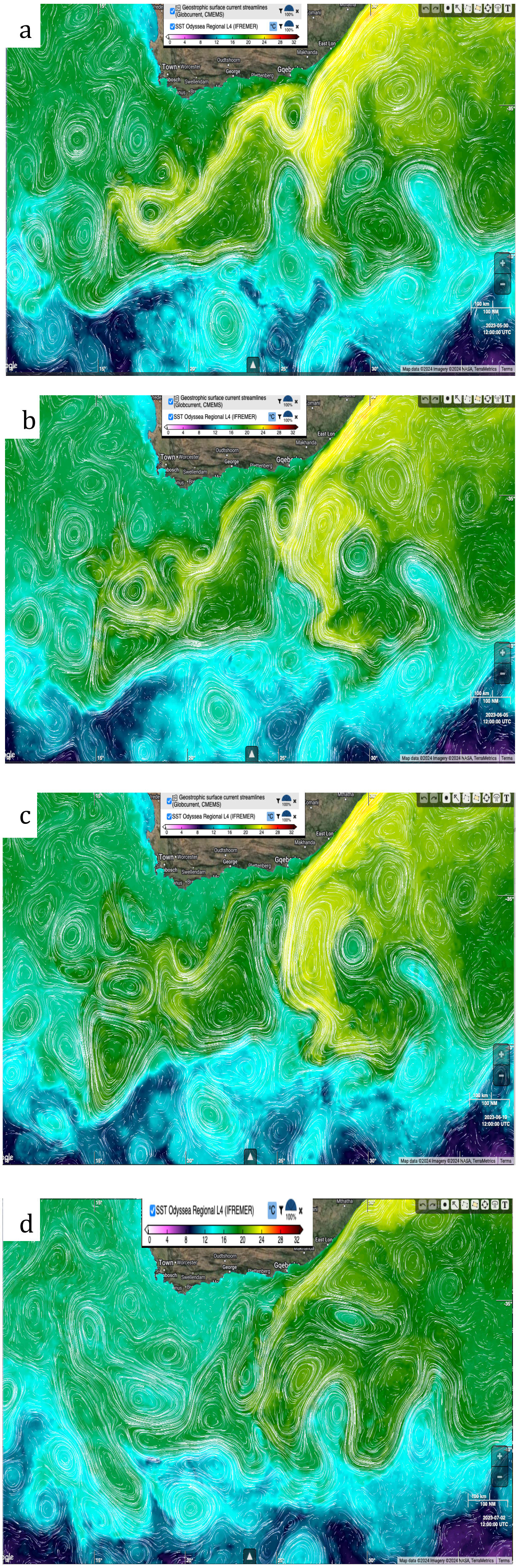

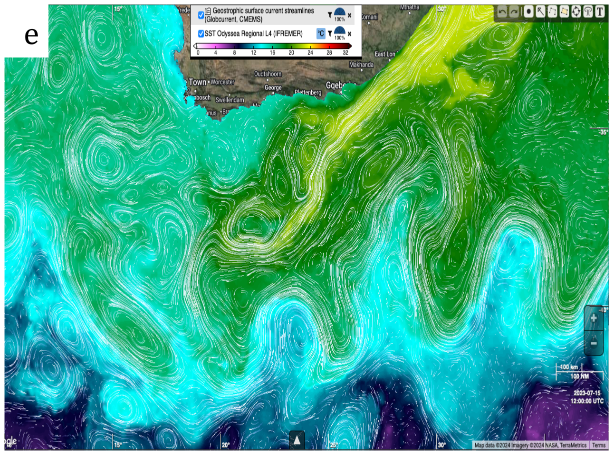

Figure 4. Evolution in the fields of SST (color) overlaid surface geostrophic current (white lines) from 30 May (a), 5 June (b), 10 June (c), 2 July (d) to 15 July (e) 2023. The inserted SST color scale ranges from around 8° to 25° C.

the satellite-based monitoring and data assimilation capabilities an *early retroflection indicator (ERI)* for the greater Agulhas Current regime could be developed. This may, for instance, be connected to the preconditioning phase (ERI-1 to ERI-3), the formation and duration period (ERI-4) and the phase connected to the breakdown and return to nominal state (ERI-5) as suggested below:

- ERI-1: A Natal pulse is generated south of Durban.
- ERI-2: A big meander in the Agulhas Return Current located over the Agulhas Plateau is formed.
- ERI-3: The Natal pulse propagates south-westward until it aligns with the big meander at about 25° E.
- ERI-4: An early retroflection is formed.
- ERI-5: The breakdown of the early retroflection starts followed by a gradual return to the nominal greater current regime.

Capitalizing on this indicator the corresponding time scales for ERI-1 to ERI-3, ERI-4 and ERI-5 can be identified and used to build a look-up table for studying early retroflection characteristics, both in time and space as well as regarding possible impact and consequences for the greater Agulhas Current regime.

4. Summary and Outlook

The greater Agulhas Current system is a fantastic natural laboratory for systematic exploitation of satellite-based remote sensing data synergy. As such, distinct 2D expressions in SST, SSH, Chl, waves, wind and surface current are combined and co-located to study complex and intense mesoscale to synoptic scale features and variability in space and time. In particular, we have again documented the evolution of an early retroflection event consistent with the concept suggested by Johannessen et al., (2020). Moreover, the robustness of this concept allows us to propose an early retroflection indicator (ERI) including a preconditioning phase (ERI-1 to ERI-3), the formation and duration period (ERI-4) and the phase from breakdown to the return to nominal state (ERI-5).

Furthermore, inspection of the SST and surface current fields delivered by the Copernicus Marine Environment Monitoring Service (CMEMS) in the period from 20 May to 15 July 2023 confirms that the early retroflection can be properly simulated thanks to assimilation of the satellite-based SST and SSH data. The characteristics of the 3D hydrography and velocity fields as well as changes in the coupled physical-biological structures might then also be explored. This, in turn, is expected to strengthen our understanding of the impact of early retroflections on air-sea interaction, wave-current refraction, regional weather, eddy shedding, as well as heat, salt and volume transports from the Indian Ocean to the Atlantic Ocean.

References

Bang, N. D. (1970). "Dynamic interpretations of a detailed surface temperature chart of the Agulhas Current retroflection and fragmentation area". South African Geographical Journal. **52**: 67–76. doi:10.1080/03736245.1970.10559466.

Chapron, B. et al (2019), GlobCurrent Analyses and Interpretation Framework, Technical Report, (http://globcurrent.ifremer.fr)

Bryden, H.L., Beal, L.M., Duncan, L.M., (2005) Structure and Transport of the Agulhas Current and its temporal variability. Journal of Oceanography, 61, 479-492. https://doi.org/10.1007/s10872-005-0057-8.

Dencausse, G., M. Arhan, S. Speich (2010), Spatio-temporal characteristics of the Agulhas Current retroflection. *Deep Sea Research Part I*: Oceanographic Research Papers November 2010, Vol. 57, Issue 11, pp. 1392-1405 http://dx.doi.org/10.1016/j.dsr.2010.07.004

Gordon, A.L., Lutjeharms, J.R.E., and Gründlingh, M.L. (1987), Stratification and circulation at the Agulhas Retroflection. Deep-Sea Research, 34, 565-599. https://doi.org/10.1016/0198-0149(87)90006-9.

Johannessen, J.A., B. Chapron, F. Collard, M.-H. Rio, G. Quartly and C. Donlon (2018), Advances in Surface Current Observations from Space: The GLOBCURRENT Case. *Proceedings IEEE International Geoscience and Remote Sensing Symposium (IGARSS 2018), pp. 153- 157;* IEEE Catalog Number: CFP18IGA-ART ISBN: 978-1-5386-7150-4.

Johannessen, J.A., T. Lamont, C. Russo, Roshin P. Raj, F. Collard and B. Chapron (2020), Using advanced visualization tool to study the dynamics of the Agulhas Current: The Early retroflection. *In Proceedings of the Nansen-Tutu Center 10-years Anniversary Symposium*, Cape Town, South Africa, 10-12 March 2020.

Lutjeharms, J. R. E. (2006). "Three decades of research on the greater Agulhas Current" (PDF). *Ocean Sci. Discuss.* ***3****: 939–995.* OCLC 800498605.

Lutjeharms, J. R. E (1981). "Features of the southern Agulhas Current circulation from satellite remote sensing". South African Journal of Science. 77: 231–236.

Rio, M.-H., S. Mulet, *and* N. Picot, (2014), Beyond GOCE for the ocean circulation estimate: Synergetic use of altimetry, gravimetry, and in situ data provides new insight into geostrophic and Ekman currents, *Geophys. Res. Lett.,* 41, 8918–8925.

Rouault, M. and J.R.E. Lutjeharms, Estimation of sea-surface temperature around southern Africa from satellite-derived microwave observations, S. Afr. J. Sci., 99 (2003), pp. 489-494.

Rouault, M.J., Mouche, A., Collard, F., Johannessen, J.A., Chapron, B., 2010. Mapping the Agulhas Current from space: an assessment of ASAR surface current velocities. J. Geophys. Res. 115, 1–14.

Russo, C.S., Lamont, T., M.J. Krug (2020), Spatial and temporal variability of the Agulhas Retroflection: Observations from a new detection method, *Remote Sensing of Environment,* 253, 112239.

Russo, C.S. Lamont, T. (2024). Is the Agulhas Current increasing its tendency to early retroflect? In: Huggett, J.A., Lamont, T., Haupt, T., Halo, I., Kirkman, S.P. (Eds.), Oceans and Coasts Annual Science Report 2023, Report No. 23, (accepted).

van Aken HM., J.R.E. Lutjeharms, M. Rouault, C. Whittle, and W.P.M. de Ruijter (2013) Observations of an early Agulhas Retroflection event in 2000: a temporary cessation of inter-ocean exchange south of Africa? *Deep Sea Research Part I*: Oceanographic Research Papers, vol. 72.

Nutrient fluxes in the greater Agulhas system: from lateral advection to (sub)mesoscale vertical nitrogen supply

T. A. Marshall[1], D. M. Sigman[2], L.M. Beal[3], A. Foreman[4], A. Martínez-García[4], S. Blain[5], E. Campbell[6], F. Fripiat[7], R. Granger[1,8], E. Harris[1,9], G. H. Haug[4], D. Marconi[2], S. Oleynik[2], P. A. Rafter[10], R. Roman[1], K. Sinyanya[1], S. M. Smart[1,11], and S. E. Fawcett[1,12]

[1]Department of Oceanography, University of Cape Town, South Africa

[2]Department of Geosciences, Princeton University, USA

[3]Rosenstiel School of Marine, Atmospheric, and Earth Science, University of Miami, USA

[4]Department of Climate Geochemistry, Max Planck Institute for Chemistry, Germany

[5]Laboratoire d'Océanographie Microbienne, Sorbonne Université, France

[6]School of Oceanography, University of Washington, USA

[7]Department of Geosciences, Environment and Society, Université Libre de Bruxelles, Belgium

[8]Microbiology & Biogeochemistry, Royal Netherlands Institute for Sea Research, Netherlands

[9]Marine Science, King Abdullah University of Science and Technology, Saudi Arabia

[10]Department of Earth System Science, University of California, Irvine, USA

[11]Department of Geological Sciences, University of Alabama, USA

[12]Marine and Antarctic Research centre for Innovation and Sustainability and (MARIS), University of Cape Town, South Africa

Abstract: The Agulhas Current, the western boundary current (WBC) of the South Indian Ocean, is known for its major role in driving significant heat and salt fluxes, yet its biogeochemical fluxes remain largely uncharacterised. Here, we use nitrate isotopes (δ^{15}N, δ^{18}O, and Δ(15-18) = δ^{15}N-δ^{18}O) to evaluate nutrient supply mechanisms that ultimately support new production in the southwest Indian Ocean. The δ^{15}N (and Δ(15-18)) of Agulhas thermocline nitrate is lower than that of both the underlying Subantarctic Mode Water and the upstream source waters, which we attribute to local N_2 fixation. Using a one-box model, we estimate a local N_2 fixation rate of 7–25 Tg N.a^{-1}. Mixed-layer nitrate Δ(15-18) is also low, due to both N_2 fixation and coupled partial nitrate assimilation and nitrification. Similarly low-Δ(15–18) nitrate in Agulhas rings indicates leakage of low-δ^{15}N nitrogen into the South Atlantic, which should be recorded in the organic matter sinking to the seafloor, providing a potential tracer of past Agulhas leakage. Along with N_2 fixation, the nitrate isotopes reveal three physical mechanisms of upward nitrate supply: i) entrainment at the edges of a mesoscale eddy, ii) inshore upwelling driven by a submesoscale oscillation of the current, and iii) entrainment at the offshore edge of the current core driven by submeso- and mesoscale instabilities. All three events manifest as upward injections of high-Δ(15-18) nitrate into the thermocline and surface where nitrate Δ(15-18) is otherwise low. The physical dynamics driving the nitrate supply events are common to all WBCs, suggesting that the WBC-facilitated nitrate flux is significant globally. We posit that N_2 fixation and submeso- and mesoscales upward nitrate supply enhance ocean fertility and possibly carbon export in the South Indian Ocean.

1. Introduction

Nutrient supply strongly shapes global ocean productivity. In the southwest Indian Ocean, our understanding of nutrient supply mechanisms is limited. The Agulhas Current, the western boundary current (WBC) of the South Indian Ocean, laterally transports heat and salt from the Indian to the Atlantic Ocean, thereby modulating climate (Beal, et al., 2011). Additionally, the high kinetic energy of this WBC system drives mixing and turbulence at submeso- and mesoscales ((sub)mesoscales). The horizontal and vertical nutrient flux in this region should thus be substantial. Nitrate isotopes, a geochemical tracer, can be used to characterise and at times quantify nutrients fluxes across multiple temporal and spatial scales.

In the low-latitude ocean, nitrogen (N) availability primarily limits ocean productivity. N_2 fixation, the biologically mediated process that converts N_2 gas to bioavailable N, is the ultimate source of N to the ocean. Some geochemical models predict broad-spread N_2 fixation across the South Indian Ocean (e.g., Wang et al., 2019); however, areal rates of N_2 fixation based on observations for this region are lacking. Additionally, there is considerable uncertainty surrounding the influence of (sub)mesoscale processes on vertical nutrient supply and ocean fertility. The high-energy Agulhas Current system, coupled with its oligotrophic surface waters and nutrient-rich thermocline waters, prime this region for potentially significant upward nutrient supply to the surface waters.

Here, we use nitrate isotope ratios ($\delta^{15}N$, $\delta^{18}O$, and $\Delta(15\text{-}18) = \delta^{15}N\text{-}\delta^{18}O$) along with other data to quantify a local N_2 fixation rate and three mechanisms of upward nitrate supply in the southwest Indian Ocean. N_2 fixation introduces low-$\delta^{15}N$ (and low-$\Delta(15\text{-}18)$) nitrate to the thermocline while incidences of high-$\Delta(15\text{-}18)$ in the surface waters (where $\Delta(15\text{-}18)$ is otherwise low) can be used to trace upward nitrate supply driven by (sub)mesoscale mixing because it is conserved during both mixing and phytoplankton assimilation of nitrate (Rafter et al., 2016 ; Marshall et al., 2023b).

2. Data and methods

Samples for nitrate isotope ratios were collected onboard the SA Agulhas II during the Agulhas Climate System Array (ASCA) cruise in winter (July) 2016. Samples from twenty full depth stations were collected using Niskin bottles. The dual isotope ratios of nitrate, both N and oxygen (O), were measured at Princeton University following the 'denitrifier' method and using a custom-built gas bench coupled to an isotope ratio mass spectrometer. The N and O isotope ratios are reported in delta notation ($\delta^{15}N$ and $\delta^{18}O$) and in units of per mil (‰). Nitrate $\Delta(15\text{-}18)$ is calculated by their differencing.

3. Results

Three water masses dominate the upper 500 m of the Agulhas Current system, Subantarctic Mode Water (SAMW), Thermocline waters, and Surface waters (Figure 1). Over the upper 500 m, nitrate $\Delta(15\text{-}18)$ is highest in Subantarctic Mode Water due to partial nitrate assimilation in the Southern Ocean surface waters (=3.4‰, orange shading), lower in the thermocline due to local N_2 fixation (=2.6‰, purple shading), and lowest at the top of the thermocline and in the surface mixed layer due to coupled partial nitrate assimilation and nitrification (=1.5‰, pink shading) (Marshall et al., 2023b).

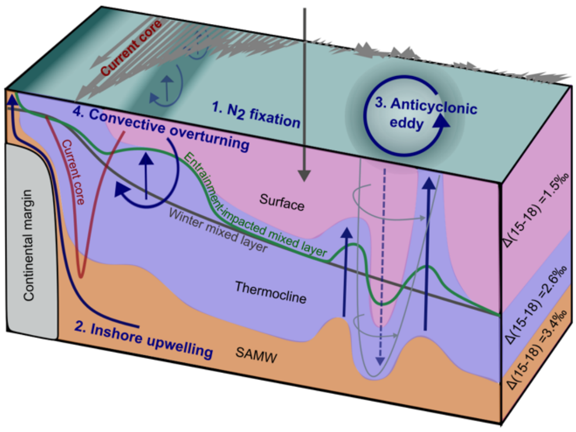

Figure 1: Schematized depth section of nitrate $\Delta(15\text{-}18)$ across the Agulhas Current showing four fluxes of nitrogen to the surface ocean, fuelling new production.

Low-$\delta^{15}N$ and -$\Delta(15\text{-}18)$ thermocline nitrate indicate a N_2 fixation signal (grey arrow in Figure 1) generated via the production and remineralisation of low-δ15N organic matter; (e.g., Knapp et al., 2008). Using nutrient and N isotope data from the three source regions to the Agulhas Current, along with an estimate of the lateral volume fluxes entering the system, we estimated a local N_2 fixation rate via a box model. Our approach revealed that the N_2 fixation rate in the greater Agulhas system ranges from 7–25 Tg $N.a^{-1}$ (Marshall et al., 2023a).

In Figure 1, the Agulhas Current core (southwest speeds >1 m s^{-1}) is shown as a red V-shaped contour and its horizontal shear at the surface is indicated by grey velocity vectors from the shipboard acoustic Doppler current profiler (ADCP). The horizontal dark grey contour represents the typical depth of the winter mixed layer, which generally follows the top of the thermocline, while the green contour shows how (sub)mesoscale entrainment events can shoal the mixed layer. The navy blue arrows show the physical processes that supply deep nitrate to shallow waters: 1) an anticyclonic eddy entrains thermocline nitrate into the mixed layer and surface at its edges. Cyclonic eddies should similarly entrain thermocline nitrate at their cores; 2) inshore upwelling entrains high-Δ(15-18) SAMW nitrate onto the shelf. Inshore upwelling of thermocline waters, which also occurs in this system, would supply lower-Δ(15-18) nitrate; 3) large horizontal density and velocity shears at the edges of the current core generate (sub)mesoscale instabilities, temporarily shoaling the mixed layer relative to its mean wintertime depth and inducing secondary vertical velocities that entrain nitrate into sunlit waters. The increase in nitrate availability that results from these three (sub)mesoscale mechanisms is indicated by the darker green shading at the surface of Figure 1.

4. Discussion

Both N_2 fixation and upward nitrate supply contribute to fuelling new and export production, which increases productivity (Dugdale & Goering 1967; Eppley & Peterson 1979). While both these N fluxes increase regional productivity, N_2 fixation also contributes to carbon sequestration and thus lowering atmospheric CO_2 concentrations. Nevertheless, the high (sub)mesoscale turbulence characteristic of all subtropical WBC systems should enhance the episodic nutrient supply and productivity in otherwise oligotrophic regions. An increase in the upward nitrate supply in WBC systems driven by an ongoing increase in their eddy kinetic energy could partially offset the decline in subtropical ocean productivity predicted under global warming.

References

Beal, L. et al., 2011. On the role of the Agulhas system in ocean circulation and climate. Nature Review, Volume 472, 429-436. https://doi.org/10.1038/nature09983

Dugdale, R. & Goering, J., 1967. Uptake of new and regenerated forms of nitrogen in primary productivity. Limnology and Oceanography, 12(2), 196–206https://doi.org/10.4319/lo.1967.12.2.0196

Eppley, R. & Peterson, B., 1979. Particulate organic matter flux and planktonic new production in the deep ocean. Nature, Volume 282, 677-680. https://doi.org/10.1038/282677a0

Knapp, A., DiFiore, P., Deutsch, C. & Sigman, D., 2008. Nitrate isotopic composition between Bermuda and Puerto Rico: Implications for N2 fixation in the Atlantic Ocean. Global Biogeochemical Cycles, Volume 22, GB3014. https://doi.org/10.1029/2007GB003107

Marshall, T. et al., 2023a. The Agulhas Current transports local and remote signals of Indian Ocean nitrogen cycling. Journal of Geophysical Research: Oceans, e2022JC019413. https://doi.org/10.1029/2022JC019413

Marshall, T. A., Beal, L., Sigman, D. M., & Fawcett, S. E. (2023b). Instabilities across the Agulhas Current enhance upward nitrate supply in the southwest subtropical Indian Ocean. AGU Advances, 4, e2023AV000973. https://doi.org/10.1029/2023AV000973

Rafter, P., DiFiore, P. & Sigman, D., 2013. Coupled nitrate nitrogen and oxygen isotopes and organic matter remineralization in the Southern and Pacific Oceans. Journal of Geophysical Research: Oceans, Volume 118, 47781–4794. https://doi.org/10.1002/jgrc.20316

Wang, W., Moore, K., Martiny, A. & Primeau, F., 2019. Convergent estimates of marine nitrogen fixation. Nature Article, Volume 566, 205–211. https://doi.org/10.1038/s41586-019-0911-2

Using the LACCE monitoring tool to investigate the variability in the Agulhas Current System

C.S. Russo[1], T. Lamont[1,2,3,4].

[1] Oceans & Coasts Research, Department of Forestry, Fisheries and the Environment, Cape Town, South Africa

[2] Bayworld Centre for Research and Education, Cape Town, South Africa

[3] Department of Oceanography, University of Cape Town, Cape Town, South Africa

[4] Nansen-Tutu Centre for Marine Environmental Research, Department of Oceanography, University of Cape Town, South Africa

Abstract: The Agulhas Current (AC), the strongest Western Boundary Current (WBC) in the Southern Hemisphere, forms a key component of the global thermohaline circulation through its facilitation of the Indian-Atlantic inter-ocean exchange of heat and salt, which takes place at the Agulhas Retroflection. Understanding and monitoring variations in the structure and persistence of the AC, among other WBCs, is crucial, as any changes in speed, width, and mean location can have both local and global implications. The AC, much like other WBCs, is ideal to map from space because it is characterised by strong velocity and temperature gradients. The Location of the Agulhas Current Core and Edges (LACCE) monitoring tool was developed for daily, near-real time operational use by the South African National Oceans and Coastal Information Management System (OCIMS). LACCE is unique in its ability to identify the core and edges throughout the greater Agulhas Current system, including the AC, the Agulhas Retroflection, and the Agulhas Return Current. LACCE was applied to daily reprocessed satellite altimetry data and the Mercator Global Oceans Physical Reanalysis (GLORYS-12v1) model output to investigate the variability in the AC system. Long-term trends in the AC's core location, computed along 100 virtual transects along the length of the east and south coasts of South Africa, suggest the current has migrated offshore over the years from 1993 to 2023. LACCE has proven to be a useful tool for monitoring AC variability, and as such application of LACCE to other WBC systems is currently underway.

1. Introduction

The warm and fast-flowing Agulhas Current (AC), located along the east coast of South Africa (Fig. 1), is the strongest and largest Western Boundary Current (WBC) in the Southern Hemisphere. The AC plays a major role in the global thermohaline circulation, through its facilitation of the inter-basin exchange of heat, salt and energy, between the Indian and Atlantic Oceans, which takes place in the Agulhas Retroflection region (Beal and Elipot 2016). The AC strongly influences the conditions of the adjacent shelf ecosystem, as well as the local weather and global climate (Yang et al. 2016, Beckley and van Ballegooyen 1992, Russo et al. 2019, Beal and Elipot 2016).

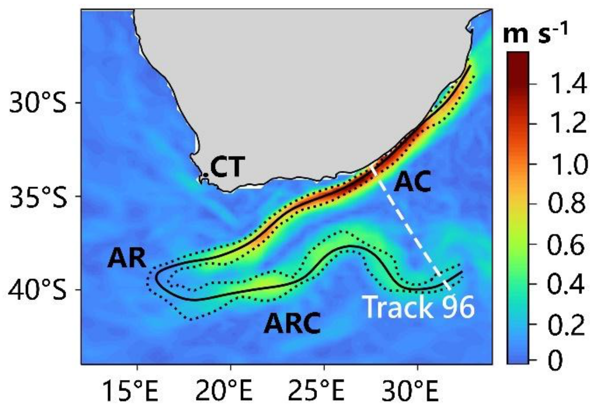

Figure 1: Mean (1993-2023) LACCE-identified location of the Agulhas Current's (AC) core (solid black line) and edges (dotted black line), highlighting the system's components including the AC Proper, the Agulhas Retroflection (AR) and the Agulhas Return Current (ARC). The location of satellite ground track #96, which is collocated with the ASCA monitoring line (dashed white line), is overlaid.

In recent years, interest in monitoring the variability in the AC system has increased due to the current's far-reaching influence combined with the increased frequency and intensity of extreme environmental events. Monitoring any variations in the structure and persistence of the AC, including changes in speed, width, and mean location, is crucial to improve our understanding of the system's variability, as well as the impacts thereof.

Due to the AC's size and its dynamic nature, *in situ* monitoring can be difficult and expensive, but also dangerous. However, similar to other WBCs, the AC is characterised by strong velocity and temperature gradients making it ideal to map from space (Krug et al. 2014). The LACCE (Location of the Agulhas Current Core and Edges) algorithm, developed for and used by the South African National Oceans and Coastal Information Management System (OCIMS), when applied to either satellite data or model output, identifies the core and edges of the current throughout the entire AC system. The current study investigates the spatial and temporal variability of the AC's path along the entirety of the South African east and south coasts through the application of LACCE to both satellite data and global ocean reanalysis output.

2. Data and Methods

Daily reprocessed gridded 1/4° satellite altimetry data (https://doi.org/10.48670/moi-00148), and 1/12° Global Ocean Physics Reanalysis (GLORYS) data (https://doi.org/10.48670/moi-00021), spanning from January 1993 to June 2023, were acquired from the Copernicus Marine Environment Monitory Systems (CMEMS) website (http://marine.copernicus.eu/). Russo et al. (2021) documented a detailed description of the LACCE algorithm. In this study, we applied LACCE to both the satellite and reanalysis datasets to identify the location of the AC's core and edges. The daily location of the AR, defined as the westernmost point in the AC system was extracted (Fig. 2a). In addition, the daily distance between the AC core and the coast, along track #96, was calculated and used as a proxy with which to monitor the occurrence and intensity of Agulhas Current meanders (Fig. 2b). We also computed the long-term (1993–2023) linear trends in the distance between the AC core and the coast (Fig. 3).

3. Results and Discussion

The AC is unique from other WBCs, such that it undergoes a change direction of flow which is known as the AR. The AC typically retroflects just south of Cape Town (CT; Fig. 1) between 16 and 22°E (Russo et al. 2021), however, on occasion it has been observed to retroflect further east than usual. These anomalous easterly retroflections also known as an Early Retroflections (ERs). LACCE proved successful in monitoring the occurrence of these events by defining any retroflection occurring east of 22.77°E as an ER (Fig. 2a). Five such ERs were observed which occurred in 1999, 2000, 2008, 2013 and 2019 (Fig. 2a). While ERs can substantially impact the regional shelf ecosystems (Roberts and Mullon 2010), they can also alter the amount of Agulhas leakage which makes its way into the Atlantic Ocean (van Sebille et al. 2009), which could have considerable global implications.

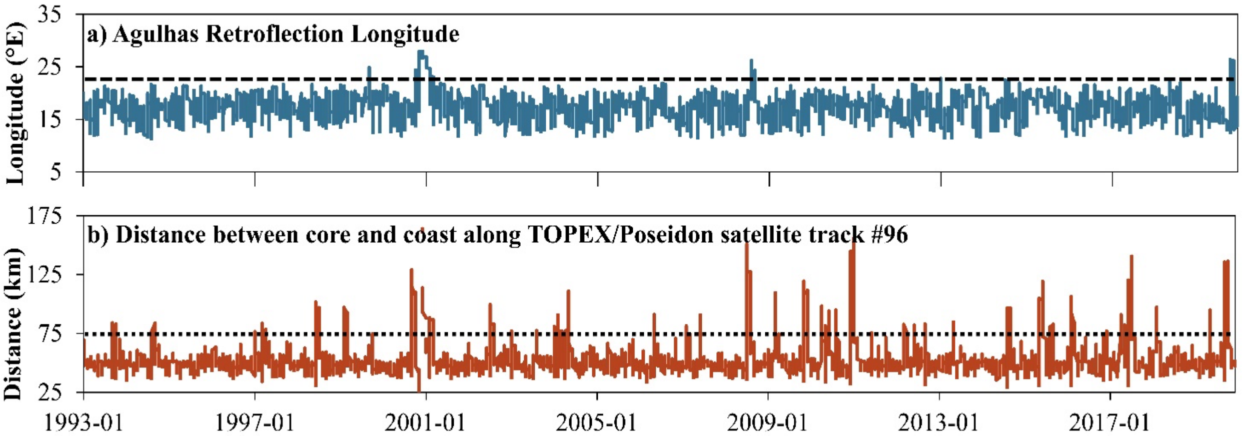

Figure 2: a) Longitudinal position of the Agulhas Retroflection identified as the westernmost point of the LACCE-identified current core obtained from satellite altimetry data. b) Distance of the LACCE-identified current core from the coast calculated along TOPEX/Poseidon track #96.

While Agulhas Current meanders form part of the triggering mechanism for ERs, their occurrence also has a considerable influence on the hydrography and biology of the adjacent shelf ecosystem (Russo et al. 2019). As a result, monitoring their occurrence is also important. Agulhas Current meanders were identified as any deviation greater than one standard deviation from the mean location of the AC (Krug et al. 2014) along track #96 (Fig. 2b). A larger number of meanders occurred in the latter half of the timeseries, after 2006. Suggesting a possible increased instability in the AC, however further investigation into this is required.

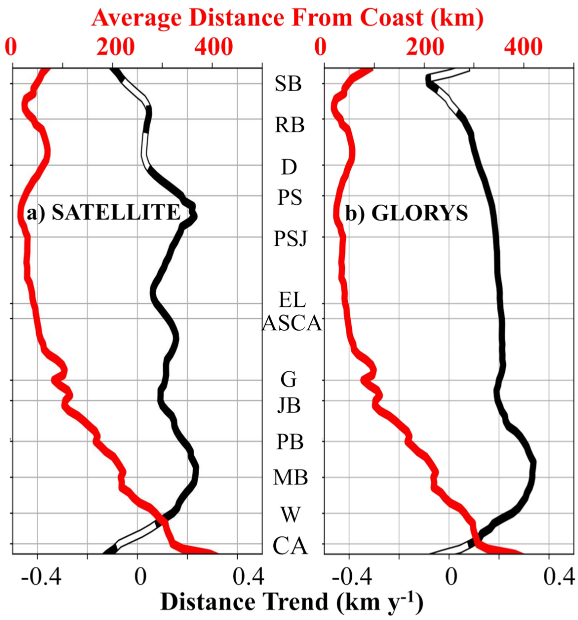

Figure 3: Mean distance of the LACCE-identified Agulhas Current core from the coast obtained from a) the satellite data and b) the GLORYS output. Statistically significant (black line) and non-significant (white line) trends for the distance of the AC core from the coast are shown. Locations indicated from north to south along the coast are Sodwana Bay (SB), Richards Bay (RB), Durban (D), Port Shepstone (PS), Port St John's (PSJ), East London (EL), Agulhas System Climate Array monitoring line (ASCA), Port Alfred, Gqeberha (G), Jeffrey's Bay (JB), Plettenberg Bay (PB), Mossel Bay (MB), Witsand (W) and Cape Town (CT).

Overall, the mean location of the AC as obtained from the GLORYS output agreed with that observed from the satellite data (Fig. 3). Given that the AC is topographically steered, it flows tightly along the slope of the continental shelf (Roberts et al. 2010), from Sodwana Bay (SB) to near Cape Agulhas (CA; Fig. 3). As a result, the distance of the AC's core from the coast, in both the satellite and GLORYS data (Fig. 3), increases as the shelf widens, specifically between Richards Bay (RB) and Port Shepstone (PS). The same pattern occurred off East London (EL), where the Transkei shelf widens before ultimately forming the Agulhas Bank.

Calculated long-term linear trends for the position of the AC's core relative to the coast, suggest that the AC has migrated offshore, specifically between RB and CA. This was observed in both the satellite and GLORYS data (Fig. 3). While two regions showed peaks in the trend calculated from the satellite data (Fig. 3a), only one of these regions showed a similar peak for the GLORYS data (Fig. 3b). The satellite data suggests that the AC migrated offshore at a maximum rate of approximately 0.24 km y^{-1} between PS and Port St Johns (PSJ), as well as between Plettenberg Bay (PB) and Mossel Bay (MB). In comparison, GLORYS suggested that the AC migrated offshore at a relatively higher maximum rate of approximately 0.35 km y^{-1} between PB and MB (Fig. 3b). While the current was observed to be migrating offshore along the majority of the coast, shoreward migration trends were observed near SB in both the satellite and GLORYS data. The satellite data also showed shoreward migration of the current near CA (Fig. 3a), but this was not observed in GLORYS (Fig. 3b).

4. Preliminary Conclusions

LACCE illustrated that the majority of the AC was migrating offshore during the 1993–2023 period, with the exception of a few locations. While this offshore migration was related specifically to the AC core, further investigation is required to ascertain whether similar trends are observed for the edges of the current. Although these results are preliminary, they demonstrate that LACCE is a useful tool for monitoring this aspect of the AC variability. Further investigation into the other aspects of the AC system's variability is currently underway. In addition, investigations are also underway to test the application of LACCE to other WBC systems.

References:

Beal, L. M., & Elipot, S. (2016). Broadening not strengthening of the Agulhas Current since the early 1990s. *Nature, 540*(7634), 570-573.

Beckley, L. E., & Van Ballegooyen, R. C. (1992). Oceanographic conditions during three ichthyoplankton surveys of the Agulhas Current in 1990/91. *South African Journal of Marine Science*, *12*(1), 83-93.

Krug, M., Cipollini, P., & Dufois, F. (2014). Observing the Agulhas Current with sea surface temperature and altimetry data: challenges and perspectives. In *Remote Sensing of the African Seas* (233-249). Springer, Dordrecht. doi:10.1007/978-94-017-8008-7_12

Roberts, M.J., van der Lingen, C.D., Whittle, C., van den Berg, M.A., 2010. Shelf currents, lee-trapped and transient eddies on the inshore boundary of the Agulhas Current, South Africa: their relevance to the KwaZulu-Natal sardine run. *African Journal of Marine Science*, *32*, 423–447. doi: 10.2989/1814232X.2010.512655.

Russo, C. S., Lamont, T., & Krug, M. (2021). Spatial and temporal variability of the Agulhas Retroflection: Observations from a new objective detection method. *Remote Sensing of Environment, 253*, 112239.

Russo, C. S., Lamont, T., Tutt, G. C. O., van den Berg, M. A., & Barlow, R. G. (2019). Hydrography of a shelf ecosystem inshore of a major Western Boundary Current. *Estuarine, Coastal and Shelf Science*, *228*, 106363. doi:10.1016/j.ecss.2019.106363

Yang, H., Lohmann, G., Wei, W., Dima, M., Ionita, M., & Liu, J. (2016). Intensification and poleward shift of subtropical western boundary currents in a warming climate. *Journal of Geophysical Research: Oceans, 121*(7), 4928-494

Patterns in the plankton: bottom-up or top-down forcing of copepods on the Agulhas Bank?

J. Huggett[1,2], J. Carstensen[3], M. Noyon[4], D. Walker[5]

[1] Oceans and Coastal Research, Department of Forestry, Fisheries and the Environment, Cape Town, South Africa.

[2] Department of Biological Sciences, University of Cape Town, Rondebosch, South Africa.

[3] Aarhus University, Roskilde, Denmark.

[4] Nelson Mandela University, Gqeberha, South Africa.

[5] Cape Peninsula University of Technology, Cape Town, South Africa.

Abstract: Copepods dominate the zooplankton community on the Agulhas Bank, where they provide an important food resource for pelagic fish and other biota. Previous studies have shown the dominant large copepod *Calanus agulhensis* to be strongly associated with the productive cold ridge of upwelled water on the central and eastern Agulhas Bank. However, there is little information available on other copepod taxa, and whether the Agulhas Bank community has changed over time in response to environmental variability or other ecosystem changes, such as the eastward shift in pelagic fish distribution. We used environmental and zooplankton data collected annually in late spring to explore spatio-temporal variability in copepod biomass and species composition on the Agulhas Bank over a 24-year period, from 1988 to 2011. Functional traits were used to interpret the observed patterns. Total copepod biomass declined significantly over the time series, as did all stages of *C. agulhensis* and the small calanoid copepods, but no long-term trends were observed for other copepod taxa. There was no obvious shift in copepod biomass in response to the eastward shift in pelagic fish in ca. 1996, but there were significant negative relationships between copepod biomass and pelagic fish biomass. This suggests predation pressure has an important top-down influence on copepod biomass on the Agulhas Bank. Bottom-up forcing from environmental drivers cannot be ruled out, however, despite ambiguous results from *in situ* and remote data series, and long-term warming due to climate change is expected to negatively impact ecosystem productivity at the large scale.

1. Introduction

Plankton are the foundation of most marine food webs, providing food to higher trophic levels such as fish, seabirds and marine mammals. Copepods typically dominate the zooplankton in terms of both abundance and biomass and form the intermediate trophic link between phytoplankton and fish. They play a key role in carbon export via the biological pump, and are ideal indicators of climate change, responding rapidly to changes in the environment (Richardson, 2008).

Zooplankton sampling over the Agulhas Bank during annual acoustic surveys from 1988 onwards showed zooplankton biomass to be dominated by a large calanoid copepod *Calanus agulhensis*, which comprised between 53 and 82% of total copepod biomass over the entire Agulhas Bank (Verheye et al., 1994). Highest densities of *C. agulhensis* were found on the central to eastern Agulhas Bank, with greatest biomass associated with the cold ridge of upwelled water south of Mossel Bay. This distribution pattern was ascribed to higher chlorophyll *a* concentrations, which would enhance growth rates, as well as localised retention of copepods due to the semi-closed, cyclonic circulation around the ridge (Peterson et al., 1992).

As most subsequent research effort has focused on *C. agulhensis*, there is scant information on the other copepod taxa that contribute to the Agulhas Bank community, including their distribution and abundance, and whether these have changed over time. Several studies have highlighted marked environmental or ecosystem changes on the Agulhas Bank over the past few decades, including the so-called ‘eastward shift’ of pelagic fish in 1996, with severe implications for top predators such as seabirds (Blamey et al., 2015). The question of whether there have been parallel changes in the lower trophic levels, in particular the zooplankton community, remains to be addressed. In this study we used a 24-year time series to explore spatial and temporal variability in the dominant copepod taxa on the Agulhas Bank during austral spring between 1988 and 2011. We also explored relationships between copepod and pelagic fish biomass for a perspective on potential top-down predation.

2. Data and methods

Sampling was conducted on the Agulhas Bank during annual hydro-acoustic stock-assessment surveys of pelagic fish in late spring (late October to early December) between 1988 and 2011 (Fig. 1). Vertical profiles of temperature and chlorophyll *a* (chl *a*) were obtained for the upper 200 m of the water column. Zooplankton samples were collected from the upper 200 m using a vertically hauled Bongo net (0.57 m diameter, 200-µm mesh) equipped with a General Oceanics flowmeter and were preserved in a 5% buffered formaldehyde-seawater solution. In the laboratory, copepods were counted and identified microscopically to stage, species or taxonomic category. The spatial distribution for copepod biomass for each year was calculated using a two-step procedure, consisting of a Generalized Additive Model (GAM) to produce the mean spatial distribution across all years, and an Ordinary Kriging (OK) analysis of residuals from the GAM analysis to produce spatial distributions for individual years (Huggett et al., 2023).

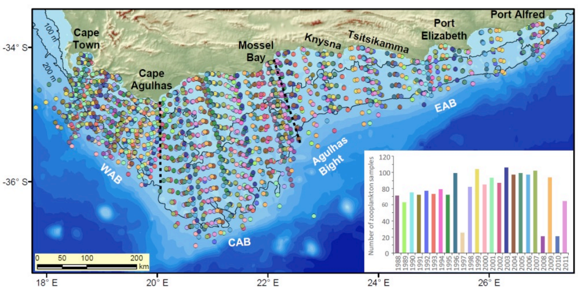

Figure 1: Map of zooplankton sampling locations on the Agulhas Bank during annual surveys in November–December from 1988–2011. Dashed lines delineate the western (WAB), central (CAB) and eastern (EAB) regions of the Bank. Inset shows number of zooplankton samples analysed per survey.

3. Results

Copepod biomass was concentrated over the outer shelf of the Agulhas Bank, beyond the 100 m isobath (Fig. 2a). Peak biomass (>1400 mg C m^{-2}) was located near the southern tip of the CAB and was relatively low (<800 mg C m^{-2}) over the entire inner shelf. Areas of greatest copepod biomass overlapped broadly with the region of elevated chl *a* at 30 m depth, as delineated by the 0.9 mg m^{-3} contour.

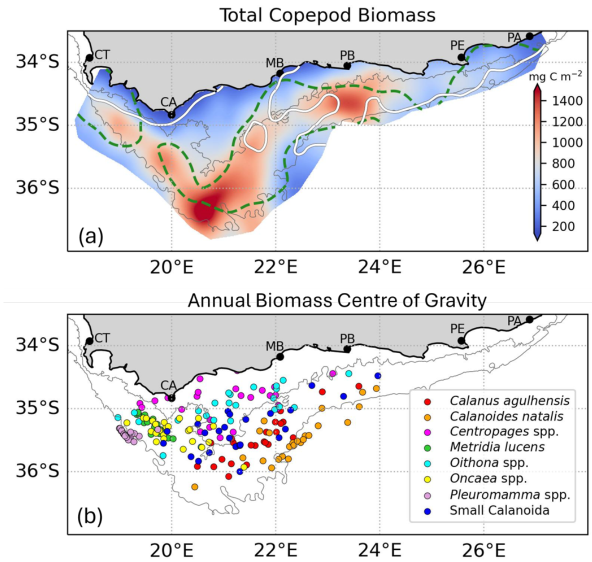

Figure 2: (a) Estimated mean copepod biomass (mg C m^{-2}) on the Agulhas Bank during November–December from 1988 to 2011. The solid white line indicates the mean 17°C isotherm at a depth of 30 m, and the dashed green line indicates the mean 0.9 mg m^{-3} chl *a* isoline at 30 m depth. The grey lines correspond to the 100 and 200 m isobaths. (b) Centre of gravity of upper 10% of highest biomass values for dominant copepod taxa each year (each dot represents one survey).

Eight species or taxonomic groups of copepods, along with large calanoid nauplii, collectively comprised 98% of total copepod abundance and 94% of total copepod biomass (Huggett et al., 2023). *C. agulhensis* comprised 50% of total copepod biomass and ranked third overall in abundance (17.1%). The small Calanoida (Para- and Clausocalanidae) were the most abundant group overall (37% of total abundance), and the second most important group in terms of biomass (23%). The tiny (<1 mm) Oithonidae were the second-most abundant taxon (18%) but comprised <1% of total biomass. The spatial distribution of annual centres of gravity (CoGs, centres of the upper 10% of highest biomass values) for the dominant taxa (Fig. 2b) showed lowest variability (tightest clustering) for the strong vertical migrants *Pleuromamma* spp. and *Metridia lucens*, but were more broadly distributed for the other species, indicating greater interannual variability in the location of peak biomass. The upwelling-associated species *Calanoides natalis* was most concentrated along the shelf edge, particularly near the Agulhas Bight. This suggests a link with shelf-edge upwelling, and potentially with sporadic shear edge cyclonic eddies in the Agulhas Bight region, which would both stimulate production through core upwelling and enhance retention of entrained plankton.

Mean copepod biomass declined significantly over the 24-year time series (R^2 = 0.52, $p < 0.001$; Fig. 3). The decline was significant for all three regions of the Bank but was most marked for the CAB (R^2 = 0.44; $p < 0.001$). Patterns of interannual variability differed between the dominant copepod taxa. There was a significant long-term decline in total biomass of *C. agulhensis* (R^2 = 0.48, $p < 0.001$), as well as for each copepodite stage, and in the proportion of total copepod biomass comprised by this species. The proportion of larger *C. agulhensis* stages (C4, C5, females) declined, while the proportion of smaller stages (C1–C3) increased. There was also a significant decline in biomass of the small Calanoida (R^2 = 0.33, $p < 0.01$), although the proportion of total copepod biomass comprised by this group increased over time. Collectively, these trends resulted in a net decrease in copepod size over the time series. There were no significant trends for any of the other taxa.

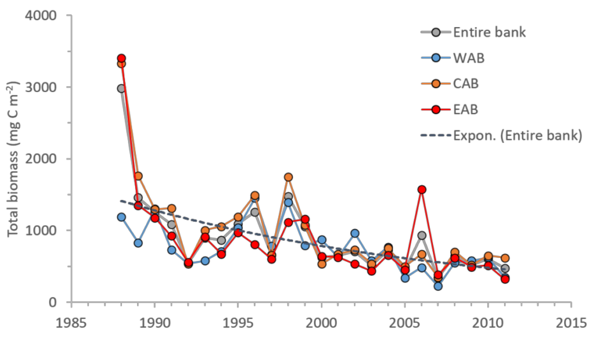

Figure 3: Time series of estimated mean total copepod biomass (mg C m^{-2}) over the entire Agulhas Bank during late spring (Oct–Dec) from 1988 to 2011, and for the western (WAB), central (CAB) and eastern (EAB) sectors. All regions showed significant negative linear trends; exponential (best) fit shown for entire bank.

There were no significant long-term trends for *in situ* temperature (sea surface temperature, temperature at 30 m depth, and the depth of 17°C isotherm), for area or volume of upwelled water (coastal or cold ridge), or for surface (5 m) or integrated (upper 100 m) chl *a*, but there was a significant long-term increase in chl *a* at 30 m. Remotely-sensed data from other studies indicate long-term warming for the Agulhas Current system as well as a significant increase in upwelling on the Agulhas Bank over the past 3–4 decades, while there was a slight but significant decline in net primary production (NPP) rates, and contrasting seasonal trends in chl *a* for the Bank, since 1997/1998 (see Huggett et al., 2023 for references).

Total pelagic fish biomass estimates (combined data for anchovy, sardine and redeye for the entire Agulhas Bank), showed a generally contrasting trend to estimated copepod biomass over the time series. Despite the interannual variability within both data sets, there was a significant negative relationship (R^2 = 0.25, $p < 0.05$, n = 24) between total copepod and total pelagic fish biomass, and mean copepod biomass was significantly lower after 1996 (the year of the eastward shift for anchovy; Roy et al., 2007) compared to before. There were also significant negative relationships between anchovy and copepod biomass (total and *C. agulhensis*), and between redeye and copepod biomass (total and *C. agulhensis*), but none with sardine biomass.

4. Discussion

Copepod biomass on the Agulhas Bank during late spring was strongly dominated by the large calanoid *Calanus agulhensis* and small calanoids of the Para- and Clausocalanidae. Collectively these two groups accounted for over 50% of total copepod abundance and over 70% of total biomass. Their distribution was closely aligned with the region of greatest subsurface chl *a* biomass, downstream from coastal and cold ridge-associated upwelling. This suggests that both small and large predominantly herbivorous calanoid copepods benefit from elevated phytoplankton biomass associated with the cold ridge. The significant decline observed for total copepod biomass on the Agulhas Bank over the 24-year time series was also seen in each developmental stage of *C. agulhensis*, from the nauplii through to the adults, as well as in the small Calanoida, but was not apparent for any of the other major copepod taxa.

Long-term changes in zooplankton may be mediated by environmental factors influencing food availability (bottom-up forcing), by predation pressure (top-down forcing), or a combination of the two, although they can be difficult to disentangle. Although there was no obvious shift in copepod biomass in response to the eastward shift in pelagic fish in ca. 1996, the significant negative relationship between total copepod biomass and total pelagic fish biomass suggests an important top-down influence from predation pressure by zooplanktivorous fish on the Agulhas Bank copepod community. The influence of environmental forcing (such as long-term warming and decreased NPP) may also be a contributing factor to the long-term reduction in copepod biomass on the Agulhas Bank. An emerging shift towards smaller zooplankton, as observed during this study, will tend to favour sardine over anchovy, since sardine feed on smaller zooplankton prey compared to anchovy (van der Lingen et al., 2009). However, the decline in larger zooplankton contributes to a decline in total zooplankton biomass over time, and hence total food availability for all zooplanktivorous species on the Agulhas Bank, most notably the pelagic fish. A similar outcome is expected to accompany increased warming of the ecosystem in the long term, as copepods have been shown to follow Bergmann's rule, whereby body size decreases with increasing temperature. The long-term ecosystem effects of a warming ocean due to climate change will result in a plankton assemblage dominated by smaller copepods, yielding lower copepod biomass overall, and consequently potentially lower fisheries production as well as carbon sequestration.

References

Blamey, L. K., Shannon, L. J., Bolton, J. L., Crawford, R. J. M., Dufois, F., Evers-King, H., Griffiths, C. L., Hutchings, L., Jarre, A., Rouault, M., Watermeyer, K. E., Winker, H. (2015). Ecosystem change in the southern Benguela and the underlying processes. Journal of Marine Systems, 144, 9–29. https://doi.org/10.1016/j.jmarsys.2014.11.006

Huggett, J. A., Noyon, M., Carstensen, J., Walker, D. (2023) Patterns in the plankton – Spatial distribution and long-term variability of copepods on the Agulhas Bank. Deep-Sea Research II, 208, 105265. https://doi.org/10.1016/j.dsr2.2023.105265

Peterson, W. T., Hutchings, L., Huggett, J. A., Largier, J. L. (1992), Anchovy spawning in relation to the biomass and the replenishment rate of their copepod prey on the western Agulhas Bank. In: Payne, A. I. L., et al. (Eds.), *Benguela Trophic Functioning*, South African Journal of Marine Science, 12, 487–500.

Richardson, A. J. (2008), In hot water: zooplankton and climate change. ICES Journal of Marine Science, 65, 279–295. https://doi.org/10.1093/icesjms/fsn028

Roy, C., van der Lingen, C.D., Coetzee, J.C., Lutjeharms, J.R.E., 2007. Abrupt environmental shift associated with changes in the distribution of Cape anchovy *Engraulis encrasicolus* spawners in the southern Benguela. African Journal of Marine Science, 29 (3), 309–319.

https://doi.org/10.2989/AJMS.2007.29.3.1.331.

van der Lingen, C. D., Bertrand, A., Bode, A., Brodeur, R., Cubillos, L. A., Espinoza, P., Friedland, K., Garrido, S., Irigoien, X., Miller, T., Möllmann, C., Rodriguez-

Sanchez, R., Tanaka, H., Temming, A. (2009), Chapter 7. *Trophic dynamics*. In: Checkley, D., Alheit, J., Oozeki, Y., Roy, C. (Eds.), Climate Change and Small Pelagic Fish. Cambridge University Press.

Verheye, H. M., Hutchings, L., Huggett, J. A., Carter, R. A., Peterson, W. T., and Painting, S. J. (1994), Community structure, distribution and trophic ecology of zooplankton on the Agulhas Bank with special reference to copepods. South African Journal of Science, 90, 154–165.

Investigating the seasonality of an inshore shelf edge upwelling along the Agulhas Current.

S. S. Taukoor [1,2,3], P. Penven[2], I. J. Ansorge[1], T. Mashifane[4]

[1] Department of Oceanography, University of Cape Town, South Africa

[2] Laboratoire d'Océanographie Physique et Spatiale, Université de Bretagne Occidentale, Plouzané, France

[3] Nansen-Tutu Centre for Marine Environmental Research, Department of Oceanography, University of Cape Town, South Africa

[4] Council for Scientific and Industrial Research, South Africa |Southern Ocean Carbon–Climate Observatory, Cape Town, South Africa

Abstract

Seasonal changes in wind patterns, ocean currents, and water temperature can strongly influence upwelling on the inshore edge of western boundary currents. In this study, we investigate the seasonality of Port Alfred upwelling, located on the southeast African shelf, on the inshore edge of the Agulhas Current. Upon analysing the temperature and vertical velocity from varying spatial resolutions of a CROCO model and observational datasets (WOA 2018 and OSTIA), we found a slightly stronger upwelling signature in summer and this was possibly linked to the increasing velocity of the Agulhas current.

1. Introduction

Upwelling on the shelf edge of western boundary currents has been observed to be driven by a combination of several driving mechanisms such as current, wind and eddies (e.g Cabo Frio upwelling along Brazil current (Castelao and Barth, 2005) and upwelling along East Australian current (Roughan and Middleton 2002). Along the coastal zone of the Agulhas current, there are several upwelling sites (e.g Natal Bight upwelling, Port Alfred upwelling, Algoa bay upwelling) and in this study we are investigating the seasonal pattern of the Port Alfred upwelling (see Figure 1).

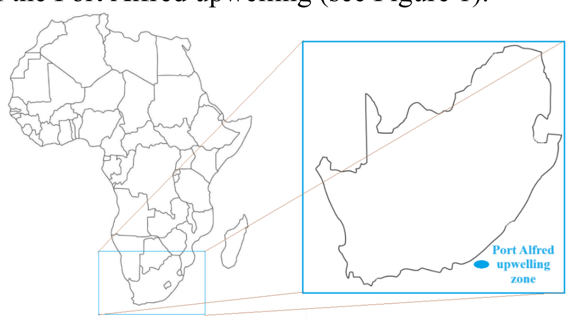

Figure 1: Location of Port Alfred upwelling

There are several possible driving mechanisms which are linked to the Port Alfred upwelling e.g northeasterly wind (Goschen et al, 2012), Agulhas current (Leber et al, 2017), meander events (Leber et al, 2017) and coastal trapped waves (Malan et al, 2013). Hence exploring the seasonality of this upwelling would be beneficial as it would allow us to shed more light on the potential driving mechanisms of this upwelling.

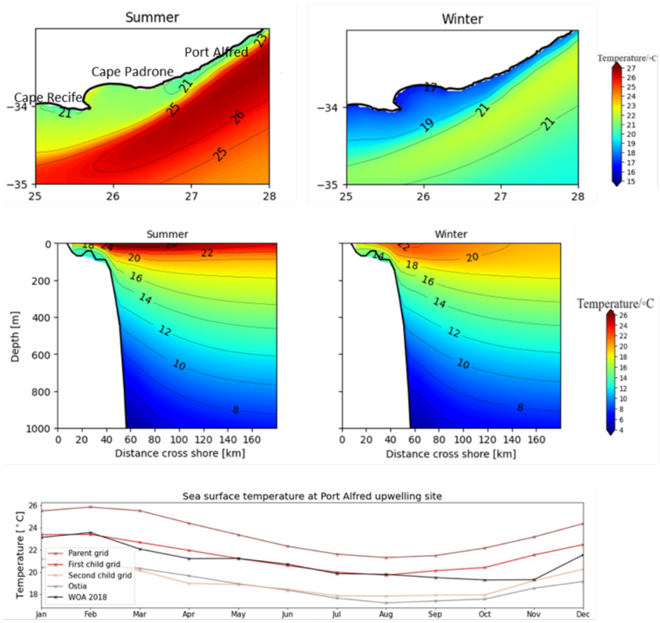

Figure 2: (upper) maps of summer (left) and winter (right) sea surface temperature of the 1/36° (Second child) CROCO grid, (middle) maps of vertical temperature for summer (left) and winter (right) of the 1/36° (Second child) CROCO grid, (lower) monthly mean of sea surface temperature of WOA2018, OSTIA, the 3 CROCO grids: 1/4° (parent), 1/12° (First child) and 1/36° (Second child)

2. Data and method

We computed the temperature and vertical velocity generated from 3 different CROCO grids, the 1/36° grid (~2.5km and 60 vertical levels), 1/12° grid (~7.5km and 60 vertical levels) and the 1/4° grid (22.5km and 60 vertical levels) from Jan 1993 to Dec 2014. We also computed the monthly temperature values from the observational datasets OSTIA and WOA 2018.

3. Results

Temperature

Figure 2 illustrates the sea surface temperature field and vertical distribution for summer and winter. It also shows the climatological monthly mean of temperature in the Port Alfred upwelling zone from the observational datasets of WOA2018 and OSTIA dataset as well as the 1/4° (Parent), 1/12° (First child) and 1/36° (Second child) CROCO grids. In summer, a strong presence of the current was characterized by a temperature of 27°C at the core, and ranging from 25°C to 27°C while the current had weakened in winter, ranging from 21°C to 23°C. In the Port Alfred upwelling zone, the temperatures are much lower at the coast ranging from 17°C to 19°C in winter compared to temperatures ranging from 19°C to 21°C in summer. The vertical temperature also showed that summer displayed a strong presence of the current. From a depth of 100m to the surface, the temperature ranged between 22°C to 26°C in summer while it ranged from 20°C to 22°C in winter. We could observe an isotherm of 10°C on the shelf during summer compared to an isotherm of 14°C in winter. This would indicate a stronger upwelling in summer, possibly due to the current. The climatological monthly mean of each dataset was also computed. Each dataset identified February as the hottest month and August as the coldest one. The maximum difference between the 1/36° CROCO grid and OSTIA was less than 1°C and for most months they displayed relatively the same temperature values, ranging from 17° to 21°C. The WOA2018 and the 1/12° CROCO grid also displayed similar temperature most of the times, but both were at least 2°C hotter than the 1/36° CROCO grid and OSTIA. As for the1/4° CROCO grid, it was likely that it was overestimating the Port Alfred upwelling region with temperatures ranging approximately from 22° to 26°C. On a seasonal scale, while the temperature was colder at the surface in the upwelling zone in winter, this would not necessarily imply that the upwelling had a seasonal signal. Since the vertical structure of the temperature revealed colder isotherms in summer, it was likely that the upwelling triggered by the current was more pronounced in summer.

Vertical velocity

In Figure 3, we plotted the vertical velocity at 100m and the vertical distribution of the vertical velocity for summer and winter. We also plotted the climatological monthly mean of vertical velocity computed at a depth of 100m from the 1/4° (Parent), 1/12° (First child) and 1/36° (Second child) CROCO grid in the Port Alfred upwelling zone. Unfortunately, the vertical velocity did

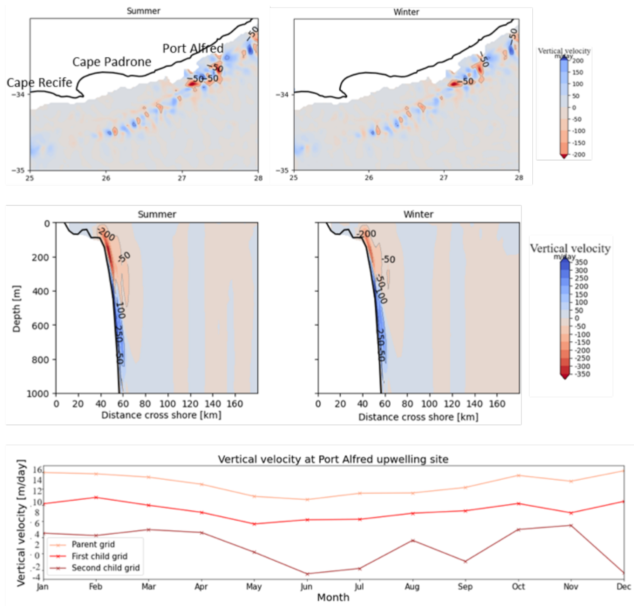

Figure 3: (upper) maps of horizontal section of vertical velocity for summer (left) and winter (right) at a depth of 100m of the 1/36° (Second child) CROCO grid, (middle) maps of cross section of vertical velocity for summer (left) and winter (right) of the 1/36° (Second child) CROCO grid, (lower) monthly mean of vertical velocity at 100m of the 3 CROCO grids: 1/4° (parent), 1/12° (First child) and 1/36° (Second child).

exhibit a considerable noise signal. At a depth of 100m, the signal at the Port Alfred region was marked by high variability upwelling anddownwelling zones ranging from -50 to 50 m/day. On the overall, summer was characterised by stronger upwelling and downwelling compared to winter despite a noisy signal. More distinct downwelling was observed from a depth of 100 to 300m along the continental slope in summer, whereby it reached -200 m/day due to a stronger presence of the current in summer. The presence of upwelling was observed along the continental slope from a depth of 400m to 900m. This strong positive vertical velocity ranging from 50 to 250 m/day in both summer and winter reinforces the hypothesis that throughout the year, upwelling is constantly occurring in the bottom boundary layer due to bottom Ekman veering (Leber et al, 2017). We can observe a slightly stronger upwelling in summer compared to winter. At the continental shelf in the upwelling zone, the variation of the vertical velocity was much smaller whereby the output from 1/36° CROCO grid showed a peak of vertical velocity of 4 m/day in summer and a drop of -4 m/day in winter. The 1/4° and 1/12° CROCO grid showed mostly a positive vertical velocity. However, the 1/4° and 1/12° CROCO grid possibly overestimated the vertical velocity in the upwelling region whereby16 m/day was recorded by the 1/4° CROCO grid and 10 m/day in the 1/12° CROCO grid.

4. Discussion

Investigating the temperature and vertical velocity through its seasonal state revealed that this upwelling was much more complex and there were many forcing mechanisms possibly driving this upwelling. The seasonal state of sea surface temperature showed that the Agulhas Current was generally weaker in winter with a lower temperature of the current's core recorded in winter. As for the vertical velocity, winter was characterized with less downwelling in the Agulhas region compared to summer.

In conclusion, the upwelling seemed to be slightly stronger in summer due to a more intense Agulhas Current. Hence this could reinforce the hypothesis that this upwelling is triggered by bottom Ekman veering. However, we would still require to explore the seasonality of other atmospheric and oceanographic fields in this region for a clearer understanding of its driving mechanisms.

5. Acknowledgements

This study was funded by IRD (ARTS scholarship), SANAP and UCT (Science faculty scholarship)

References

Castelão, R.M., and J.A. Barth. 2006. Upwelling around Cabo Frio, Brazil: The importance of wind stress curl. Geophysical Research Letters 33: L03602.

Goschen, W. S., Schuman, E. H., Bernard, K. S., Bailey, S. E., and Deyzel, S. H. P. (2012). Upwelling and ocean structures off Algoa Bay and the south-east coast of South Africa. African Journal of Marine Science, 34:4(April 2013):37–41.

Leber, G.M., Beal, L.M. and Elipot, S., 2017. Wind and current forcing combine to drive strong upwelling in the Agulhas Current. Journal of Physical Oceanography, 47(1), pp.123-134.

Malan, N., 2013. Driving mechanisms of the Port Alfred upwelling cell inshore of the Agulhas Current (Master's thesis, University of Cape Town).

Roughan, M. and Middleton, J.H., 2002. A comparison of observed upwelling mechanisms off the east coast of Australia. Continental Shelf Research, 22(17), pp.2551-2572.

An evaluation of GLORYS and BRAN ocean reanalysis model outputs on the South African west coast

AM Kupczyk[1,2], T Lamont[1,3,4,5], I Halo[1,5], CS Russo[1]

[1]Oceans & Coasts Research, Department of Forestry, Fisheries and the Environment, PO Box 52126, V&A Waterfront, Cape Town, 8000, South Africa

[2]Department of Conservation and Marine Science, Cape Peninsula University of Technology, District Six, Cape Town, 7925, South Africa

[3]Department of Oceanography, University of Cape Town, Private Bag X3, Rondebosch, 7701, South Africa

[4]Bayworld Centre for Research & Education, 5 Riesling Road, Constantia, 7806, Cape Town, South Africa

[5]Nansen-Tutu Centre for Marine Environmental Research, Department of Oceanography, University of Cape Town, Private Bag X3, 7701, Cape Town, South Africa

Abstract: The Benguela Upwelling System is a highly variable and productive upwelling region. Limited *in situ* ocean observations makes understanding the spatial and temporal variability of physical oceanographic features in this region challenging. Researchers often use ocean reanalysis products to model past states of the oceanographic conditions. This study evaluated the performance of Mercator Ocean's Global Reanalysis (GLORYS) and Bluelink ReANalysis (BRAN) products by comparing them to *in situ* hydrographic data from four Integrated Ecosystem Program cruises, each with four transects, sampled along the South African west coast in 2019. Overall, GLORYS and BRAN reproduced temperature and salinity distributions across all transects reasonably well, supported by strong, positive correlations ($r = 0.80$–0.99; $p = <0.001$) at most stations. GLORYS generally outperformed BRAN, but underestimated upwelling in summer and overestimated it in winter. During summer, GLORYS was 3–6 °C and 0.2–0.4 PSU higher than *in situ* data, but 1–2 °C and 0.1–0.3 PSU lower in winter. BRAN consistently underestimated temperature by 2–5 °C and salinity by 0.2–0.7 PSU during all cruise periods. Both models appeared to perform better subsurface than in the surface, and simulated temperature better than salinity. Model performance appeared to vary with latitude, with generally stronger correlations along the Scarborough transect in the south compared to the Kleinsee transect in the north, especially for salinity. The performance of GLORYS and BRAN highlights the need for refining global models with sub-grid scale parameters and accurate input data for better characterization of upwelling, advection, and mixing rates in this dynamic environment.

1. Introduction

The Benguela Upwelling System (BUS), located off the west coast of Africa, is one of the most productive Eastern Boundary Upwelling Systems (EBUSs) in the world (Lamont et al. 2015). The South African west coast forms part of the Southern Benguela Upwelling System (SBUS) and is associated with intense upwelling events during the austral spring and summer months. These upwelling events occur due to strong southeasterly winds facilitated by the South Atlantic Atmospheric Anticyclone (Lamont et al. 2015, Russo et al. 2022). Enhancing the current understanding of the complex ocean dynamics in this region is important for promoting sustainable management and to mitigate the risks of potential marine disasters such as harmful algal blooms (HABs), among others.

Hydrodynamic models and ocean reanalysis products are valuable tools for studying ocean conditions because they offer a comprehensive simulated view of the ocean state over time periods not possible from available *in situ* observations. However, their global resolution may limit their accuracy in representing regional and local ocean dynamics. Regional oceanographic complexities can also affect their performance (Russo et al. 2022). Global simulations may exclude critical coastal features like tides, local wind forcing, surface waves and the realistic shape of the coastline (de Souza et al. 2021, Russo et al 2022). Therefore, it is important to evaluate their efficiency in simulating regional ocean dynamics, particularly in the context of coastal and shelf ecosystems, such as the SBUS.

Research cruises, while valuable for collecting ocean data, have limited spatial and temporal coverage due to weather constraints and high operational expenses. Therefore, achieving a consistent year-round *in situ* dataset for the South African west coast is a challenge. In contrast, ocean reanalysis products, like Mercator Ocean's Global Reanalysis (GLORYS) and Bluelink ReANalysis (BRAN) offer a cost-effective alternative by having the potential to provide consistent, high-resolution data at various depths and locations. This study evaluated the performance of GLORYS and BRAN by comparing them against cross-shelf *in situ* hydrographic observations taken from four Integrated Ecosystem Program (IEP) research cruises along the South African west coast in 2019.

2. Data and method

Temperature and salinity measurements were obtained from observational datasets collected from Conductivity-Temperature-Depth (CTD) casts during four IEP cruises on the RS *Algoa* in 2019 (1-7 March, 21-26 May, 14-20 August, and 21-27 November). The casts were sampled along four monitoring transects: Kleinsee, Namaqualand, St Helena Bay, and Scarborough (Fig. 1). Version 1 of the GLORYS reanalysis (CMEMS, https://marine.copernicus.eu/) and the 2020 release of the BRAN reanalysis (NCI, https://research.csiro.au/) products were utilized. These products provide daily-averaged simulated data with spatial resolutions of 1/12° and 1/10°, respectively (Russo et al. 2022, Amaya et al. 2023). To perform evaluations, the model outputs from both products were co-located with the *in situ* data in time and space. The analyses included vertical section comparisons, bias analyses, as well as qualitative comparisons of temperature-salinity plots and Pearson's correlation coefficients.

3. Results

Overall, GLORYS and BRAN reproduced temperature and salinity distributions across all transects reasonably well (Fig. 2). This is indicated by strong positive correlations (r = 0.80 to 0.99; $p < 0.001$) between model output and *in situ* data. Since the correlation patterns for temperature and salinity were consistent across all transects and months, Figure 2 illustrates the results of the Kleinsee transect only.

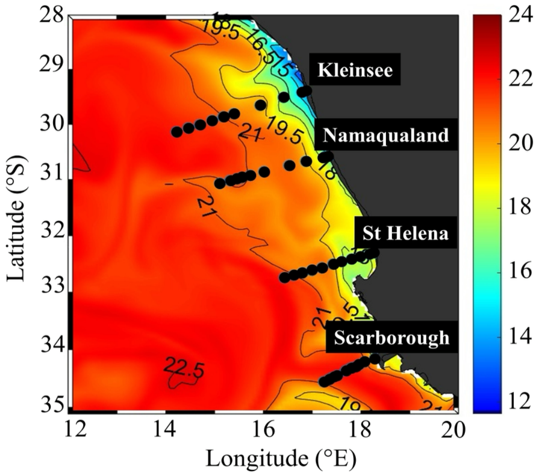

Figure 1: Sea surface temperature (°C) simulated by GLORYS (1 March 2019) to show typical surface temperature distributions off the South African west coast. Black dots indicate CTD stations along the Kleinsee, Namaqualand, St Helena Bay, and Scarborough monitoring transects.

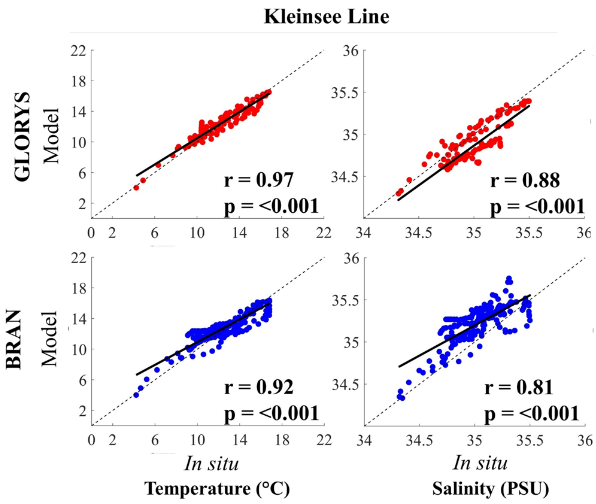

Figure 2: Relationships of temperature (°C) and salinity (PSU) between model-derived data and *in situ* data for August 2019 along the Kleinsee transect. Correlation coefficients (r) and significance values (p) are included.

During summer, GLORYS was 3–6 °C and 0.2–0.4 PSU higher than *in situ* data, but 1–2 °C and 0.1–0.3 PSU lower in winter (Fig. 3). BRAN underestimated temperature by 2–5 °C and salinity by 0.2–0.7 PSU during all cruise periods. This is indicated in Figure 3 where simulated data points for BRAN were consistently lower than the CTD data points. Both models appeared to perform better at deeper depths (roughly indicated by temperature less than 8 °C) than at the surface (Fig. 3), and also simulated temperature better than salinity.

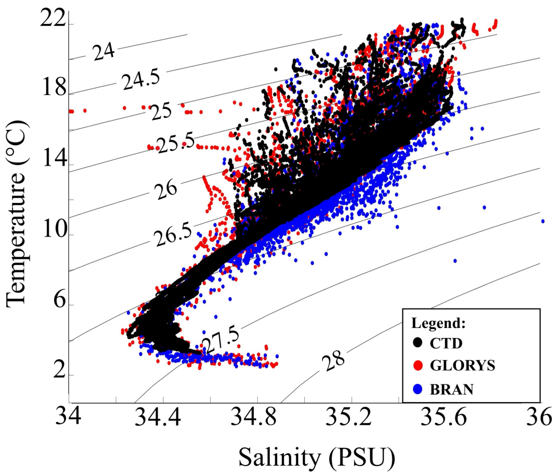

Figure 3: Temperature–Salinity relationship for *in situ* CTD data, and GLORYS and BRAN output for the four cruises in 2019.

4. Discussion

Overall, GLORYS generally performed better than BRAN in reproducing temperature and salinity on the South African west coast. These results align with findings from de Souza et al. (2021) and Russo et al. (2022) where GLORYS (with a slightly higher resolution of 1/12°) had outperformed other reanalysis products such as the Hybrid Coordinate Ocean Model (HYCOM) in simulating major oceanographic features. HYCOM has a similar spatial resolution to BRAN (1/10°). However, it is important to remember that, when compared to *in situ* data from the four cruises, GLORYS did not appear to reproduce realistic seasonal variability, and generally underestimated upwelling in the summer months (March and November) while overestimating it in the winter months (May and August). BRAN on the other hand, consistently underestimated temperatures across all four months, without significant changes in the representation of seasonal patterns.

GLORYS and BRAN are forced by the ERA5 (previously ERA-Interim) and Japanese 55-year (JRA-55) atmospheric reanalysis products, respectively (Lellouche et al 2021, Chamberlain et al. 2021). Rivas and Stofflen (2019) and Taboada et al. (2019) found that ERA5 exhibited better performance compared to JRA55 in EBUS systems. The use of ERA5 by GLORYS could be a possible reason for the model's better performance in simulating coastal upwelling processes compared to BRAN. Similar to the findings of Amaya et al. (2023), both models simulated temperature conditions better than salinity, particularly at the inshore stations closer to the coast. Amaya et al. (2023) also found that GLORYS represented nearshore ocean parameters in the California Current system reasonably well, which is another EBUS with similar marine environmental conditions as the BUS. Similar to the findings in this study, GLORYS also overestimated sea surface temperatures in the California Current system.

In order to continuously gather data and information on the ocean conditions along the South African west coast, ocean reanalysis products offer a valuable alternative to research cruises. However, this study showed similar findings to existing literature that highlights the limitations of model output in the shelf and nearshore regions. Possible reasons for the observed discrepancies include the models' representation of coastal dynamics such as land-sea interactions and nearshore bathymetry. Additionally, the complexity of upwelling processes and the influence of oceanic fronts and jet currents in the shelf and nearshore regions may not be fully captured by the models.

The performance of GLORYS and BRAN in simulating the physical oceanographic behaviour on the west coast emphasises the need to refine global models with finer details, sub-grid scale parameters, and more accurate input data for assimilation. This is important for better model characterisation of upwelling, advection, and mixing rates within this dynamic environment.

References

Amaya, D.J., M.A. Alexander, J.D. Scott, J.D. and M.G. Jacox (2023), An evaluation of high-resolution ocean reanalyses in the California current system. Progress in Oceanography, 210(102951).

de Souza, J.M.A.C., P. Couto, R. Soutelino and M. Roughan (2021), Evaluation of four global ocean reanalysis product for New Zealand waters – A guide for regional ocean modelling. New Zealand Journal of Marine and Freshwater Research, 55, 132-155.

Chamberlain, M.A., P.R. Oke, R.A.S Fielder, H.M. Beggs, G.B. Brassington and P. Divakaran (2021), Next generation of Bluelink ocean reanalysis with multiscale data assimilation: BRAN2020. Earth System Science Data, 13: 5663-5688.

Lamont, T., L. Hutchings, M.A. van den Berg, W.S. Goschen and R.G. Barlow (2015), Hydrographic variability in the St Helena Bay region of the southern

Benguela ecosystem. Journal of Geophysical Research: Oceans, 120(4), 2920-2944.

Lellouche, J., E. Greiner, R. Bourdalle-Badie, G. Garric, A. Melet, M. Drévillon, C. Bricaud, T. Candela, C. Testnut, F. Gasparin, G. Ruggiero, M. Benkiran, Y. Drillet and P. Le Traon (2021), The Copernicus global 1/12° oceanic and sea ice GLORYS12 reanalysis. Frontiers in Earth Science, 9, Article id. 698876.

Russo, C.S., J. Veitch, M. Carr, G. Fearon and C. Whittle (2022), An intercomparison of global reanalysis products for southern Africa's major oceanographic features. Frontiers in Marine Science, 9, Article id. 837906.

Rivas, M. and A. Stoffelen (2019), Characterizing ERA-Interim and ERA5 surface wind biases using ASCAT. Ocean Science Discussions, 15: 831-852.

Taboada, F.G., C.A. Stock, S.M. Griffies, J. Dunne, J.G. John, R.J. Small and H. Tsujino (2019), Surface winds from atmospheric reanalysis lead to contrasting oceanic forcing and coastal upwelling patterns. Ocean Modelling, 133, 79-111.

Eddy variability in the Benguela: A comparative study between the northern and southern Benguela eddy fields

T. Nkadimeng[1], T. Lamont[2,3,4], I. Halo[2,3], C. Russo[2]

[1]Department of Oceanography, University of Cape Town, Cape Town, South Africa

[2]Department of Forestry, Fisheries and the Environment, Oceans and Coasts Research, Cape Town, South Africa

[3]Nansen-Tutu Centre for Marine Environmental Research, Department of Oceanography, University of Cape Town, Private Bag X3, 7701, Cape Town, South Africa

[4]Bayworld Centre for Research & Education, 5 Riesling Road, Constantia, 7806, Cape Town, South Africa

Mesoscale eddies (Agulhas rings) shed from the Agulhas retroflection region transfer warm, salty waters from the southwest Indian Ocean into the southeast Atlantic Ocean. The Indian Ocean properties trapped in these eddies interact with the Benguela region. This study utilises output from an eddy tracking algorithm which was applied to satellite altimetry data to investigate the spatiotemporal characteristics of eddies within the Northern (NB, north of 26°S) and Southern (SB, south of 26°S) Benguela regions from 1993 to 2020. Comparative results between the NB and SB revealed that eddy occurrences in the SB exceeded those of the NB by more than 3.5-fold. Anticyclonic eddies were found to form a in slightly greater proportion in the NB (54% anticyclonic) than in the SB (51% anticyclonic). Eddies in the SB had longer lifetimes, with 41% surviving longer than 7 days and 12% lasting more than 30 days, as opposed to the respective 21% and 6% in the NB. Cyclonic eddies survived longer than anticyclonic eddies in the SB, while an equal number (0.2%) of cyclonic and anticyclonic eddies survived longer than 120 days in the NB. The disproportionate occurrence and longer lifetimes of eddies in the SB relative to the NB indicates greater transport of water properties by eddies around the SB.

1. Introduction

Mesoscale variability more strongly manifests in the form of linear Rossby waves and nonlinear vortices or eddies. Unlike linear waves, nonlinear vortices have the capability to trap and transport momentum, heat, mass, and the chemical components of seawater, thereby playing a role in shaping the general circulation, large-scale water mass distributions, and the dynamics of ocean biology (Robinson 1983).

Development of satellite altimetry has allowed considerable research to be conducted, at global and regional scales, leading to the discovery of eddies as commonly occurring ocean features responsible for a majority of the kinetic energy associated with ocean circulation (Chelton et al. 2011). Eddies can be categorised into warm-core anticyclonic vortices and/or cold-core cyclonic vortices.

The Benguela region considered in this study includes the warm Angola Current System in the north, and the Benguela Upwelling System, and Agulhas Retroflection region in the south. The Benguela eddy field is a complex and dynamic system of mesoscale eddies present in the southeast Atlantic Ocean (Boebel et al. 2003).

The Benguela eddy field has been found to be highly variable with wide ranges of eddy lifespans, amplitudes, horizontal length scales, propagation speeds and travelling distances (Rubio et al. 2009; Bettencourt et al. 2012). Understanding the characteristics, behaviour, and influence of the Benguela eddy field is crucial, not only for comprehending the intricacies of this particular marine environment but also for its broader implications on global ocean circulation and climate processes. The objective of this study was to characterise and compare the distribution and occurrence of eddies between the northern (NB) and southern Benguela (SB).

2. Data and Method

The data used in this study were obtained from the Copernicus marine data store platform (https://data.marine.copernicus.eu/product/SE

ALEVEL_GLO_PHY_L4_MY_008_047). The product contains level-4 processed Absolute Dynamic Topography (ADT) data evaluated from all available altimeter missions and is accessible, in delayed time. The product has global coverage with a spatial resolution of 0.25° and a daily temporal resolution spanning from 1st January 1993 to present day. The variables used in this study were ADT (m), and the zonal and meridional components of absolute geostrophic velocity (m s^{-1}). The period covered in this study spans over 28 years from January 1st 1993 to December 31st 2020.
The automatic hybrid eddy detection algorithm described by Halo et al. (2014) was applied to the satellite altimetry data to identify and characterise eddies in the region of interest. Eddy lifetimes were calculated as the number of days a unique eddy was detected in the time series. Eddies were subsequently split into 3 categories based on how long they survived (≥ 7 days , ≥ 30 days and ≥ 120 days). The eddies in each lifetime category were further classified by spin (anticyclonic and cyclonic). All eddies with vorticities greater than 0 were classified as anticyclonic. Contrastingly, eddies with negative vorticities were classified as cyclonic.
The pathway of each eddy was investigated by tracking the position of its core over the time period that it was detected. The total distance travelled by each eddy was calculated using the Haversine formula. Scatter plots were created using MATLAB, plotting total distance travelled by each eddy with each eddy's mean latitude over its lifetime. MATLAB was used to compute the Pearson correlation coefficient for the relation between eddy total distance travelled and eddy lifetime. To assess the significance of the correlation between the two variables, a t-test was conducted.

3. Results and discussion

A total of 6507 eddies were identified in the NB (Fig. 1), and 1335 of those eddies survived ≥7 days, while 370 eddies survived ≥30 days, and 26 eddies survived ≥120 days. Eddies along the continental slope and in the offshore region decreased in number with increasing lifetime (Fig. 1). The longest lived eddies in the NB occurred in the southern sector and there was a decrease in eddy occurrence towards the equator. Exponential decline in eddy population with increased lifespan was also recorded by Chen and Han (2019). Similarly, Chaigneau et al. (2009) and Halo et al. (2023) also observed an equatorward decrease in eddy abundance. North of 20°S, most of the identified eddies were observed on or just offshore of the continental slope (Fig. 1). These eddies appeared to be distributed in latitudinal bands with alternating favour of cyclonic or anticyclonic eddy spin. Offshore, in the Angola Basin, eddy occurrence was sparse (Fig. 1). This was also observed by Aguedjou et al. (2019).

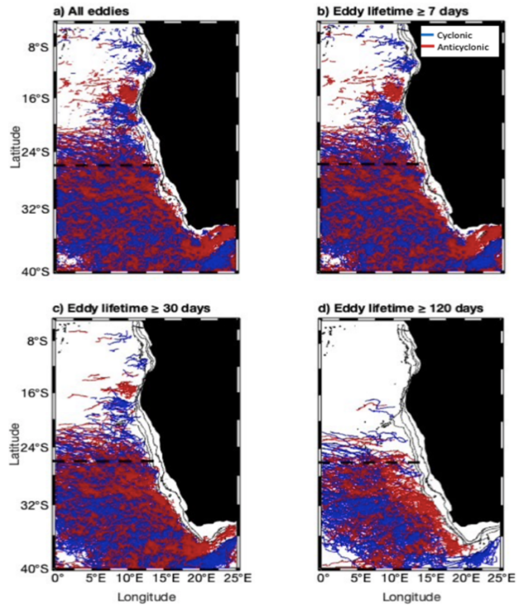

Figure 1: Cyclonic (blue) and anticyclonic (red) eddy trajectories (1 January 1993 to 31 December 2020) in the Benguela Current System. Trajectories for: a) all eddies with varying lifespans, b) eddies with lifespans equal to or greater than 7 days, c) eddies with lifespans equal to or greater than 30 days and d) eddies with lifespans equal to or greater than 120 days. Thin black contours depict isobaths of 200, 1000 and 2000 m. The thick black dashed line represents the latitude of separation (26°S) between the northern and southern Benguela.

In the SB, only 9865 eddies of the total 23 953 eddies survived 7 days or longer. Considerably fewer (2867) eddies survived 30 days or longer when compared to those with lifespans 7 days or less (Fig. 1). This was most evident along the SB shelf which had few eddies survive 30 days or longer (Fig. 1c-d). When observing longer-lived eddies (Fig. 1c-d), it is evident that the SB has a dominance of anticyclonic eddies closer to the shelf, whereas offshore there appears to be a dominance of cyclonic eddies

The occurrence of a greater number of eddies in the SB is likely due to the presence of Agulhas rings into the region. Chaigneau et al. (2009)

attributed the notably high eddy frequency south of 20°S in the Benguela to the north-westward advection of eddies originating from the Agulhas Retroflection. Additionally, Hall and Lutjeharms (2011) found that a majority of cyclonic eddies in the Cape Basin were first detected alongside passing Agulhas Rings.

A majority (62.20%) of eddies in the NB had no displacement, while 30.89 % travelled over 10 km and only 11.42% travelled further than 100 km. In the SB, 61.65% of the eddies travelled further than 10 km and 26.17% travelled further than 100 km. Both cyclonic and anticyclonic eddies showed an increase in distances travelled from 16 to 26°S, but the anticyclonic eddies represented a greater proportion of the eddies that travelled further at these latitudes. South of 30°S, cyclonic eddies were observed to have larger ranges in the distance travelled (Fig. 2). Considering the Benguela overall, there was a statistically significant correlation between eddy lifetime and total distance travelled ($r = 0.92$, $p < 0.001$) suggesting that an increase in eddy lifetime tends to result in an increase in eddy total distances travelled.

The abundance and longer lifetimes of SB eddies suggests a greater distribution of water properties by eddies in the region, particularly through the introduction of Agulhas rings which entrain warmer, more saline waters into the SB. The presence of eddies in these regions plays a role in shaping the general circulation, water mass distributions, and the dynamics of ocean biology.

References

Aguedjou, H. M. A., I. Dadou, A. Chaigneau, Y. Morel, and G. Alory (2019). Eddies in the Tropical Atlantic Ocean and their seasonal variability. Geophysical Research Letters, 46, 12,156–12,164. https://doi.org/10.1029/ 2019GL083925.

Bettencourt, J. H., C. López, and C. Hernández-García (2012). Oceanic three-dimensional Lagrangian coherent structures: A study of a mesoscale eddy in the Benguela upwelling region. Ocean Modelling, 51, pp.73-83.

Boebel, O., J. R. E. Lutjehrams, C. Schmid, W. Zenk, T. Rossby, and C. Barron (2003). The Cape Cauldron: a regime of turbulent inter-ocean exchange. Deep Sea Research Part II: Tropical Studies in Oceanography, 50(1), pp.57-86.

Chaigneau, A., G. Eldin, and B. Dewitte (2009). Eddy activity in the four major upwelling systems from satellite altimetry (1992–2007. *Progress in Oceanography* 83: 117–123.

Chelton, D. B., M. G. Schlax, and R. M. Samelson (2011). Global observations of nonlinear mesoscale eddies. Progress *in oceanography* 91: 167–216.

Chen G, Han G 2019. Contrasting short-lived with long-lived mesoscale eddies in the global ocean. *Journal of Geophysical Research: Oceans* 124: 3149–3167.

Hall, C., and J. R. E. Lutjeharms (2011). Cyclonic eddies identified in the Cape Basin of the South Atlantic Ocean. *Journal of Marine Systems* 85: 1–10.

Halo, I., B. Backeberg, P. Penven, I. Ansorge, C. Reason, and J. E. Ullgren (2014). Eddy properties in the Mozambique channel: A comparison between observations and two numerical ocean circulation models. [Software]. Deep-Sea Research, Part II, *100*, 38–53. Zenodo.

Halo, I., R. P. Raj, A. Korosov, P. Penven, J. A. Johannessen, and M. Rouault (2023). Mesoscale variability, critical latitude and eddy mean properties in the tropical South-East Atlantic Ocean. Journal of Geophysical Research: Oceans, 128, e2022JC019050. https://doi. org/10.1029/2022JC019050.

Robinson, A. R., (1983). *Overview and summary of Eddy Science', Eddies in Marine Science*.

Rubio, A., B. Blanke, S. Speich, N. Grima, and C. Roy (2009). Mesoscale eddy activity in the southern Benguela upwelling system from satellite altimetry and model data. *Progress in Oceanography*, *83*(1-4), 288-295.

Detecting impact of climate extremes on overfishing in African coastal fisheries using satellite data and the ‘ocean triad’ concept: the case of the Angolan sardinella.

Marek Ostrowski[1,2]

[1]Institute of Marine Research and Bjerknes Centre for Climate Research, Bergen, Norway

[2]Nansen-Tutu Centre for Marine Environmental Research Department of Oceanography
University of Cape Town, South Africa

Abstract: Patterns linking reproductive success of small pelagic fishes to climate variability are well-studied in Eastern Boundary Upwelling Systems. The “optimal environmental window” concept (*Cury and Roy*, 1989) has proven to be a strong predictor of reproductive outcomes in Ekman-type upwelling ecosystems. This study examines the climate-fish patterns for Angolan sardinella, whose reproductive success is independent of coastal wind dynamics. Stemming from the “ocean triad” framework, the presented findings suggest that the recent collapse of the Angolan sardinella stock was triggered by the degradation of its reproductive habitat by the intensification of extreme events in the Southeastern Atlantic since 2016.

1. Introduction

Angolan fish landings are dominated by pelagic fisheries, which account for 75 percent of the total catch. Among these, the two small pelagic fishes, the round sardinella (*Sardinella aurita*) and the flat sardinella (*S. maderensis*), comprise the largest proportion of the total pelagic catch by a significant margin. Before 2010, Angolan

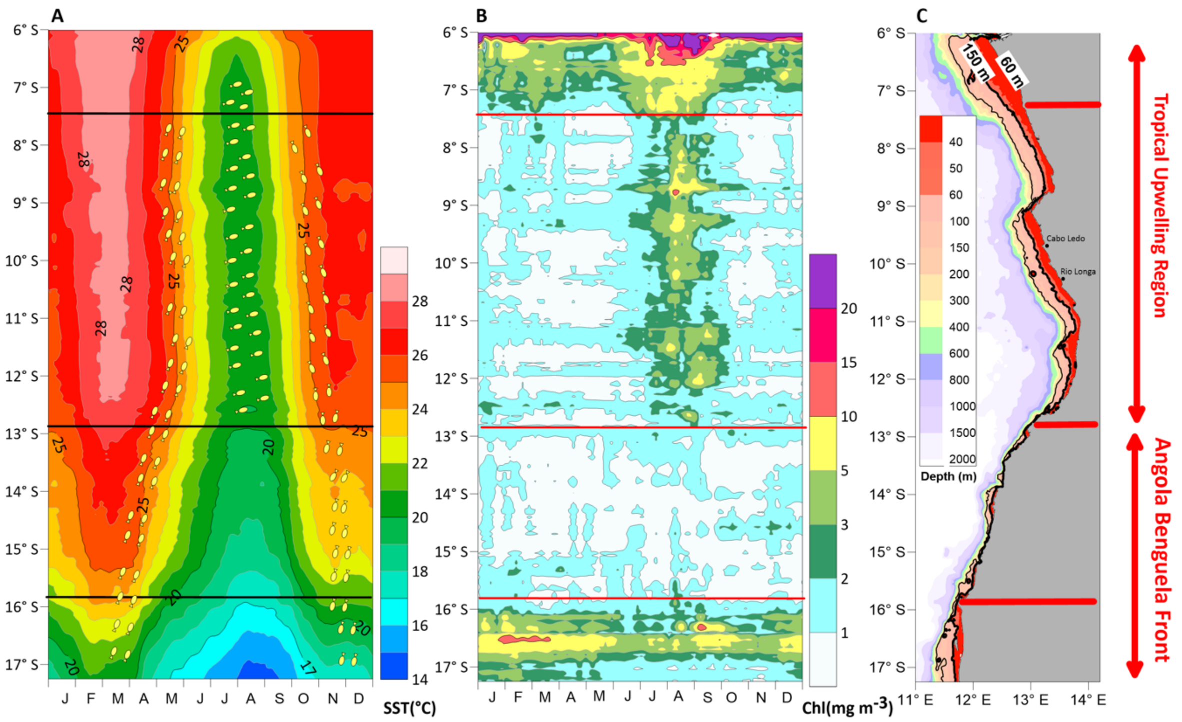

Figure 1. Environmental and bathymetric constraints on the reproductive habitat of sardinella in Angolan waters: **A:** the annual migration cycle of the sardinella spawning stock (yellow symbols) aligns with seasonal warm water intrusions; however, the lethal temperatures limit the survival of their spawning products south of 16°S during JJAS. **C:** 16°S - 13°S, extreme coastal bathymetry limits larval retention year-round in this region. **B,C:** Favourable conditions for reproductive success characterize TUR (north of 13°S) owing to high coastal ocean productivity during JAS, and broad extent of coastal nursery areas (represented by the red bands in C). Data sources: A: SST OSTIA, B: Chl-a OC-CCI climatologies of the first 4 pixels nearest to the coast (~20 km), C: Bathymetry – GEBCO 2022.

sardinella resources have been considered to be at biologically sustainable levels (*FAO*, 2011). The year 2012 began the sardinella peak harvest period. The period from 2012 to 2016 is thought among the most abundant to Angolan fisheries. The shift from sustainable to overexploited sardinella fisheries occurred after 2016.

Prior to the overexploitation period, the sardinella stock consisted of significant proportions of *S. aurita (FAO, 2011)*. This species undergoes large interannual fluctuations in abundance induced by natural environmental variations in their habitat (*Cury and Fontana*, 1988). Global studies on exploited small pelagic fish stocks have shown that moderate fluctuations in natural productivity of these stocks are amplified by fisheries towards major stock collapses (*Essington et al.*, 2015). The Angolan sardinella stock scenario, from sustainable state to overexploitation, was likely to follow a ratchet effect as described by *Ludwig et al.* (1993): the harvesting rates were stable during sustainable resource period. The following good years encouraged additional investment in fleets and processing capacity. When climatic conditions turned unfavourable to natural production *S. aurita*, fishing effort concentrated on *S. maderenisis*, leading to overfishing of both species (*Braham et al.*, 2024).

The natural productivity events of *S. aurita* can be detected from climatic data alone by applying conceptual frameworks linking climate to population variability (*Bakun*, 2010). Results from such detections can be then used as early warnings because grave fisheries-induced effects lag natural productivity fluctuations by 1 to 3 years (*Essington et al.*, 2015).

2. Background and Study Domain

This study compares mean climatic conditions in the reproductive habitat of *S. aurita* across three periods reported in the Angolan sardinella harvest history: the sustainable fisheries (baseline) period before 2010, the plentiful period from 2010 to 2015, and the overfishing period from 2016 to 2023. The aim is to identify whether these configurations indeed favoured reproductive success during the plentiful years and failure during the overfishing period, thereby serving as triggers for socio-economic reverberations according to a ratchet scenario outlined above.

The analysis builds on the 'ocean triad' hypothesis, which assesses reproductive success based on a configuration of three classes of physical processes within the reproductive habitat: enrichment, concentration, and retention (*Bakun*, 2010). The investigation involved several stages: determining the range of successful reproductive habitat (*Planque et al.*, 2007) for *S. aurita* in Angolan waters; identifying the physical processes that combine to stimulate reproductive success within this habitat; deriving climatologies from selected satellite products representing these processes; examining the seasonal evolution of the ocean triad to identify seasons favourable and unfavourable to reproduction; and, finally, comparing the climatologies from the plentiful and overfishing periods to the baseline climatology to determine if the harvest status during these two periods was synchronized with the quality of *S. aurita* reproductive habitat—favourable during the former period and detrimental during the latter.

The successful reproductive habitat of Angolan sardinella is confined to the Tropical Upwelling Region (TUR, 13°S - 7°30'S). Although the migration range of adult *S. aurita* extends across the Angola-Benguela Front (*Boley and Fréon*, 1980), bathymetric and environmental conditions limit the survival of its early-life stages outside of this latitude range (Figure 1).

3. Results

The ocean triad configuration in TUR was found linked to combined forcing of internal solitary waves breaking at tidal frequencies (baroclinic tides), omnipresent on this shelf, and seasonal coastally trapped waves (CTW) remotely forced from the equator (*Ostrowski et al.*, 2009). Nutrient enrichment, planktonic food encounter rates (concentration), and larval retention rates on the daily and weekly timescales are regulated by the levels of baroclinic tide-induced turbulence (*Woodson*, 2018). These turbulence levels depend on background stratification and local bathymetry configuration. A rise in stratification increases the restoring force of an internal wave train. This means more energy is required to induce instabilities and turbulent mixing (*Woodson*, 2018). As a result, there will be generally less nutrient enrichment and smaller planktonic prey encounter rates as the stratification strengthens (*Woodson*, 2018)

CTW propagations modulate enrichment and concentration processes on seasonal and interannual timescales. Upwelling propagations uplift the thermocline which, combined with internal-tide induced mixing, enhances surface cooling and nutrient enrichment in the coastal habitat of sardinella (*Körner et al.*, 2023). Downwelling propagations depress the thermocline beyond the surf zone depth range, suppressing surface cooling and enrichment in

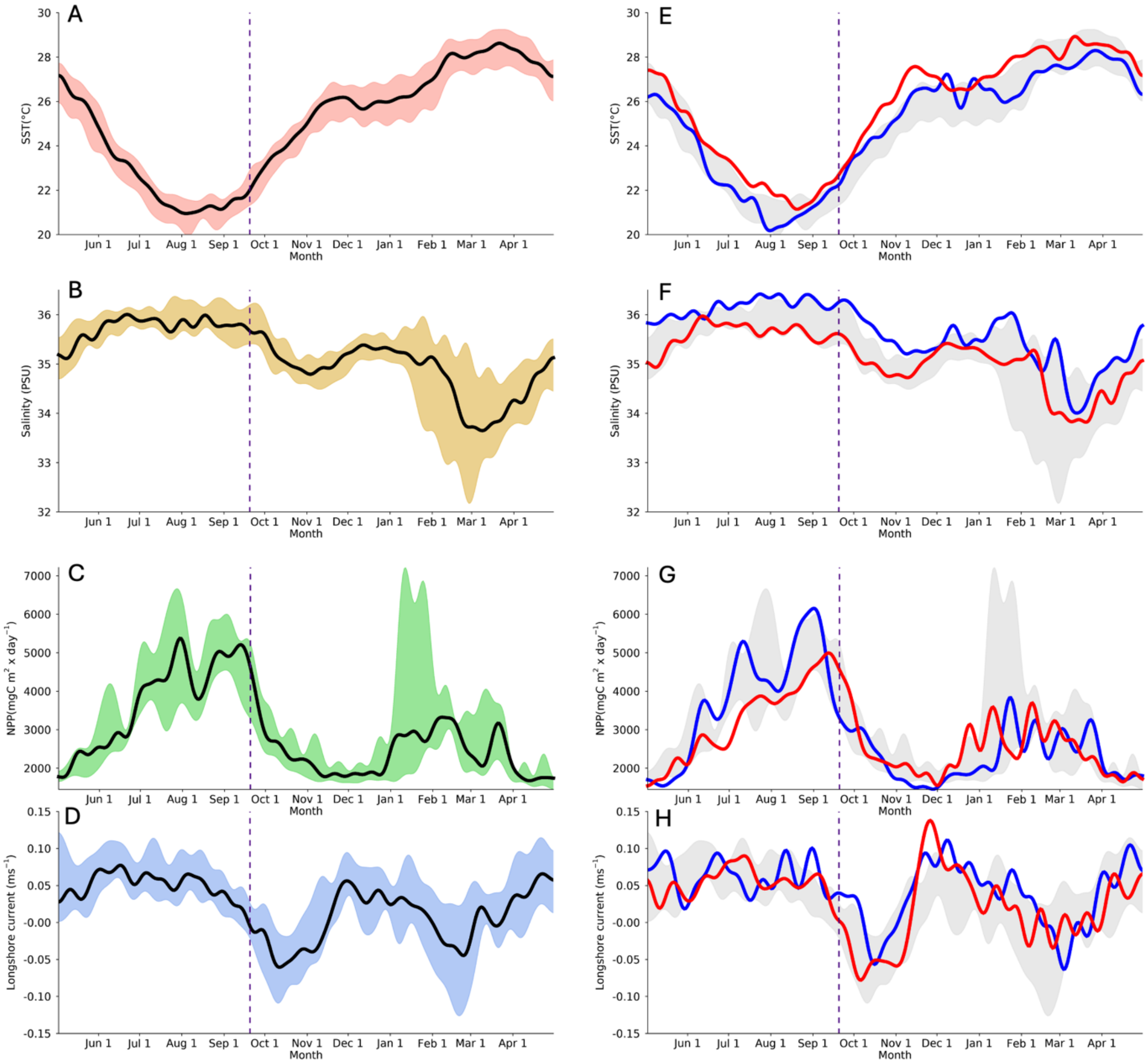

Figure 2. The charts in the left column (A-D) show the median climatologies for the historical period (until 2012). Those on the right (E-H) depict the median climatologies for the plentiful (2010-2015 - blue hued) and overfishing (2016-2023 - red hued) periods. The shaded areas represent the Q1-Q3 (first to third quartile) range of the baseline climatology. The parameters (from top to bottom): SST, SSS, NPP, and Longshore current.

these waters. The accompanying outburst of the poleward current (*Ostrowski*, 2007) reduces the retention of sardinella early life stages in the coastal waters. The associated advection of warm and low-salinity tropical waters increases coastal stratification, reduces turbulence, which in turn lowers the encounter rates of food particles for sardinella early life stages. Furthermore, desalinated and warm waters cue the adult spawning stock of *S. aurita* to migrate away from the affected areas.

The comparative analysis of the ocean triad configuration was performed using the following satellite data products: Sea Surface Temperature (OISST v2.1), Sea Surface Salinity (SMOS), Net Primary Production (Eppley VGPM), and longshore current (GlobCurrent), extracted from the 25 km coastal band nearest to the coast in TUR. The results are shown in Figure 2.

The optimal conditions for reproduction in TUR last from late May to mid-September, characterised by the minimum annual SST (Figure 2A) and peak NPP (Figure 1C), both implying peak annual nutrient enrichment; and favourable retention as the mean coastal current vanishes from the coastal zone (Figure 1D).

The CTW-driven Angolan upwelling subsides by mid-September (*Ostrowski*, 2007). In the coastal TUR, the downwelling season begins, characterized by the rising SST and declining SSS (Figure 1A, B), implying a stronger stratification. The NPP wanes (Figure 1C), caused by reduced enrichment in coastal waters as the depressed thermocline departs seawards. The southward coastal current amplifies, implying enhanced planktonic food dispersion and reduced retention of early life-stages in coastal nurseries. These conditions manifest a highly unfavourable seasonal ocean triad configuration, that persists, apart from a month-long hiatus from December to January, until the end of the austral summer in April.

Figure 2E-H, shows the comparative analysis result. During the plentiful period (2010-2015), oceanographic processes within the sardinella habitat were more favourable to reproductive success than those characterizing the long-term climatology (Figure 2A-D). The opposite relationship characterized the overfishing period, with the reproductive habitat conditions much degraded compared to both the climatology and the plentiful period.

4. Summary and Implications

The above result supports the initial hypothesis that favourable reproductive habitat conditions for *S. aurita* preceded the period of good sardinella harvests from 2012 to 2016, followed by unfavourable conditions that preceded the poor harvest years after 2016. Sustaining steady harvest rates during the transition period from favourable to unfavourable reproductive habitat conditions after 2016 could have potentially initiated the negative socio-economic chain reaction mentioned in the introduction that led to the state of overexploitation, which Angolan fisheries are now facing.

References

Bakun, A. (2010), Linking climate to population variability in marine ecosystems characterized by non-simple dynamics: Conceptual templates and schematic constructs, *J. Mar. Sys.*, *79*, 361-373.

Boley, T., and P. Fréon (1980), Coastal Pelagic Resources, in *The Fish Resources of the Eastern Central Atlantic. Part One: The Resources of the Gulf of Guinea from Angola to Mauritania.*, edited by J. P. Troadec and S. Garcia, pp. 13-76, FAO, Rome.

Braham, C.-B., M. Ahmed-Jeyid, J. Bensbai, F. Ngoum, A. Corten, and J. Gascoigne (2024), Overexploitation of round sardinella may lead to the collapse of flat sardinella: What lessons can be drawn for shared stocks, *Fish Res.*, *269*, 106873.

Cury, P., and A. Fontana (1988), Compétition et stratégies démographiques comparées de deux espèces de sardinelles (Sardinella aurita et Sardinella maderensis) des côtes ouest-africaines, *Aquatic Living Resources*, *1*(3), 165-180.

Cury, P., and C. Roy (1989), Optimal environmental window and pelagic fish recruitment success in upwelling areas, *Can. J. Fish. Aquat. Sci.*, *46*, 670-680.

Essington, T. E., P. E. Moriarty, H. E. Froehlich, E. E. Hodgson, L. E. Koehn, K. L. Oken, M. C. Siple, and C. C. Stawitz (2015), Fishing amplifies forage fish population collapses, *Proc. Natl. Acad. Sci. USA*, *Early edition April, 17*, 1-5.

FAO (2011), *Review of the State of World Marine Fishery Resources Fisheries Technical Paper 335*, FAO, Rome.

Körner, M., P. Brandt, and M. Dengler (2023), Seasonal cycle of sea surface temperature in the tropical Angolan Upwelling System, *Ocean Sci.*, *19*(1), 121-139.

Ludwig, D., R. Hilborn, and C. Walters (1993), Uncertainty, Resource Exploitation, and Conservation: Lessons From History, *Science (New York, N.Y.)*, *260*, 17-36.

Ostrowski, M. (2007), Impact of Equatorial Kelvin waves on aggregation of sardinellas (*Sardinella spp*.) in Angolan waters., *ICES CM, 2007/G:08*, 32 pp.

Ostrowski, M., J. C. B. da Silva, and B. Bazik-Sangolay (2009), The response of sound scatterers to El Nino- and La Nina-like oceanographic regimes in the southeastern Atlantic, *ICES J. Mar. Sci.*, *66*(6), 1063-1072.

Planque, B., E. Bellier, and P. Lazure (2007), Modelling potential spawning habitat of sardine (Sardina pilchardus) and anchovy (Engraulis encrasicolus) in the Bay of Biscay, *Fish. Oceanogr.*, *16*(1), 16-30.

Woodson, C. B. (2018), The Fate and Impact of Internal Waves in Nearshore Ecosystems, *Annual Review of Marine Science*, *10*(1), 421-441.

Low salinity intrusion in Angola Upwelling System and its potential impact on Angola coastal fish habitat.

F. M. Awo[1], M. Ostrowski[2], M. Rouault[1†]

[1]Nansen-Tutu Centre for Marine Environmental Research, Department of Oceanography, University of Cape Town, Cape Town, South Africa

[2]Institute of Marine Research (IMR), Bergen, Norway

[†]Deceased

Abstract: The livelihoods of Angolan coastal communities depend on fishing, which is widely developed along the Angolan coastline and is essential for economic security and employment. However, the abundance of the relevant market fish caught along the Angolan coast is under the influence of freshwater flux characterised by a low salinity, originating from the Congo River outflow and local rainfall. Along the Angolan coast, the northern region often experiences the intrusion of low salinity water from Congo river plume, while the southern region is characterized by higher salinity due to limited rainfall and nearly dry local rivers throughout the year. In this study, we found two types of Benguela Niños that occurred, one in 1995 with low salinity water intrusion on the southern Angolan coast and the other in 2010/2011 without low salinity water intrusion. Although these two types of Benguela Niños are generated by the same remote dynamic process linked to coastal trapped waves, they have different scenarios in terms of freshwater intrusion. These differences in the water column have different effects on ecosystem dynamics, which can be favourable or unfavourable for the fish species caught along the Angolan coast. The intrusion of low salinity water could prompt some fish species to migrate to other regions in search of more favourable conditions for their development or lead to the death of other species with a huge consequence for local coastal communities.

1. Introduction

The tropical Angolan Upwelling System is a very productive marine ecosystem in the southeast Atlantic and serves as the gateway for connecting the equatorial dynamics to the northern Benguela. Fisheries are widely developed along the Angolan shore and are critical for economic security and the employment of local coastal communities. In contrast to the Benguela upwelling system where productivity is sustained by the upwelling favourable winds, the Angolan system is driven by equatorial dynamic forcing that triggers Coastal trapped Waves (CTW) propagating southward along the African coast. However, the abundance of the relevant market fish caught along the Angolan coast is under the influence of low salinity water (Binet et al., 2001) originating from the Congo River run-off located at 6°S, with a maximum discharge into the ocean in early December (Martins & Stammer, 2022). The observed freshwater along the Angolan coast shows a semi-annual cycle, driven by the strengthening of the Angola Current (Awo et al. 2022). Indeed, the Angola Current brings the freshwater from the Congo River plume toward the Angolan coast, leading to a strong vertical stratification, with low-salinity water at the surface above a subsurface salinity maximum. Year-to-year changes of this low salinity intrusion are observed along the Angolan coast, especially during extreme warm events, named Benguela Niños (Martins & Stammer, 2022; Rouault, 2012; Shannon et al., 1986). For a long time, local Angolan fishermen recognized the existence of extreme warm events, but they realized that some events come with low salinity while others may come with high salinity, which define the kind of fish species they catch in abundance. Using reanalysis, this study aims to describe a set of physical conditions characterizing coastal waters during two selected extreme warm events, which may be favourable or unfavourable to fish species.

2. Data and method

For the analysis, we used the GLORYS reanalysis from Copernicus products, which is publicly available at: https://data.marine.copernicus.eu/product/GLOBAL_MULTIYEAR_PHY_001_030/services.

This monthly product covers the tropical Atlantic with a spatial resolution of 1/12° and extends over the period from 1994 to 2019.

3. Results

The Angolan coastal area is divided by 3 zones (North, Center and South). The North and Center zones are characterized by higher rainfall and consequently with perennial discharge rivers throughout the year. The southern zone (Province of Namibe), covered by the Kalahari Desert and closest to the Angolan Benguela front, is characterized by a scarce rainfall with rivers almost dry throughout the year. The low salinity water could therefore be rare in the southern zone, but could appear during extreme events, especially during warm events like Benguela Niños. The Benguela Niños in 1995, 2001, 2016 and 2019, all recorded with low salinity water, while other Benguela Niños in 1997-1998 and 2010-2011 occurred with salty water.

The Benguela Niño in February 1995 was accompanied by a strong intrusion of low-salinity water (Fig. 1a), whereas the Benguela Niño from October 2010 to March 2011 was not associated with any intrusion of low-salinity water in February 2011 (Fig. 1b; Fig. 2). The surface salinity in 1995 was therefore significantly lower than in 2011 (by more than -5 psu) along the Angolan coast (Fig. 2). The salinity anomalies started developing in January 1995, extending southward in the following months, with a depth of range of 20-40m within the mixed layer, until April 1995 when the anomalies disappeared. The anomalies reached their peak in February 1995 coinciding with the semi-annual peak of low salinity intrusion along the Angolan coast (Awo et al., 2022). Contrary to the important changes in the mixed layer salinity related to Benguela Niño in 1995, during the Benguela Niño in October 2010, change in salinity is only concentrated in the northern part of Angolan coast, without any extension toward the southern Angolan coast (Fig. 1b). Both events are due to the strengthening of the Angola Current southward during the propagation of the CTW. Indeed, the CTW has a semi-annual cycle of alternating upwelling and downwelling seasons. The first downwelling occurs in February-March, followed by an upwelling in July–August, and the second downwelling occurs in October-November and ends with a weak upwelling in December–January (Ostrowski et al. 2009).

The Benguela Niño in February 1995 results in the intensification of the primary seasonal downwelling of CTW, which strengthens the Angola Current southward. The Angola Current encounters a huge pool of freshwater in February

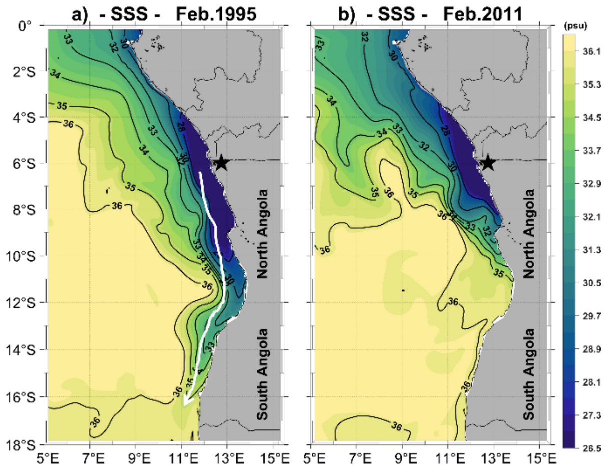

Figure 1: Monthly Sea Surface Salinity (SSS) averaged in February 1995 (a) and in February 2011 (b) using the GLORYS Mercator reanalysis products, with very high resolution (1/12°), over the period 1994-2019. The black star (at 6.2°S, 12° E) represents the position of the Congo River mouth. The white arrow (a) illustrates the trajectory of the low salinity intrusion in Angolan upwelling system.

at the outlet of the Congo River and therefore advects this freshwater of low salinity toward the Angolan coast. However, during the Benguela Niño of October 2010, despite the strengthening of the Angola Current due the prolonged intensification of the secondary annual downwelling of CTW in October, the freshwater pool was less developed off the Congolese coast and therefore could not be much more advected toward the Angola coast. Consequently, the marine ecosystem could react differently to these two coastal habitat conditions (Ostrowski & Bazika-Sangolay, 2015).

Our results suggest a potential growth of relevant market fish species (i.e., Sardinella aurita) in October 2011, as they develop favorably in warm and salty water conditions, while Sardinella aurita species might not have been potentially caught in warm and fresh water in February 1995. Sardinella aurita does not tolerate the habitat with low salinity water (Binet et al., 2001; Ostrowski & Bazika-Sangolay, 2015). The main mechanism that could explain these different scenarios of extreme warm events are the interplayed actions between the strengthening of Angola Current and the significant available flooding of freshwater discharge off the Congolese coast.

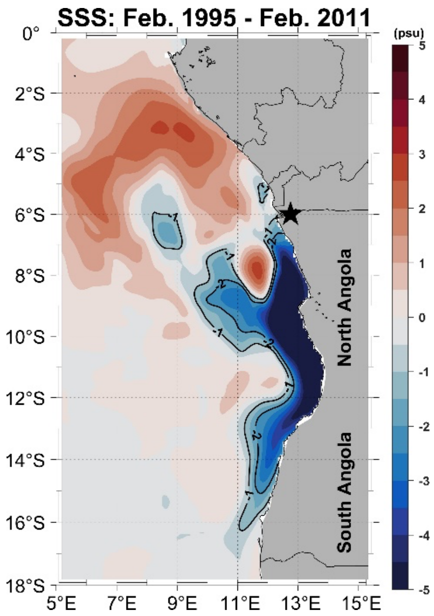

Figure 2: Same as Figure 1, but for SSS in February 1995 (Figure 1a) minus SSS in February 2011 (Figure 1b).

4. Discussion and Conclusion

In this study, we described a set of physical conditions characterizing coastal waters during two selected Benguela Niños, which may be favourable or unfavourable to fish species. Our description is mainly relying on the Angolan current that flows along the coast, the signature of Coastal trapped Kelvin waves through Sea Level Anomalies and the distribution of salinity along the coast. The behavior of the surface salinity during Benguela Niños differs from one event to another. Indeed, some Benguela Ninos were recorded with low salinity water occurrence along the Angolan coast while other warm events occurred with salty water. The Benguela Niño in February 1995 was with a strong intrusion of low salinity while the event in October 2010 was without any intrusion of low salinity in February 2011. Both events are due to the strengthening of the Angola Current related to the CTWs that propagate along the coast. The low salinity advection toward the southern Angolan coast then depends on the amount of fresh water in front of the Congo River plume, which makes the water column specific for each extreme event and therefore a different scenario of marine ecosystem dynamic. Some relevant market fish species such as Sardinella Aurita could migrate to other regions in search of more favourable conditions for their development or lead to the death of other species.

To improve our analysis related to the intrusion of low salinity water, a new high-resolution simulation of the NEMO model that includes coastal processes should be performed to quantify their contributions. As the low-salinity observed along the South Angola coast comes from Congo River plume, additional investigations are needed to better estimate the propagation speed of the low-salinity signal toward southern Angola. A more statistical distribution of fish species during extreme events are needed to improve our analysis related to the potential impact of freshwater salinity intrusion on the Angolan marine ecosystem.

References

Awo, F. M., Rouault, M., Ostrowski, M., Tomety, F. S., Da-Allada, C. Y., & Jouanno, J. (2022). Seasonal cycle of sea surface salinity in the Angola upwelling system. Journal of Geophysical Research: Oceans, 127, e2022JC018518. https://doi.org/10.1029/2022JC018518

Awo, F. M., Alory, G., Da-Allada, C. Y., Delcroix, T., Jouanno, J., Kestenare, E., & Baloïtcha, E. (2018). Sea surface salinity signature of the tropical Atlantic interannual climatic modes. Journal of Geophysical Research: Oceans, 123(10), 7420–7437. https://doi.org/10.1029/2018jc013837

Binet, D., Gobert, B., & Maloueki, L. (2001). El Nino-like warm events in the Eastern Atlantic (6N, 20S) and fish availability from Congo to Angola (1964–1999). Aquatic Living Resources, 14(2), 99-113.

Martins, M. S., & Stammer, D. (2022). Interannual variability of the Congo River plume-induced sea surface salinity. Remote Sensing, 14, 1013.https://doi.org/10.3390/rs14041013

Ostrowski M, da Silva JCB, Bazik-Sangolay B (2009). The response of sound scatterers to El Niño- and La Niña-like oceanographic regimes in the southeastern Atlantic. Ices Journal of Marine Science 66:1063-1072. https://doi.org/10.1093/icesjms/fsp102

Ostrowski, M., & Bazika-Sangolay, B. (2015, July). On physical mechanisms controlling inshore aggregations of small pelagic fish in a tropical upwelling system. In 2015 IEEE/OES Acoustics in Underwater Geosciences Symposium (RIO Acoustics) (pp. 1-7). IEEE. 10.1109/RIOAcoustics.2015.7473621

Rouault, M. (2012). Bi-annual intrusion of tropical water in the northern Benguela upwelling. Geophysical Research Letters, 39(12). https://doi.org/10.1029/2012GL052099

Shannon, L. V., Boyd, A. J., Brundrit, G. B., & Taunton-Clark, J. (1986). On the existence of an El Niño-type phenomenon in the Benguela system. Journal of Marine Research, 44, 495–520. https://doi.org/10.1357/002224086788403105

Simulating the Influence of West African Westerly Jet on Sahel Rainfall

A.I. Makinde[1], B.J. Abiodun[1,2]

[1]Climate System Analysis Group (CSAG), Department of Environmental and Geographical Science, University of Cape Town, South Africa

[2]Nasen-Tutu Research Centre for Marine Environmental Research, Department of Oceanography, University of Cape Town, South Africa

Abstract: Several studies have shown that the West African Westerly jet (WAWJ) transports moisture from the Atlantic Ocean into West Africa and plays a crucial role in Sahel precipitation, but the extent to which the jet is represented in climate models is unclear. This study examines how well the Model for Prediction Across Scales (MPAS), a global climate model with a stretched grid, simulates the WAWJ and its influences on Sahel rainfall. MPAS was used to perform two simulation experiments. In the first experiment, the model was used to simulate the climatology of WAWJ (1984 - 2015) at 60 km horizontal-grid resolution, and the results were compared with the Climate Research Unit (CRU) observation and the European Centre for Medium-Range Weather Forecast (ECMWF) Atmospheric Reanalysis (ERA5) results. In the second experiment, the sensitivity of the simulated WAWJ to changes in model convective parameterization schemes and horizontal grid resolution was tested, focusing on the weak and strong WAWJ years. The results show that MPAS simulates the characteristics of the WAWJ and its moisture transport to the Sahel as in ERA5 results. However, the jet occurs earlier and is stronger in MPAS. The link between WAWJ and Sahel rainfall is also weaker in MPAS. In addition, the location and the drivers of the simulated jet differ from that of the ERA5 results. The changes in convection schemes and horizontal resolution produce no discernible improvement in the simulated jet. Hence, for a better simulation of Sahel rainfall, there is a need to improve the representation of the characteristics and drivers of WAWJ in MPAS.

1. Introduction

West African Westerly Jet (WAWJ) plays a crucial role in West African precipitation. It transports moisture from the oceans to the subcontinent during the peak of the monsoon season (in July-September), when the southerly moisture flux and the flux convergence over the Gulf of Guinea weaken(Omotosho and Abiodun, 2007; Pu and Cook, 2012; Lélé and Leslie, 2016).) The WAWJ moisture transport contributes substantially to the spatiotemporal variation of precipitation over the Sahel (Kidson and Newell, 1977; Cadet and Nnoli, 1987; Fontaine et al, 2003; Gu and Adler, 2004; Pu and Cook, 2012; Lélé et al, 2015) and to the rainfall within the Intertropical convergence zone (ITCZ) rain band along about 10^{o}N and over the West African continent (Fontaine et al, 2003; Gu and Adler, 2004).) Hence, a reliable simulation of rainfall in the Sahel may require adequate simulation of WAWJ. However, there is a dearth of information on how well the contemporary atmospheric models represent the WAWJ and its influence on precipitation over the Sahel.

The use of variable-resolution global climate models (GCMs) is becoming more promising for regional climate studies because of their advantages over regional climate models and high-resolution uniform-resolution GCMs (Fox-Rabinovitz et al, 2008).) The newly evolving Model for Prediction Across Scales (MPAS) is an example of variable-resolution GCM with great potential for simulating the West African climate. However, while some studies have demonstrated the reliability of MPAS in capturing regional-scale processes and high-impact atmospheric features at unprecedented scales (Abiodun et al, 2008; Gu and Adler, 2004; Hagos et al, 2013; Kidson and Newell, 1977; Lélé et al, 2015),2015) there is little or no information on the capability of MPAS in simulating WAWJ and its moisture transport over West Africa. Such information is necessary for improving the weather prediction of rainfall over West Africa.

This study aims to assess the capability of MPAS in simulating WAWJ and its associated moisture transports over West Africa. It will also shed light on the sensitivity of the simulation to horizontal resolution.

2. Methodology

2.1 Data

Climate observation, reanalysis, and model simulation datasets for the period 1985 - 2014 were analyzed over the West African domain. The observational datasets, which include monthly rainfall and near-surface temperature data at a 0.5° x 0.5° grid resolution, were obtained from the Climatic Research Unit (CRU TS v4; hereafter CRU). The CRU dataset was used to evaluate the reanalysis and the model simulation dataset over West Africa. The reanalysis dataset is the 5th generation European Center for Medium-Range Weather Forecast reanalysis (hereafter, ERA5) obtained from the Copernicus Climate dataset website (https://cds.climate.copernicus.eu). The reanalysis datasets contain monthly precipitation, 2-m temperature, zonal and meridional components of the wind, vertical velocity, and geopotential height. The ERA5 reanalysis was used to evaluate how well the model simulates the characteristics of WAWJ and its influence on rainfall variability in the Sahel and West Africa.

2.2 MPAS model description and set-up

MPAS is a non-hydrostatic global atmospheric model that employs a unique variable-resolution grid structure generated by SCVT algorithms (Cadet and Nnoli,1987; Pu and Cook, 2012; Skamarock et al., 2012) The model uses two physics parameterization suites, namely: the convection-permitting suite which is for relatively high spatial resolutions (dx < 10 km), and the mesoscale-reference suite which is for coarser resolutions (> 10 km cell spacing).

The model was used to perform two experiments: climatology and sensitivity-test experiments (see Table 1). The climatology experiment aimed to simulate and evaluate the climatology of WAWJ in MPAS simulations while the sensitivity-test experiment aimed to check the sensitivity of the simulated WAWJ to changes in convection schemes and horizontal resolution. In the climatological experiment, MPAS was used to simulate the global climate at 60 km resolution (1985 - 2014). The simulation started from December 1984 to December 2014; the first-month simulation was discarded as a model spin-up while the remaining 30 years of data were analyzed for the study. The simulation used the mesoscale-reference suite and was initialized with climate variables and forced with 6 hourly SST and sea-ice data from the Climate Forecast System Reanalysis (CFSR).

The sensitivity experiment consists of three simulations. The model set-up for the first simulation (MPAS_CTR) is similar to the climatology simulation, except that it was performed for July-August of six years: 3 strong WAWJ years (1989, 1994, and 1999) and 3 weak WAWJ years (1986, 1990, and 2000), as identified from ERA5 results. The model setup of the second experiment (MPAS_GFC) is the same as that of MPAS_CTR, except that the simulation used the Grell Freitas convection scheme instead of the New Tiedtke. A comparison between MPAS_CTR and MPAS_GFC will reveal the influence of convection schemes on the simulated jet. The third simulation (MPAS_R15) used the same model set-up with MPAS_CTR, but the simulation used the stretched-grid version of the model, in which the model resolution was increased to 15 km over West Africa domain (0^oN - 30^oN and 15^oW - 20^oE) but remained 60 km elsewhere. A comparison between MPAS_CTR and MPAS_R15 will therefore reveal the influence of the increased model resolution on the simulated jet.

Table 1: MPAS model set-up for the climatology and sensitivity test experiments.

Experiment	Convection scheme	Horizontal resolution
Climatology		
• MPAS	New Tiedtke	~ 60 km
Sensitivity Test		
• MPAS_CTR	New Tiedtke	~ 60 km
• MPAS_GFC	Grell Freitas	~ 60 km
• MPAS_R15	New Tiedtke	60 - 15 km

3. Results and Discussion

3.1 Climatology of WAWJ

MPAS gives a realistic simulation of the WAWJ evolution and compares well with the reanalysis (ERA5; Fig. 1a). However, the simulated jet developed faster than the observed (Fig. 1a). Although the simulated and observed jets peak in August, the simulated jet is stronger (> 7.5 ms^{-1}) than the observed (< 5.0 ms^{-1}). The spatial distributions of the WAWJ in MPAS and ERA5 results are similar, but the core of the MPAS jet is located north of the ERA5 and the area coverage is smaller (Fig. 1b). Further analysis revealed that the discrepancies between the MPAS and ERA5 simulation can be linked to the difference in the pressure gradient force associated with the formation of the jet in MPAS and ERA5 (not shown). While ERA5 attributes the formation of the jet to a localized maximum pressure gradient force over the Atlantic Ocean, MPAS attributes it to a strong pressure gradient force over the east coast of West Africa.

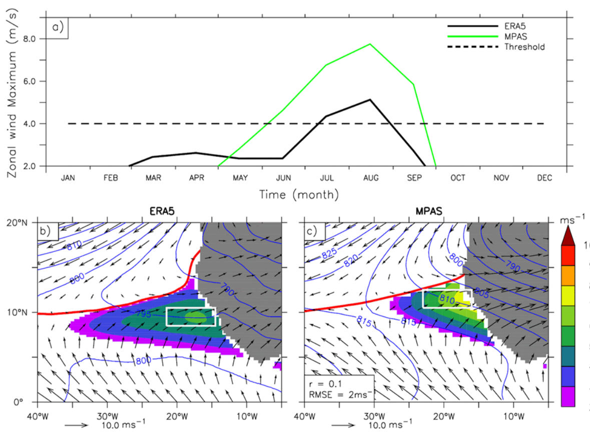

Figure 1: The climatology of WAWJ (1985 - 2014) as depicted by ERA5 and MPAS: (a) the annual cycle of WAWJ with the dashed line marking the threshold for defining the jet mature stage. (b) ERA 5 and (c) MPAS derived spatial distribution of WAWJ (shaded) for August. The white rectangle in (b) and (c) shows the location of the jet core, the blue contours show the 925 hPa geopotential height, the arrows show the corresponding winds and the red line shows the ITCZ.

The MPAS and ERA5 datasets agree on the strong relationship between WAWJ and Sahel precipitation in August (Fig. 2). Both datasets feature positive correlations between WAWJ and precipitation north of 10°N and attribute the positive correlation to moisture transports from the Atlantic Ocean into the continent. This agrees with previous studies that established the link between WAWJ strength and Sahel precipitation. However, the relationship is stronger in ERA5 (r > 0.75) than in MPAS (r = 0.65). This is because the WAWJ moisture flux convergence (over the Sahel) is weaker in MPAS than ERA5, despite stronger moisture transport in the former (Fig 2). Another notable discrepancy between MPAS and ERA5 results is that while ERA5 features weak or no correlation between WAWJ and precipitation South of 10°N, MPAS features a strong negative correlation (Fig. 2).

3.1 Sensitivity of the simulated WAWJ

Figure 3 presents the results of the sensitivity test experiment. The figure shows that changing the convection scheme from New Tiedtke to Grell Freitas does not improve the quality of the simulated WAWJ but it slightly deteriorates (i.e. by changing the correlation between the observed and simulated from 0.0 to -0.1 in the strong WAWJ composite). Note that the poor

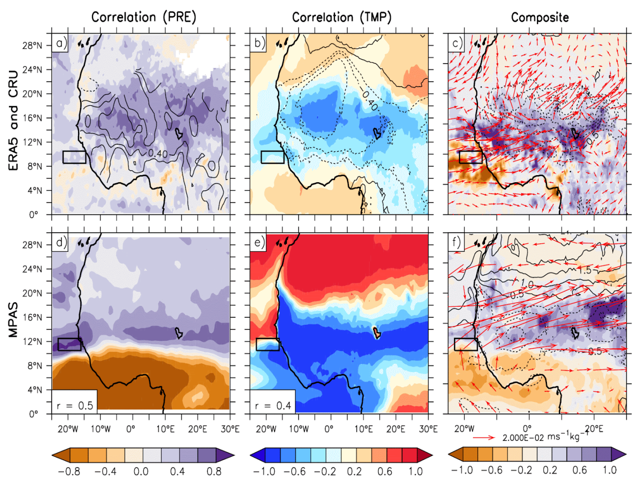

Figure 2: The spatial distribution of the relationship between the interannual variabilities of WAWJ and climate variables (i.e. precipitation and temperature) over West Africa (August 1985 - 2014) as observed in ERA5 and CRU (upper panels) and simulated in the MPAS (lower panels). In panels (a) and (b), the contours show the corresponding CRU results, and in panels (d) and (e), the correlations (r) between simulated and observed patterns are indicated. The left panels show the correlation between WAWJ and precipitation; the middle panels show the correlation between WAWJ and temperature; the right panels show the composites of moisture transport (arrows), precipitation (shaded), and temperature (contour) difference between WAWJ strong years (1989, 1994, and 1999) and weak years (1986, 1990, and 2000) (strong years composite minus weak years composite).

correlation between simulated and observed jets is due to disparity in their spatial location. Increasing the model resolution does not enhance the quality of the WAWJ either, though it slightly improves the correlation between the simulated and observed WAWJ. None of the MPAS simulations in the sensitivity test experiment reproduces localized PGF that induces WAWJ in ERA5 (not shown). Hence, all MPAS simulations attribute the formation of WAWJ to the westward extension of the continental trough, thereby positioning the jet north of the observed position.

Furthermore, the MPAS simulations show no discernible difference in characteristics of the jet during its strong and weak years as identified in the ERA5 dataset. For instance, in ERA5, the spatial coverage of the jet is wider and the jet core is stronger during the strong WAWJ years than during the weak years, because the localized PGF that induces WAWJ is higher in strong years (> 12 m s^{-2}) than in weak years (< 9 m s^{-2}). In MPAS simulations, the spatial structure of the WAWJ does not change because the PGF fields are almost identical in the WAWJ strong and weak years.

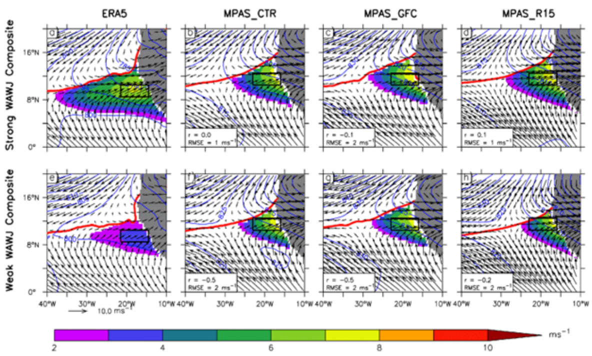

Figure 3: The composites of moisture transport (arrows), precipitation (shaded), and temperature (contour) difference between WAWJ strong years (1989, 1994, and 1999) and weak years (1986, 1990, and 2000) for ERA5, MPAS_CTR, MPAS_GFC, and MPAS_R15.

4.0 Conclusion

This study assessed the performance of the MPAS model in simulating the West African westerly jet (WAWJ) and associated moisture transports. The results of the simulations are compared with the observation (CRU) and reanalysis (ERA5) dataset. We found that MPAS realistically captured some of the evolution and spatial structure of the WAWJ well, but it simulated the jet to be earlier and stronger than the observed jet. It also locates the jet north of the observed location and too close to the coast. Despite these biases, the model still reproduces the observed link between WAWJ and the Sahel precipitation. On the other hand, the simulated WAWJ is neither sensitive to changes in the convection scheme and horizontal resolution made in the study nor to the difference in the WAWJ strong and weak years identified in the ERA5 data.

The results of the study suggest that while the WAWJs in ERA5 and MPAS have a similar influence on precipitation over the Sahel, the jets do not have the same drivers at the synoptic or inter-annual scale. Hence, there is a need for further studies on why the driver of WAWJ differs in ERA5 and MPAS. The results of such studies could improve the seasonal prediction of MPAS over West Africa.

References

Abiodun, B. J., Prusa, J. M., & Gutowski, W. J. (2008). Implementation of a non-hydrostatic, adaptive-grid dynamics core in CAM3. Part I: Comparison of dynamics cores in aqua-planet simulations. Climate dynamics, 31(7-8), 795-810.

Cadet, D. L., & Nnoli, N. O. (1987). Water vapour transport over Africa and the Atlantic Ocean during summer 1979. Quarterly Journal of the Royal Meteorological Society, 113(476), 581-602.

Du, Q., Faber, V., & Gunzburger, M. (1999). Centroidal Voronoi tessellations: Applications and algorithms. SIAM review, 41(4), 637-676.

Fontaine, B., Roucou, P., & Trzaska, S. (2003). Atmospheric water cycle and moisture fluxes in the West African monsoon: Mean annual cycles and relationship using NCEP/NCAR reanalysis. Geophysical Research Letters, 30(3).

Gu, G., & Adler, R. F. (2004). Seasonal evolution and variability associated with the West African monsoon system. Journal of climate, 17(17), 3364-3377.

Hagos, S., Leung, R., Rauscher, S. A., & Ringler, T. (2013). Error characteristics of two grid refinement approaches in aquaplanet simulations: MPAS-A and WRF. Monthly Weather Review, 141(9), 3022-3036.

Heinzeller, D., Duda, M. G., & Kunstmann, H. (2016). Towards convection-resolving, global atmospheric simulations with the Model for Prediction Across Scales (MPAS) v3. 1: An extreme scaling experiment. Geoscientific Model Development, 9(1), 77-110.

Kidson, J. W., & Newell, R. E. (1977). African rainfall and its relation to the upper air circulation. Quarterly Journal of the Royal Meteorological Society, 103(437), 441-456.

Kramer, M., Heinzeller, D., Hartmann, H., van den Berg, W., & Steeneveld, G. J. (2020). Assessment of MPAS variable resolution simulations in the grey-zone of convection against WRF model results and observations. Climate Dynamics, 55(1), 253-276.

Lélé, M. I., & Leslie, L. M. (2016). Intraseasonal variability of low-level moisture transport over West Africa. Climate Dynamics, 47(11), 3575-3591.

Lélé, M. I., Leslie, L. M., & Lamb, P. J. (2015). Analysis of low-level atmospheric moisture transport associated with the West African monsoon. Journal of Climate, 28(11), 4414-4430.

Maoyi, M. L., & Abiodun, B. J. (2021). How well does MPAS-atmosphere simulate the characteristics of the Botswana High? Climate Dynamics, 1-20.

Nicholson, S. E. (2013). The West African Sahel: A review of recent studies on the rainfall regime and its interannual variability. International Scholarly Research Notices, 2013.

Omotosho, J. B., & Abiodun, B. J. (2007). A numerical study of moisture build-up and rainfall over West Africa. Meteorological Applications: A journal of forecasting, practical applications, training techniques and modelling, 14(3), 209-225.

Pu, B., & Cook, K. H. (2012). Role of the West African westerly jet in Sahel rainfall variations. Journal of Climate, 25(8), 2880-2896.

Skamarock, W. C., Klemp, J. B., Duda, M. G., Fowler, L. D., Park, S. H., & Ringler, T. D. (2012). A multiscale nonhydrostatic atmospheric model using centroidal Voronoi tesselations and C-grid staggering. Monthly Weather Review, 140(9), 3090-3105.

Zhao, C., Xu, M., Wang, Y., Zhang, M., Guo, J., Hu, Z., ... & Skamarock, W. (2019). Modeling extreme precipitation over East China with a global variable-resolution modeling framework (MPASv5. 2): impacts of resolution and physics. Geoscientific Model Development, 12(7), 2707-2726.

Fox-Rabinovitz, M., Cote, J., Dugas, B., Deque, M., McGregor, J. L., & Belochitski, A. (2008). Stretched-grid Model Intercomparison Project: decadal regional climate simulations with enhanced variable and uniform-resolution GCMs. Meteorology and atmospheric physics, 100(1), 159-178.

Occurrence of marine heatwaves in the Agulhas bank

D. M. Dimoune[1,2,3], D. Mawren[1], M. Ostrowski[3], M. Rouault[1,2†], I. Ansorge[1,2]

[1] Department of Oceanography, University of Cape Town, South Africa

[2] Nansen Tutu Center for Marine Environmental Research, Department of Oceanography, University of Cape Town, South Africa

[3] Institute of Marine Research (IMR), Bergen, Norway

Abstract: The longest and largest marine heatwave event in the Agulhas Bank (19°E-23°E, 34°S-36°S) is identified and studied using satellite-based high-resolution global optimum interpolation sea surface temperature data and the ERA5 wind velocity and geopotential height, for the period 1982-2022. The result shows that this event occurred from November 2, 2004 to January 19, 2005 and is associated with an anomalous warming offshore of the western part of the Agulhas Bank. The investigation shows that this event is driven by an atmospheric process that induces a heat gain from the ocean and a warming in the Agulhas Bank. Apart from this specific event, the annual mean of marine heatwave metrics over the same period indicates that more frequent and prolonged events are also occurring in the Agulhas Bank region, which may disrupt the marine ecosystem and fisheries, making this area particularly important for future studies.

1. Introduction

Marine heatwaves (MHWs) are the extreme sea surface temperature (SST) events that negatively affect the marine ecosystems and fisheries (Hobday et al., 2016; 2018; Oliver et al., 2017). In recent years, the Agulhas Bank (AB) region, one of the most productive areas in the Southern Ocean (Diver et al., 2012; Brandt et al., 2023), has been experiencing a series of MHW events, which may impact its marine ecosystem, fisheries, and the economy of South Africa (Schlegel et al., 2017a, b). For instance, using in situ data from multiple locations, Schlegel et al. (2017a) demonstrated

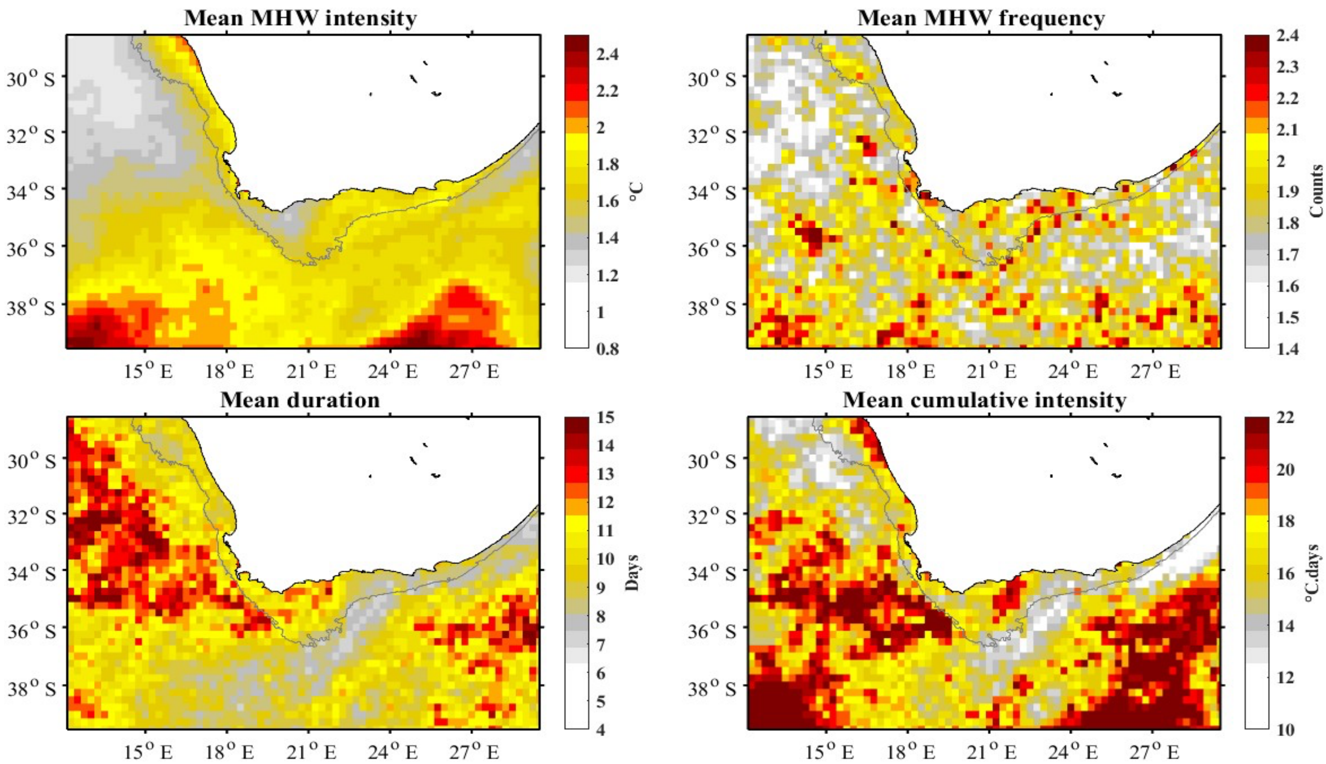

Figure 1: Mean marine heatwaves metrics off South Africa coast. The gray lines on the panels shows the 200-depth isobath.

that MHW events are becoming more frequent in the AB, especially in the western and southern AB, and can occur in any season. Building on this work, Schlegel et al. (2017b) found that these events are driven by both atmospheric and oceanic processes. In this study, our objective to identify all the MHW events in the Agulhas Bank (34°S-36°S,19°E-23°E), using optimum interpolation SST product over the period 1982-2022; and to examine the largest and longest event identified in this timeframe.

2. Data and method

For this study we used:

- the daily optimal interpolated SST from NOAA over the period 1982-2022. The spatial resolution is 0.25° x 0.25° (Kawai et al., 2006).
- ERA5 daily products: the wind velocity at 10-m, and the 850 hPa geopotential. The spatial resolution is 0.25° x 0.25° (Hersbach et al., 2020).

A marine heatwave (MHW) is defined as an anomalously warm event lasting five or more days, with temperatures warmer than the 90th percentile of the climatological value (Hobday et al., 2016) and each MHW can be characterized by their intensity, cumulative intensity and duration. The Matlab detection algorithm is available at: https://github.com/Zijie ZhaoM MHW/m_mhw1.0.

3. Results

The annual mean of MHW metrics off the coast of South Africa (Figure 1) shows intensities between 1.2°C and 2°C in the AB, but lower compared to the region southward in the offshore (Figure 1 top left). In the AB, the highest values of mean duration and mean frequency (14 days and 2 counts, respectively) occur randomly (Figure 1 lower left and upper right, respectively), while the highest values of mean cumulative intensity (>20°C.days) occur in the eastern AB (Figure 1 lower right).

Considering the 4 boxes from Figure 1 of Roy et al. (2007), we computed the linear trend of the mean MHW metric. All boxes show statistically significant positive trends (Table 1). However, the positive trend of the cumulative intensity in the central AB inner region (CABC) is highest (2.33 °C.days) compared to the others.

Table 1: Trends of the MHW metrics (counts, mean intensity, and mean cumulative intensity) in different areas of the Agulhas bank from Roy et al. (2007).

	Count/decade	Mean Intensity/decade	Mean cumulative Intensity/decade
WABC	0.62	0.04 (°C)	2.19 (°C.days)
CABC	0.23	0.08 (°C)	2.33 (°C.days)
EABC	0.41	0.11 (°C)	1.22 (°C.days)
CABO	0.59	0.07 (°C)	1.46 (°C.days)

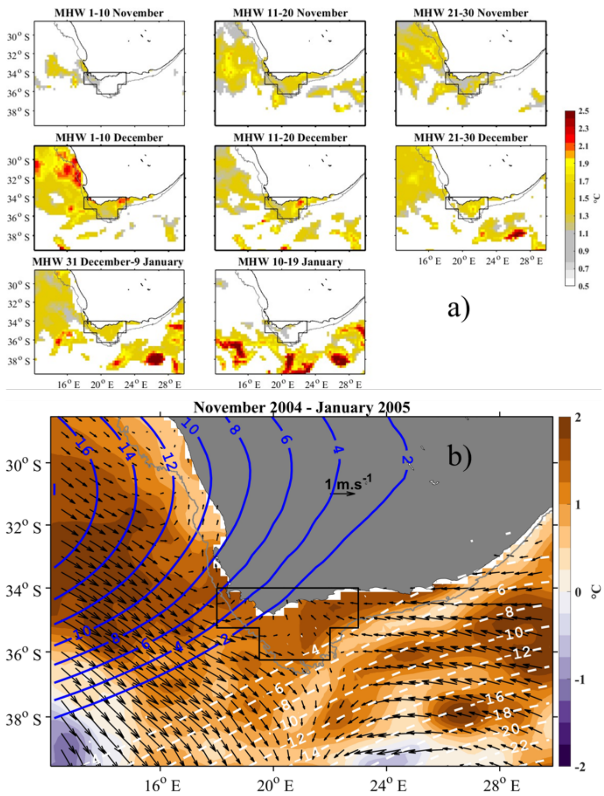

Figure 2: a) 10-days average of marine heatwaves evolution during the November 2004-January 2005 period; b) 850 hPa geopotential height anomaly (blue contour lines and dashed white contour lines for the positive and the negative anomalies, respectively: 2 m contour interval) and 10-m wind anomaly (black arrows) superimposed on the SST anomaly. The external boundaries of the 4 boxes of the Agulhas Bank from Roy et al. (2007) are shown in the black boxes in a) and b). The gray lines on the panels shows the 200-depth isobath.

The longest and largest event in the AB is found from November 2, 2004 to January 19, 2005 (Figure 2a). The warming spreads from the western offshore into the AB (black boxes in Figure 2) and is strong, occupying the entire basin from November 10 to December 20. 2004. From December 21, 2004, to January 19, 2005, the event began to decay until it completely disappeared.

To investigate the mechanism driving this event and the SST anomaly, the 850 hPa geopotential height anomaly and the wind speed anomaly off the coast of South Africa were computed for this period (Figure 2b). The SST anomaly in the basin is shown to be associated with the western offshore warming, while the anomaly in the path of the Agulhas Current is negative. The wind anomaly also shows a weakening of wind speed across the entire basin, particularly in the western part.

4. Discussion

As in previous studies by Schlegel et al. (2017a, b), we found that the Southern Ocean, including the Agulhas bank region, is experiencing recurrent marine heat wave events as a result of global warming (Figures 1 and 2, Table 1). Particularly in this study, we found that the largest and longest event in the Agulhas Bank in the period 1982 to 2022 lasted 71 days and occurred during the austral summer of 2004/2005.

The investigations show that the warmer SST during this period is associated with westerly offshore warming and the southeasterly anomaly of wind speed. The situation corresponds to an atmospheric blocking, indicated by the positive geopotential anomaly over the entire basin, which favors the heat gain in the southern ocean and causes the warming and marine heatwave event on the upper AB (Figure 2b).

References

Brandt, S., Karenyi, N. plus Sink, K., 2023. Macrobenthic fauna of the Agulhas Bank shelf edge, African Journal of Marine Science, 45:4, 265-272, doi: 10.2989/1814232X.2023.2273362

Driver, A., Sink, K.J., Nel, J.L., Holness, S., Van Niekerk, L., Daniels, F., Jonas, Z., Majiedt, P.A., Harris, L. & Maze, K., 2012. National Biodiversity Assessment 2011: An assessment of South Africa's biodiversity and ecosystems. Synthesis Report. South African National Biodiversity Institute and Department of Environmental Affairs, Pretoria.

Hersbach, H., Bell, B., Berrisford, P., Hirahara, S., Horányi, A.,Muñoz-Sabater, J., Nicolas, J., Peubey, C., Radu, R., Schepers, D.,Simmons, A.,Soci,C., Abdalla,S., Abellan,X., Balsamo,G.,Bech-told, P., Biavati, G., Bidlot, J., Bonavita, M., Chiara, G., Dahlgren,P., Dee, D., Diamantakis, M., Dragani, R., Flemming, J., Forbes,R., Fuentes, M., Geer, A., Haimberger, L., Healy, S., Hogan, R.J.,Hólm, E., Janisková, M., Keeley, S., Laloyaux, P., Lopez, P., Lupu,C., Radnoti, G., Rosnay, P., Rozum, I., Vamborg, F., Villaume, S. and Thépaut, J.N., 2020. The ERA5 global reanalysis.Quarterly Journal of the Royal Meteorological Society, 146(730), 1999–2049. https://doi.org/10.1002/qj.3803.

Hobday, A.J., Alexander, L.V., Perkins, S.E., Smale, D.A., Straub, S.C., Oliver, E.C., Holbrook, N.J., 2016. A hierarchical approach to defining marine heatwaves. Progress in Oceanography 141:227–238

Hobday, A.J., Oliver, E.C., Gupta, A.S., Benthuysen, J.A., Burrows, M.T., Donat, M.G., Smale, D.A., 2018. Categorizing and naming marine heatwaves. Oceanography 31(2):162–173.

Kawai, Y., Kawamura, H., Takahashi, S., Hosoda, K., Murakami, H., Kachi, M., and Guan, L., 2006, Satellite-based highresolution global optimum interpolation sea surface temperature data, Journal of Geophysical Research, 111, C06016, doi:10.1029/2005JC003313.

Olivier, E.C.J., Benthuysen, J.A., Bindoff, N.L., Hobday, A.J., Holbrook, N.J., Mundy, C.N. and Perkins-Kirkpatrick S.E., 2017. The unprecedented 2015/16 Tasman Sea marine heatwaves. Nature Communications 8 :1610, https://doi.org/10.1038/ncomms16101

Roy, C., van der Lingen, C. D., Coetzee, J. C., and Lutjeharms, J. R. E. (2007). Abrupt environmental shift associated with changes in the distribution of Cape anchovy *Engraulis encrasicolus* spawners in the southern Benguela, African Journal of Marine Science, 29:3, 309-319, DOI: 10.2989/A JMS.2007.29.3.1.331.

Schlegel, R.W., Oliver, E. C. J.,Wernberg, T., and Smit, A. J., 2017. Nearshore and offshore co-occurrence of marine heatwaves and cold-spells. Progress in Oceanography 151, 189–205. doi: 10.1016/j.pocean.2017.01.004.

Schlegel, R. W., Oliver, E. C., Perkins-Kirkpatrick, S., Kruger, A., and Smit, A. J., 2017. Predominant atmospheric and oceanic patterns during coastal marine heatwaves. Front. Marine Science 4, 323. doi: 10.3389/fmars.2017.00323

Marine Heatwave Characteristics in the South Atlantic and South Indian Oceans

AK Sneddon [1], T Lamont[1, 2, 3, 4], CJC Reason[1], CS Russo[2]

[1]Oceanography Department, University of Cape Town, Cape Town, South Africa

[2]Oceans & Coasts Research Branch, Department of Forestry, Fisheries, and the Environment, Cape Town, South Africa

[3]Bayworld Centre for Research and Education, Constantia, Cape Town, South Afric

[4]Nansen-Tutu Centre for Marine Environmental Research, Department of Oceanography, University of Cape Town, Cape Town, South Africa

Abstract: Marine heatwaves (MHW) are extreme warm water events, and have been shown to cause significant negative impacts on marine ecosystems and economies. Their frequency and intensity are increasing due to climate change. This study compared MHW characteristics in the South Atlantic and South Indian Ocean basins, finding longer durations and higher frequencies in specific regions like the Agulhas Retroflection. On average, MHW lasted longer in the South Atlantic (~30 days) than in the South Indian Ocean (~25 days). Regions like the Agulhas Retroflection and the Brazil-Malvinas Confluence exhibited higher MHW frequency and mean intensity. In the Agulhas Retroflection region, the longest and most intense MHW lasted 87 days with a maximum intensity of 4.6ºC above the 90th percentile threshold. Understanding the MHW characteristics is crucial for improving the ability to adapt and mitigate the effects of these events in the future.

1. Introduction

A marine heatwave (MHW) is defined as a "prolonged discrete anomalously warm water event that can be described by its duration, intensity, rate of evolution, and spatial extent" (Hobday et al., 2016). MHW have been shown to be increasing in frequency and intensity under anthropogenic climate change (Holbrook et al., 2020, Oliver et al., 2018). This will have major implications for ecosystems and the environment (Oliver et al., 2017), making it imperative to understand the characteristics of MHW events.

Up to this point, some work has been done to understand MHW in general and the associated patterns of the oceans and atmosphere around southern Africa (Mawren et al., 2021, Schlegel et al., 2017). While MHW have also been studied in the western South Atlantic (Costa and Rodrigues, 2021), the tropical Indian Ocean (Saranya et al., 2022) in the South Indian Ocean (Azarian et al., 2023) and in the Southern Ocean (Montie et al., 2020, Su et al., 2021), those studies are mostly region-specific, with little work done to compare characteristics of MHW across the ocean basins around southern Africa.

As little is known about MHW in the South Atlantic, South Indian, and Southern Oceans, their potential responses to changing climate conditions are uncertain. This study aims to better understand the characteristics of MHW in and across oceans basins around southern Africa through the analysis and comparison of MHW characteristics in the South Atlantic, South Indian and Southern Oceans.

2. Data and Methods

To identify the characteristics of MHW in the three ocean basins, a MHW MATLAB toolbox (https://github.com/ZijieZhaoMMHW/m_mhw1.0) which detects and analyses MHW events, initially created by Oliver (2016) and adapted by Zhao (2019) was used. It was applied to daily Sea Surface Temperature data from Global Ocean OSTIA Sea Surface Temperature and

Sea Ice Reprocessed (OSTIA) satellite data in the region from 0°S to 55°S and from 50°W to 90°E (for 1992 to 2021). The characteristics extracted for the identified MHW included: the mean frequency (The average count of MHW occurring at a point per year.), mean duration (The mean number of days between the start and end dates of MHW), mean intensity (The mean intensity shows the average temperature anomaly over the duration of events.), cumulative intensity (The integrated temperature anomaly over an event's duration) and the mean number of MHW days per year (The mean number of days over which a MHW occurs in an average year in the region). In addition, a case study was carried out on a small area of interest within the Agulhas Current Retroflection (ACR) region to gain further insight into the MHW that occurred there and their respective characteristics.

3. Results and Discussion

The mean frequency of MHW in the study region ranged from 1 to 3.5 MHW per year (Fig. 1). Figure 1 illustrates that the highest frequencies were observed in the ACR region (between 40ºS to 38ºS and 15ºE to 20ºE), the Agulhas Current (AC) (along the east coast of South Africa), and Agulhas Return Current (ARC) which extends eastward from the Retroflection region. The Antarctic Circumpolar Current (ACC) region, which extends from west to east at approximately 50ºS also exhibited high frequencies of MHW, but more so in the Indian Ocean section than in the Atlantic Ocean section (Fig. 1).

The mean intensity of MHW refers to the temperature in ºC above the 90th percentile threshold for each point, averaged over the time period (Hobday et al., 2016). The mean intensity of MHW ranged from 0.5–4.5ºC above the threshold for each location in the study region (Fig. 1). The highest mean intensity of 4.0–4.5ºC was observed in the region of about 42–44ºS; 22–24ºE, slightly south-east of the ACR region. Higher mean intensities extended eastward into the ARC and also extended southward toward the South West Indian Ridge at approximately 30ºE (Fig. 1).

The AC, ACR and ARC exhibited a distinct pattern of mean intensities ranging from 1.5–3.0ºC above the 90th percentile threshold, with the ARC visible as a band of mean intensities

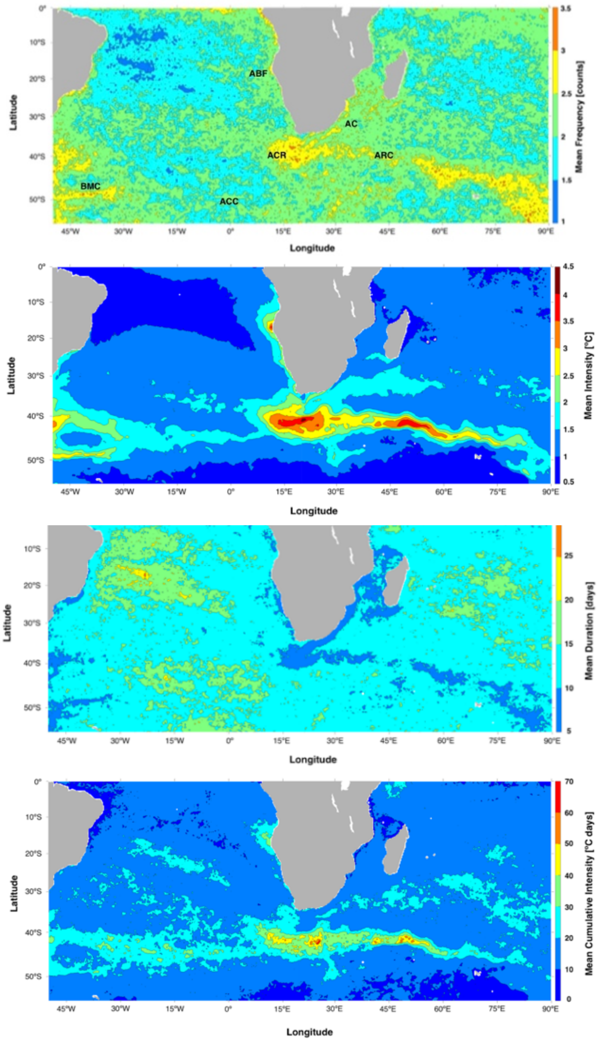

Figure 1: Spatial map showing: (a) the mean frequency of MHW, i.e. the mean number of MHW per year; b) the mean intensity of MHW, measured in ºC above the 90th percentile, for each location over the time period; c) the mean duration of MHW in days in the study region; d) the mean cumulative intensity of MHW in ºC days for the study region.

of 1.5–2.0ºC which extended eastward into the South Indian Ocean (Fig. 1). Evidence of Agulhas Leakage, the flow of warm, salty water from the Indian Ocean into the South Atlantic (Lutjeharms, 2006), is visible in the form of patches of higher mean intensities extending westwards from the ACR into the South Atlantic Ocean (Fig. 1). The region of the Angola-Benguela Frontal (ABF) Zone also exhibited high mean intensities, bulging in a westward direction off the coast.

The mean duration of MHW in the study region ranged from 5 days, the minimum required days for an anomalous heating event to be classified as a MHW, to a maximum of 30 days (Fig. 1). On average, the subtropical gyres exhibited longer durations for MHW than the surrounding ocean regions, with the South Atlantic Subtropical Gyre exhibiting slightly longer mean durations than the South Indian Ocean Gyre (Fig. 1). The MHW with the lowest average durations were observed to occur mostly along the coasts inshore of both the Eastern and the Western Boundary Currents. The AC, ACR, ARC, Benguela Current region and the Brazil-Malvinas Confluence (BMC) regions displayed MHW with low mean durations (<10 days) (Fig. 1).

The mean cumulative intensity, measured in ºC days, refers to the sum of the daily intensities during the MHW (Hobday et al., 2016). The mean cumulative intensity of the study region ranged from 0ºC days to 70ºC days (Fig. 1). The highest mean cumulative intensities were observed at about 43ºS; 26ºE, but there was a band of elevated mean cumulative intensities between 40ºS and 47ºS, from about 10ºE to 60ºE (Fig. 1). There was also a band of moderately high mean cumulative intensities extending southwards from the ACC in the region of the South West Indian Ridge (Fig. 1), as well as in the region of the Angola-Benguela Frontal Zone.

A small region in the ACR was studied in more detail, and a time series analysis was performed to better understand MHW in the region. Figure 2 shows two consecutive MHW that were the second and third longest MHW in this section of the study region, lasting 71 and 70 days respectively. The first event had a maximum intensity of 2.4ºC and a cumulative intensity of 143.1 ºC days, and ended 15 days before the onset of the second event (Fig. 2). The second event had a maximum intensity of 4.1ºC and a cumulative intensity of 195.5ºC days, the second highest cumulative intensity in this region (Fig. 2).

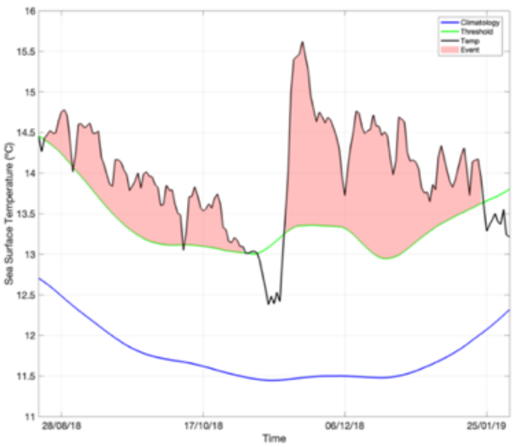

Figure 2: Time series showing the second and third largest MHW events in the Agulhas Retroflection region during the study period, occurring within 15 days of each other.

This study investigated marine heatwaves (MHW) in the South Atlantic, South Indian, and Southern Oceans, analysing their frequency, intensity, and duration. Different ocean regions showed distinct MHW patterns, with boundary currents having more frequent, intense, and shorter MHW compared to Subtropical Gyres. However, a comprehensive understanding requires more detailed analyses of the associated heat budget, occurrence of multiple MHW events, and subsurface data. While some MHW events seemed to be associated with climate modes, further research is needed to understand their drivers and impacts on ocean ecosystems, especially given their projected increase. This underscores the importance of raising awareness about extreme oceanic events alongside terrestrial ones.

References:

Azarian, C., Bopp, L., Pietri, A., Sallée, J. B., d'Ovidio, F. (2023), Current and projected patterns of warming and marine heatwaves in the Southern Indian Ocean. Progress in Oceanography. 215: 103036.

Costa, N.V., Rodrigues, R.R. (2021), Future Summer Marine Heatwaves in the Western South Atlantic. Geophysical Research Letters. 48(22).

Hobday, A.J., Alexander, L.V., Perkins, S.E., Smale, D.A., Straub, S.C., Oliver, E.C.J., Benthuysen, J.A., Burrows, M.T., Donat, M.G., Feng, M, Holbrook, N.J., Moore, P.J., Scannell, H.A., Gupta, A.S., Wernberg, T. (2016), A hierarchical approach to defining marine heatwaves. Progress in Oceanography. 141: 227–238.

Holbrook, N.J., Sen Gupta, A., Oliver, E.C.J., Hobday, A.J., Benthuysen, J.A., Scannell, H.A., Smale, D.A., Wernberg, T. (2020), Keeping pace with marine heatwaves. Nature Reviews Earth and Environment. 1: 482–93.

Lutjeharms, J.R.E. 2006. The Agulhas Current.

Mawren, D., Hermes, J., Reason, C.J.C. (2021), Marine heatwaves and tropical cyclones - Two devastating types of coastal hazard in South-eastern Africa. Estuarine Coastal and Shelf Science. 277(2): 108056.

Montie, S., Thomsen, M.S., Rack, W., Broady, P.A. (2020), Extreme summer marine heatwaves increase chlorophyll-a in the Southern Ocean. Antarctic Science. 32(6): 508–509.

Oliver, E.C.J., Benthuysen, J.A., Bindoff, N.L., Hobday, A.J., Holbrook, N.J., Mundy, C.N., Perkins-Kirkpatrick, S.E. (2017), The unprecedented 2015/16 Tasman Sea marine heatwave. Nature Communications. 8(1):1–12.

Oliver, E.C.J., Perkins-Kirkpatrick, S.E., Holbrook, N.J., Bindoff, N.L. (2018), Anthropogenic and natural influences on record 2016 marine heat waves. Bulletin of the American Meteorological Society. 99: S44–S48.

Saranya, J. S., Roxy, M.K., Dasgupta, P., Anand, A. (2022), Genesis and Trends in Marine Heatwaves Over the Tropical Indian Ocean and Their Interaction With the Indian Summer Monsoon. Journal of Geophysical Research. 127(2).

Su, Z., Pilo, G. S., Corney, S., Holbrook, N. J., Mori, M., Ziegler, P. (2021), Characterizing Marine Heatwaves in the Kerguelen Plateau Region. Frontiers in Marine Science. 7: 531297.

Zhao, Z., Marin, M. (2019), A MATLAB toolbox to detect and analyze marine heatwaves. Journal of Open Source Software, 4(33): 1124.

Marine heatwaves and Warm Events in the Cape Peninsula Upwelling Cell, Southern Benguela

K. Petzer [1,2], T. Lamont[1,2,3,4] and M. Rouault[1,4†]

[1] Department of Oceanography, University of Cape Town, Private Bag X3, Rondebosch, 7701, South Africa.

[2] Oceans & Coasts Research, Department of Forestry, Fisheries and the Environment, PO Box 52126, V&A Waterfront, Cape Town, 8000, South Africa.

[3] Bayworld Centre for Research & Education, 5 Riesling Road, Constantia, 7806, Cape Town, South Africa.

[4] Nansen-Tutu Centre for Marine Environmental Research, Department of Oceanography, University of Cape Town, Private Bag X3, 7701, Cape Town, South Africa.

Abstract: Marine Heatwaves (MHWs) are considered to be one of the emerging threats to marine ecosystems globally. Extreme warm Sea Surface Temperature (SST) anomalies can cause severe ecological impacts. MHWs were identified in the Cape Point Council for Scientific and Industrial Research (CSIR) half-hourly in situ SST, with a focus on MHW duration and maximum SST values as well as a focus on the influence of the wind on the formation and dissipation on MHWs and warm events (WEs). MHWs are defined events in which the SST exceeds the climatological 90th percentile for at least five days, while the WEs events SST values must exceed the climatological 90th percentile for at least three days. The observed average event duration is between 7 to 8 days, but the longest events occurred during periods of decreased upwelling, while the highest maximum SSTs occurred during periods of upwelling dominance. The dominant wind during the formation of MHWs and WEs is a north-westerly wind, indicating the main driver of events at the CSIR Cape Point mooring is the movement of warm water masses to the mooring location. The dominant wind direction at the end of the MHWs and WEs is a south-easterly wind indicating that coastal upwelling limits the duration of warm water events at the Cape Point mooring. MHWs are expected to worsen with climate change by lasting longer with high temperature increases but the projected increase in southeasterly winds could further limit the duration of MHWs in the Southern Benguela Upwelling System.

1. Introduction

Due to global warming, Marine Heatwaves (MHWs) are considered to be one of the emerging threats to marine ecosystems globally (Holbrook et al., 2019). South Africa's fisheries and coastal communities depend on the Southern Benguela's upwelling to sustain the high marine productivity in the region (Kämpf & Chapman, 2016). MHWs are prolonged periods of extreme warm Sea Surface Temperatures (SST) anomalies which could have severe ecological impacts on marine ecosystems by decreasing biodiversity, negatively affecting cold water species, and increasing ocean stratification (Hobday et al., 2016).

2. Data and method

This study examined the Cape Point Council for Scientific and Industrial Research (CSIR) half-hourly *in situ* SST data over 17-years from 2003 to March 2020 to identify MHW events (Figure 1). The fifth generation ECMWF atmospheric reanalysis (ERA5) wind time series, comprised of model and observational data, was also used to determine the influence of wind conditions on the formation and cessation of MHWs.

The MHW events were identified using the Hobday et al. (2016) method, which identifies such an event when the SST exceeds the climatological 90th percentile for at least five consecutive days. Due to the high variability of SST in the Southern Benguela upwelling system, this study also investigated Warm Events (WE) events, which were defined when the SST exceeded the climatological 90th percentile for at least three (but less than five) consecutive days. The duration of MHWs and WEs was computed as the number of days between the start (first day of SST exceeding the 90th climatological percentile) and end (last day of SST exceeding the 90th climatological percentile) of the events. The maximum SST values reached during each of the MHW and WE events was also determined. These parameters were compared across the upwelling (October to March) and non-upwelling (April to September) seasons to determine if there were any seasonal differences in the characteristics of the MHWs and WEs.

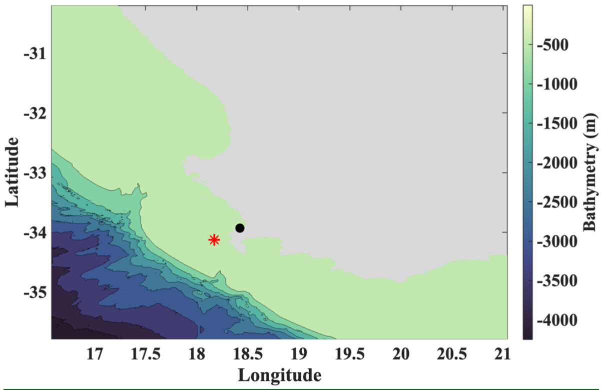

Figure 1. Bathymetric map of the South African coast. The location of Cape Town is indicated by a black circle, while the red asterisk indicates the position of the CSIR mooring 5km off the coast.

3. Results and Discussion

A total of 14 MHWs and 21 WEs occurred over the 17-year period of this study. The average duration of these events was between 7 to 8 days, but the longest events occurred during periods of decreased upwelling (April to September; Figure 2). The non-upwelling season also has more events lasting fewer days than in the upwelling season, with four events lasting three days (Figure 2).

In contrast to the seasonal pattern observed for the duration of MHWs and WEs (Figure 2), the highest maximum SSTs of these events occurred during the periods of upwelling dominance (October to March; Figure 3). The average maximum temperature during the upwelling season is 18°C, which is over 2°C higher than the non-upwelling season (Figure 3).

Of the 14 MHWs and 21 WEs which were identified during the 17-year period, a total of 27 events began with northwesterly winds, while a total of 30 events ended with southeasterly winds.

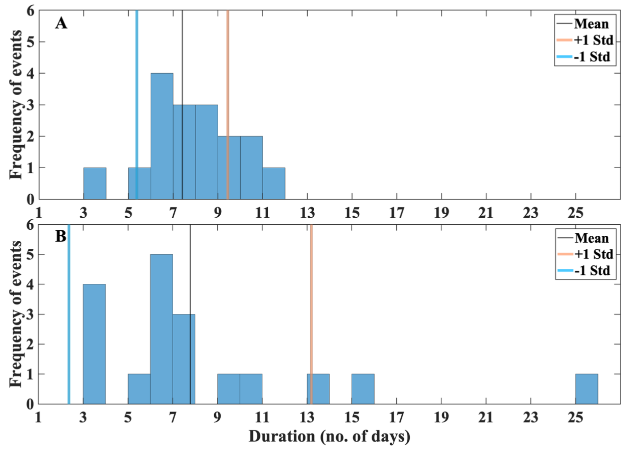

Figure 2. The frequency of the duration of MHWs and WEs per event during the (A) upwelling and (B) non-upwelling seasons with the +1 standard deviation (orange), -1 standard deviation (light blue) and the mean (black) duration indicated.

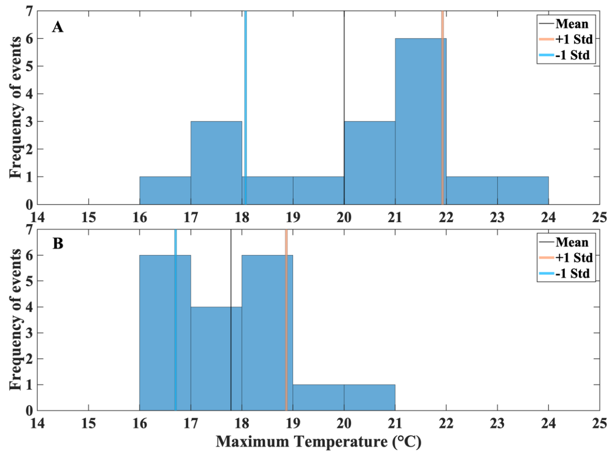

Figure 3. The frequency of MHWs and WEs against the maximum SST (°C) of the events during the (A) upwelling and (B) non-upwelling seasons, with the +1 standard deviation (orange), -1 standard deviation (light blue) and the mean (black) SST indicated.

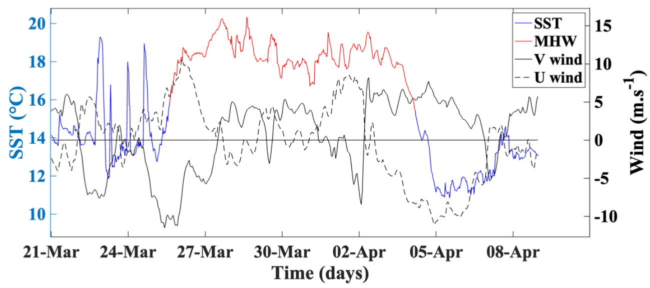

Figure 4. SST (°C) and ERA5 wind speed components (m s^{-1}) from 21 March to 8 April 2014. SST during the MHW is highlighted in red, while SST before and after the MHW is indicated in blue. The V (meridional) component indicates northward (positive) and southward (negative) wind speeds, while the U (zonal) component indicates eastward (positive) and westward (negative) wind speeds.

Figure 4 illustrates an example of such an event. This event lasts more than 10 days, reaches a maximum SST of 20.35°C, and ends with an upwelling event which decreased the SST to 11°C (Figure 4).

The dominance of northwesterly winds during the formation of the MHWs and WEs, suggests that the main driver of these events at the Cape Peninsula Upwelling cell is the movement of warm surface waters from offshore toward the mooring location. As southeasterly winds drive upwelling at this location, the occurrence of these winds at the end of the MHWs and WEs suggests that the onset of upwelling events, together with the offshore transport of upwelled waters, may be an important mitigator of MHWs and WEs. Further research is required to understand the influence of other physical oceanographic forcing mechanisms, such as currents, among others, on the formation and dissipation of MHWs and WEs.

4. Conclusion

MHWs are expected to worsen with climate change by lasting longer with increased peak temperatures. However, numerous studies have demonstrated that there has been a long-term increase in upwelling in the poleward regions of upwelling systems such as the Southern Benguela (Xiu et al., 2018). The associated increase in southeasterly winds has led to an observed decrease, in recent years, in the occurrence of MHWs in the Southern Benguela upwelling system (Holbrook et al., 2019). These findings highlight the need for continued monitoring and more detailed investigations of such events in order to better understand their variability, their driving mechanisms, and their impacts on the ecosystem.

References

Hobday, A.J., Alexander, L.V., Perkins, S.E., Smale, D.A., Straub, S.C., Oliver, E.C., Benthuysen, J.A., Burrows, M.T., Donat, M.G., Feng, M. and Holbrook, N.J. 2016. A hierarchical approach to defining marine heatwaves. *Progress in Oceanography*. 141:227-238.

Holbrook, N., Scannell, H., Sen Gupta, A., Benthuysen, J., Feng, M., Oliver, E., Alexander, L., Burrows, M., Donat, M., Hobday, A., Moore, P., Perkins-Kirkpatrick, S., Smale, D., Straub, S. and Wernberg, T. 2019. A global assessment of marine heatwaves and their drivers. *Nature Communications*. 10(1).

Kämpf, J. and Chapman, P. 2016. Upwelling Systems of the World. A Scientific Journey to the Most Productive Marine Ecosystems. *Springer International Publishing*.

Xiu, P., Chai, F., Curchitser, E.N. and Castruccio, F.S. 2018. Future changes in coastal upwelling ecosystems with global warming: The case of the California Current System. *Scientific reports*. *8*(1):2866.

Origin of the recent warming along the Angolan and Namibian coasts

F.S. Tomety[1], S. Illig[2,1], M. Ostrowski[1,3], F. M. Awo[1], M-L Bachèlery[4], N. Keenlyside[4], and M. Rouault[1]

[1] Department of Oceanography, Nansen Tutu Center, University of Cape Town, Cape Town, South Africa.

[2] Laboratoire d'Etudes en Géophysique et Océanographie Spatiale (LEGOS), CNRS/IRD/UT3/CNES, Toulouse, France

[3] Institute of Marine Research and Bjerknes Centre for Climate Research, Bergen, Norway

[4] Geophysical Institute, University of Bergen and Bjerknes Centre for Climate Research, Bergen, Norway

The Angola and Namibia coastal zones are renowned for their highly productive marine ecosystems. Over the past few decades, these regions have undergone significant long-term changes. This study aims to investigate the long-term in different seasons and explore the underlying processes using a numerical ocean model. The results reveal a clear seasonal dependence in the sea surface temperature (SST) trends along the Angolan and Namibian coasts with alternating positive and negative trends. There is an overall annual warming trend in the modelled SST in the Angola coastal region, with a pronounced warming trend observed during austral summer (November-January) and Autumn (March-May). Conversely, the Namibian coastal region exhibits an overall annual cooling trend in the modelled SST, particularly from austral autumn to earlier spring (February-October). The analysis of the mixed-layer heat budget reveals that the summer warming trend in the Angolan coastal zone is associated with an acceleration of the meridional advection term linked to an intensification of a warm coastal poleward flow and a reduction of cooler coastal equatorial flow into the region. These long-term changes in SST have significant implications for the annual cycle of temperature fluctuations in the Angola region, potentially impacting the local ecosystem.

1. Introduction

The Angola Upwelling System (AUS) and the North Benguela Upwelling System (NBUS) are two highly productive marine ecosystems of the southeastern Atlantic Ocean. They play a crucial role in ensuring food security and supporting the economic livelihoods of local communities (Hutchings *et al.*, 2009; Sowman and Cardoso, 2010). In both systems, coastal upwelling initiates the rise of the thermocline, transporting cold, nutrient-rich water from the deep to the euphotic zone. This process creates an optimal environment for feeding and reproduction of small pelagic fish. However, the availability of these abundant fish stocks is affected by oceanic variability and the effects of climate change. There is therefore an urgent need to improve our understanding of the variability within the AUS and NBUS, to describe their long-term changes and to identify the underlying mechanisms and their potential impact on fisheries. In this study, we investigate the decadal linear trend in AUS and NBUS across different seasons and identify the mechanisms driving these changes.

2. Data and method

The Coastal and Regional Ocean Community model (CROCO, Shchepetkin and McWilliams, 2005; Penven *et al.*, 2006; Debreu *et al.*, 2012) was implemented in this study to produce a multi-decadal (1982-2015) simulation over the tropical Atlantic. With a horizontal resolution of 1/12° and 37 terrain-following vertical levels, the model domain covers 62.25°W-17.25°E and 30°S to 10°N. The bathymetry is derived from the GEBCO database. The model is forced by momentum, heat, and freshwater fluxes derived using bulk formulae based on the daily-averaged surface fields from the DRAKKAR Forcing Set v5.2; the open boundary conditions are from the CARS2009 climatology. The model timestep is 600 seconds. We store 3-day averages of the state variables and surface fluxes, along with daily averages of the Mixed-Layer (ML) heat budget tendencies. This configuration has been successfully used to study Benguela Niños (Illig et al., 2020).

The ensemble-mean of satellite-derived SST data from OISST at 1°×1° and 0.25°×0.25° spatial resolution; and the 1°×1° Hadley SST, is used in this study to validate the decadal linear trend in the model. Classical linear least squares regression method is used to access the linear trend and the non-parametric Mann-Kendall and seasonal Kendall tests are used to estimate statistical significance.

3. Results

3.1. Long-term and climatological SST decadal trends

Figure 1 shows the observed and modeled long-term trends in SST at both annual (**Fig.1a**) and seasonal (**Fig.1b and c**) scales. The observations exhibit a mean warming trend larger than 0.1°C per decade (°C/dec) along most parts of the Angolan and Namibian coasts. Southern Angola, between 12°S and 17°S, undergoes the largest warming trend over the 1982-2015 period (>0.25°C/dec). The southern Namibian coastal region (22°S-25°S) only shows a weak warming trend of less than 0.05°C/dec.

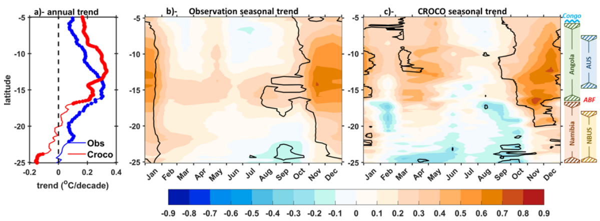

Figure 1: Linear trend (in °C/dec) of the SST averaged within the 1°-wide coastal fringe along the Angola-Namibia coast over the period 1982-2015. (a) Annual long-term SST trends. (b, c) Hovmöller diagrams of the monthly climatological decadal linear SST trends for the observations and CROCO, respectively. Dashed contours indicate statistically significant values at the 95% confidence level, from Tomety et al. [submitted].

At the seasonal scale (**Fig.1b**), the observed SST trend along the Angolan and Namibian coasts exhibits a clear seasonal dependence with alternating positive and negative trends. Our observational dataset highlights a statistically significant warming trend during the austral spring and summer (September-January), with a peak exceeding 0.8°C/dec at 14°S in November-December in the Angola Benguela Front (ABF). In contrast, the rest of the year experiences a moderate coastal cooling trend of up to -0.2°C/dec, except in the ABF zone where a warming trend persists throughout the year. Along the coasts of Angola, the pronounced warming trend in austral spring/summer underlies the overall annual warming trend reflected in the annual observed SST trend (**Fig.1a**). Contrastingly, south of 19°S, the counterbalance of the austral winter cooling trend and the spring/summer warming trend in the southern Namibian coastal zone results in the very weak annual trend of the observed SST.

A comparison between the SST long-term trend in CROCO and in the observations (**Fig.1a**) reveals that CROCO reproduces well the annual warming trend in the Angolan and North Namibian coastal region (North of 20°S) with a maximum value of +0.33°C/dec at 13°S. However, the model fails to capture the weak positive trend along the south Namibian coast, instead showing a cooling trend up to -0.16°C/dec south of 20°S, in agreement with Vizy *et al.* (2018). On a seasonal scale (**Fig.1c**), the model successfully reproduces the strong warming trend in the austral spring/summer and the cooling trend in the winter along both the Angolan and the Namibian coasts. However, CROCO overestimates the warming trend in March-April off Angola and the cooling trend in the Namibian coastal region. This results in an overall annual cooling trend in the model south of 20°S (**Fig.1a**). Possible explanations for this bias in the model include unrealistic acceleration trends in equatorward coastal winds, which would lead to excessive upwelling and evaporation, and to stronger equatorward horizontal currents advecting cold water northward. These discrepancies between model and observations could also be attributed to the coarse resolution of satellite data, which struggles to accurately capture the coastal upwelling (García-Reyes *et al.*, 2015; Carr *et al.*, 2021). Despite these differences, the good agreement between the modeled and observed SST trends at the seasonal scale gives confidence on the use of the CROCO outputs to unravel the mechanism responsible for the decadal climatological changes in SST observed along the Angolan and Namibian coasts. This is done in the following sections.

Processes driving the Mixed-Layer Temperature (MLT) trend

We examine the potential drivers of the decadal climatological trend of the MLT and analyze the monthly decadal trend of each term of the monthly ML heat budget. We found that the long-term summer warming along the Angola Namibia coast is mainly due to the decadal changes of the coastal horizontal advection during spring and earlier summer (not shown). Similarly, the demise of the long-term summer warming is mainly due to the increase of the horizontal advection cooling. A decomposition of the horizontal advection into its zonal and meridional components shows that the positive and negative trends of horizontal advection during the austral spring and summer (not shown) are predominantly driven by the trends in the meridional advection process (not shown), which is attributed to the modulation of the Angola Current and Benguela current. We, therefore, analyze the monthly trend of the horizontal coastal currents along the coast of Angola and Namibia

Role of the horizontal current evolution in the seasonal trend.

The current averaged in the ML shows a distinct seasonal pattern (**Fig.2a**), which is particularly pronounced along the coastal region of Angola. The meridional component of the coastal currents in the AUS flows southward in January-February and August-October, and reverses to north during the rest of the year, reaching intensities of up to 18 $cm.s^{-1}$. The southward flow is strong in August-October with maximum values up to 16 $cm.s^{-1}$ in September, while it is weaker in January-February with values less than 6 $cm.s^{-1}$. In the ABF region, the meridional current flows consistently southward throughout the year, with two maxima. The first peak, with intensities up to 14 $cm.s^{-1}$, is observed in February, while the second maximum, with values up to 28 $cm.s^{-1}$, is prominent in September-October. Further south, in the NBUS region, the current maintains a northwestward flow throughout the year, with maximum values up to 14 $cm.s^{-1}$ in austral winter. The monthly decadal trend analysis of the horizontal ML currents (**Fig.2b**) shows that the southward current in the AUS has intensified up to 3 $cm.s^{-1}$/dec in September-October over the last three decades. Conversely, the northward current has weakened by 2.5 $cm.s^{-1}$/dec in November, both contributing to the AUS warming trend in austral spring. Similarly, in the austral summer, the northward current has strengthened by up to 4 $cm.s^{-1}$/dec in December-January and the southward current has weakened up to -3 $cm.s^{-1}$/dec in February. During the austral winter, the AUS northward current has increased by up to 4 $cm.s^{-1}$/dec.

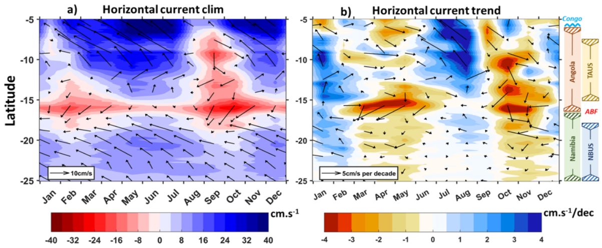

Figure 2: Hovmöller diagram of: a) climatological horizontal current averaged in the ML ($cm.s^{-1}$, arrows) and its meridional current ($cm.s^{-1}$, shading). b) same as (a) but for the monthly decadal trend from the surface to 250 m depth, (right panel) the corresponding trend ($cm.s^{-1}$/dec).

4. Discussion

In this study, we analyzed the climatology of the long-term changes of the upper layer temperature in the productive marine ecosystems of the southeastern tropical Atlantic off Angola (AUS) and Namibia (NBUS). We investigated the main processes responsible for these changes based on the analysis of the ML heat budget from a ~9 km resolution regional ocean model over the period 1982-2015. Our results revealed a clear seasonal dependence of the decadal SST trends in the first 100 km (1° band along the coast) along the Angolan and Namibian coasts. The overall annual warming trend in the AUS is mainly the result of a pronounced warming trend in late austral spring and summer (October-January), with no significant change observed in austral winter and autumn (February-September). In contrast to the AUS, the weak annual trend in the NBUS results from a counterbalance of the austral winter cooling trend and the austral summer warming trend.

On the analysis of the processes driving the long-term surface temperature changes, our results showed that, whilst the AUS and the NBUS undergo different dynamics, their climatological long-term trends are driven by the same process, i.e. the horizontal advection. The latter controls the monthly climatological decadal warming trend of the austral spring and summer ML in the AUS. It also controls the austral summer ML warming trend and the late austral winter and spring cooling trends in the NBUS.

We further disentangled the role of currents vs. horizontal gradients in the contribution of zonal and meridional advections. Our analyses showed that, in both regions, the changes in the horizontal advection are primarily attributed to changes in the coastal currents. In the AUS, the warming trend of the MLT in austral spring and early summer, followed by its demise in late austral summer, can be attributed to the southward intensification of the Angola Current. This current brings warm water from the equator into the region in austral spring and early summer, while the northward intensification of the reverse Angola Current in late austral summer contributes to the dissipation of this warming trend. Similarly, in the NBUS, the warming trend of the MLT during the austral early summer can be attributed to a weakening of the northwestward Benguela Current, which brings cold water from the south into the NBUS region.

References

Debreu, L., P. Marchesiello, P. Penven, and G. Cambon (2012), Two-way nesting in split-explicit ocean models: Algorithms, implementation and validation, *Ocean Modelling*, *49*, 1-21.

Carr, M., T. Lamont, and M. Krug (2021), Satellite Sea surface temperature product comparison for the Southern African marine region, *Remote Sensing*, *13*(7), 1244.

García-Reyes, M., W. J. Sydeman, D. S. Schoeman, R. R. Rykaczewski, B. A. Black, A. J. Smit, and S. J. Bograd (2015), Under pressure: Climate change, upwelling, and eastern boundary upwelling ecosystems, *Frontiers in Marine Science*, *2*, 109.

Hutchings, L., C. Van der Lingen, L. Shannon, R. Crawford, H. Verheye, C. Bartholomae, A. Van der Plas, D. Louw, A. Kreiner, and M. Ostrowski (2009), The Benguela Current: An ecosystem of four components, *Progress in Oceanography*, *83*(1-4), 15-32.

Illig, S., M. L. Bachèlery, and J. F. Lübbecke (2020), Why do benguela Niños lead atlantic Niños?, *Journal of Geophysical Research: Oceans*, *125*(9), e2019JC016003

Penven, P., L. Debreu, P. Marchesiello, and J. C. McWilliams (2006), Evaluation and application of the ROMS 1-way embedding procedure to the central California upwelling system, *Ocean Modelling*, *12*(1-2), 157-187.

Shchepetkin, A. F., and J. C. McWilliams (2005), The regional oceanic modeling system (ROMS): a split-explicit, free-surface, topography-following-coordinate oceanic model, *Ocean modelling*, *9*(4), 347-404.

Vizy, E. K., K. H. Cook, and X. Sun (2018), Decadal change of the south Atlantic Ocean Angola–Benguela frontal zone since 1980, *Climate Dynamics*, *51*, 3251-3273,

Characterisation of Late 2019 Marine Heatwaves and Extremes Sea Levels in the Gulf of Guinea

Franck Eitel Kemgang Ghomsi[1,2], Daneeja Mawren[1], Roshin P. Raj[3], Antonio Bonaduce[3], Babatunde J. Abiodun[1,4], Folly S. Tomety[1], Founi M. Awo[1], Djiorka M. Dimoune[1], Graham D. Quartly[5]

[1]Nansen-Tutu Center for Marine Environmental Research, Dept of Oceanography, University of Cape Town, South Africa.

[2]Geodesy Research Laboratory, National Institute of Cartography, P.O. Box 157, Yaoundé, Cameroon3

[3]Nansen Environmental and Remote Sensing Center and Bjerknes Center for Climate Research, Bergen, Norway

[4]Climate Systems Analysis Group, Department of Environmental and Geographical Science, University of Cape Town, Cape Town, South Africa

[5]Plymouth Marine Laboratory, UK

Abstract: The Gulf of Guinea (GoG) is a vital marine ecosystem located between the Mauritanian-Senegalese and Namibian Boundary upwelling systems. Despite its ecological importance, the region faces challenges from environmental changes, including marine heatwaves and rising sea levels. In late 2019, unprecedented positive sea surface temperature (SST) anomalies occurred, coinciding with significant sea level anomalies (SLA). This study examines these phenomena using data from 1993 to 2021. The analysis reveals a pronounced Marine Heatwave (MHW) event from October 2019 to March 2020, with a peak in severity in February 2020. At the same time, Extreme Sea Level (ESL) events show variability, with significant increases observed along the Equator and coastlines. The discussion underscores the interconnected nature of oceanic processes in the GoG and highlights the urgency of integrated coastal risk management and climate adaptation strategies to enhance resilience in the face of ongoing environmental changes.

1. Introduction

Nestled between two of the world's most important upwelling systems, the Mauritanian-Senegalese and Namibian Boundary upwelling systems, the Gulf of Guinea (GoG) is a vast area of marine richness and ecological importance (Fig. 1). As a large marine ecosystem (LME), the GoG serves as a crucible of biodiversity and productivity, and exerts a profound influence not only on the coastal states that border it, but also on the dynamics of the global ocean (Wiafe et al., 2016; Ghomsi et al., 2024a). Encompassing the coastal areas of West Africa, the GoG is a nexus of ecological diversity and socio-economic vitality.

Its strategic location places it at the confluence of major oceanic currents, including the Guinea Current, which flows eastward along the coast, driving coastal upwelling and high primary productivity (Wiafe et al., 2016; Alory et al., 2022). This complex web of oceanic forces supports thriving fisheries and the livelihoods of millions of people along its shores. The GoG's ecological importance extends beyond its borders, contributing to the broader dynamics of the Atlantic Ocean and beyond. As

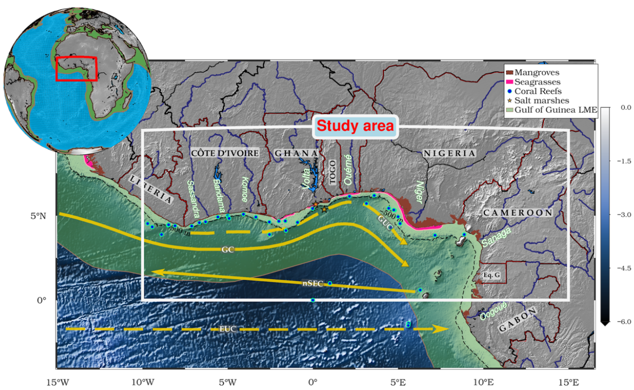

Figure 1: The Gulf of Guinea LME encompasses four key ecological niches namely seagrasses, mangroves, salt marshes, and coral reefs (see legend). Annotation used: EUC – Equatorial Undercurrent, Eq.G – Equatorial Guinea, GC – Gulf of Guinea Current, GUC- Gulf of Guinea Undercurrent, nSEC – north South Equatorial Current. Major rivers are labeled in light green. The dashed line represents the 500m isobath. The inset shows the location of the GoG LME along the African continent.

a transition zone between the nutrient-rich upwelling systems to the north and south, the GoG serves as a crucial corridor for marine species migration and nutrient transport (Hardman-Mountford and McGlade, 2002). Its role in regulating regional climate patterns underscores its importance, with effects reaching far inland and influencing weather patterns across the African continent. However, the GoG is not immune to the forces of environmental change. As global temperatures rise and anthropogenic pressures increase, the GoG faces growing challenges, including the spectre of rising sea levels and marine heat waves (MHWs), defined as temporary periods of exceptionally high ocean temperatures that can have severe and long-lasting effects on the structure and function of marine ecosystems (Hobday et al., 2016). In late 2019, unprecedented positive Sea Surface Temperature (SST) anomalies were reported, marking the most prominent anomalies in the last three decades over the tropical Atlantic (Richter et al., 2022). A notable positive sea level anomaly (SLA), which is characterized by the propagation of coastal trapped waves over the GoG, coexisted with these anomalies. This research aims to understand the drivers and characterise the mechanisms that lead to marine heatwaves and compound effects in the GoG (Ghomsi et al., 2024b). By bridging the gap between scientific research and practical application, our study aims to highlight the importance of monitoring oceanic drivers to effectively inform policy-making and empower stakeholders to safeguard the future of this invaluable marine ecosystem in the face of ongoing global warming and increasing frequency of extreme events.

2. Data and method

2.1. Data

To detect MHWs and their main characteristics (frequency and total days), we used a daily gridded high-resolution (0.05° × 0.05°) SST dataset from the Copernicus Marine Environment Monitoring Service (CMEMS) website. This dataset, from 1 January 1982 to 31 December 2021, is freely available on the following website: (https://resources.marine.copernicus.eu/?option=com_csw&view=details&product_id=SST_GLO_SST_L4_REP_OBSERVATIONS_010_011). This product merges different satellite sensors and in situ observations to produce daily gap-free SST maps. The CMEMS SST reprocessed (REP) global dataset provides a reliable and consistent long-term SST time series for the GoG, produced for climatic applications. To quantify sea level variability, daily gridded SLAs were extracted from the CMEMS (https://doi.org/10.48670/moi-00148[1]). This dataset covers the period 1993–2022, with a horizontal spatial resolution of 1/8° x 1/8°. This product is a combination of several altimeter missions (Jason-3, Sentinel-3A, HY-2A, Saral/AltiKa, Cryosat-2, Jason-2, Jason-1, T/P, ENVISAT, GFO, ERS1) (Pujol et al., 2016).

2.2. Methods

To identify MHWs and extreme sea level (ESL) events in the GoG using daily SST and SLA datasets from 1993 to 2021, we followed the definitions outlined by Hobday et al. (2016). All MHW characteristics, including frequency, total number of days, duration, mean intensity, cumulative intensity and maximum intensity, were examined. These were compared to a 29-year baseline climatology (1993-2021). The use of a seasonally varying 90th percentile threshold allowed us to identify MHWs across all seasons, not just the summer months. The equations describing the primary characteristics of MHWs are detailed by Hobday et al. (2016). As elucidated by Darmaraki et al. (2019), each MHW event is delineated by its start and end dates, denoted by the mean and maximum intensity in degrees Celsius (i.e., the mean and maximum SSTs relative to the 90th percentile during the event's duration in days), with the same approach employed for the SLA. Cumulative MHW intensity, quantified in degrees Celsius days, reflects the summation of daily SSTs relative to the 90th percentile during the event's duration, as elucidated by Darmaraki et al. (2019). Following this methodology, annual statistics were calculated, which include the annual frequency of MHW events. The total number of MHW days per year serves as a metric to identify temporal variations in the frequency of MHW events at each grid point, according to the metrics outlined by Hobday et al. (2016).

[1] Accessed November 2023

3. Results

The monthly evolution of MHWs and ESL events, characterized above the 90th percentile from October 2019 to March 2020, is illustrated in Fig. 2. Initiation of the MHW (Fig. 2a) in November 2019 is observed in the Northern GoG (outlined in black), persisting until December 2019 with temperatures hovering around 1°C. Subsequently, temperatures peak at 1.5°C one month later, intensifying further to 2°C by February 2020, reaching a maximum severity across the basin, with a widespread MHW above 1.25°C. By March 2020, the MHW tends to dissipate, with temperatures stabilizing around a dominant mean state of 1°C.

As known, during MHWs, abnormal increases in SSTs lead to thermal expansion of seawater, resulting in a rise in sea levels, referred to as a positive SLA. This phenomenon is often observed concurrently with increased SSTs during MHW events. The warming of surface waters during MHWs not only contributes to higher SSTs but also exacerbates thermal expansion, further elevating sea levels in affected regions.

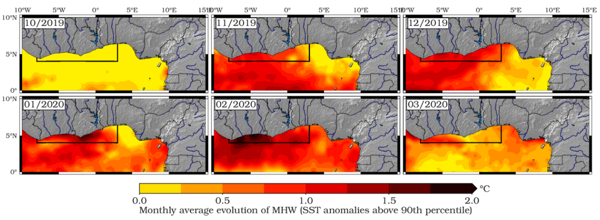

(a)

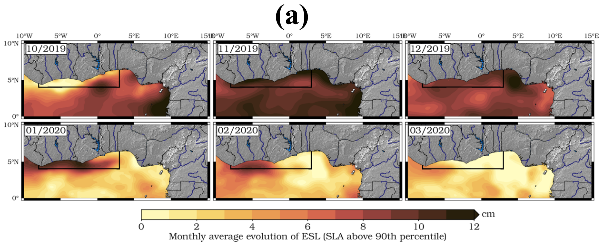

(b)

Fig. 2 : Monthly average evolution of (a) ESL and (b) MHW events over the Northern GoG from Oct 2019 to Mar 2020.

Fig. 2b illustrates the ESL over the GoG during the Late 2019 Atlantic Niño event. From October 2019 to March 2020, the ESL varied from 0 to 12 cm, with a significant rise observed in October 2019 along the Equator at (0°, 9°E), peaking at 12 cm. Between November 2019 and February 2020, this rise propagated westward along the coast, persisting for two months off the coast of Côte d'Ivoire, before dissipating later in March 2020. Interestingly, the ESL tends to exhibit a slight delay compared to the onset of MHWs. However, a good synchronization is observed between the establishment of MHWs and ESL events in the GoG.

4. Discussion

The co-occurrence of MHW and ESL events in the GoG highlights the interrelated nature of oceanic processes and their impact on coastal regions. MHWs, characterised by prolonged periods of elevated SST, can trigger seawater thermal expansion, contributing to positive SLAs during extremes. These anomalies exacerbate the effects of ESL events, increasing coastal flooding and erosion along the GoG's vulnerable coastlines. In modulating the intensity and duration of MHW and ESL events in the GoG, the underlying physics of ocean dynamics play a critical role. Characterised by a coastal upwelling system, the GoG influences SST patterns by bringing cooler, nutrient-rich waters to the surface. Changes in the intensity or frequency of upwelling can disrupt thermal gradients and SST distributions (de Coëtlogon et al., 2023), increasing the likelihood of MHWs and their associated impacts on SLAs. In late 2019, during the period of the MHW and ESL events in the GoG, significant flooding was recorded on land due to extreme precipitation coinciding with the West African monsoon rains, resulting in intense rainfall over coastal regions (Padi et al., 2021), leading to widespread inundation and displacement of populations. The synergy between extreme rainfall events and sea-level rise further exacerbated the flooding impacts, highlighting the complex interactions between atmospheric and oceanic processes.

In conclusion, the co-occurrence of MHW, ESL events and extreme precipitation during the West African monsoon rainy season underscores the interconnected nature of climatic and oceanic processes in the GoG. By addressing the underlying drivers of these events and implementing proactive adaptation measures, we can increase the resilience of coastal regions to future climate variability and extremes.

References

Alory, G., Da-Allada, C. Y., Djakouré, S., Dadou, I., Jouanno, J., & Loemba, D. P. (2021). Coastal upwelling limitation by onshore geostrophic flow in the Gulf of Guinea around the Niger River plume. Frontiers in Marine Science, 7, 607216.

Darmaraki, S., Somot, S., Sevault, F., Nabat, P., Cabos Narvaez, W. D., Cavicchia, L., ... & Sein, D. V. (2019). Future evolution of marine heatwaves in the Mediterranean Sea. Climate Dynamics, 53, 1371-1392.

de Coëtlogon, G., Deroubaix, A., Flamant, C., Menut, L., & Gaetani, M. (2023). Impact of the Guinea coast upwelling on atmospheric dynamics, precipitation and pollutant transport over southern West Africa. Atmospheric Chemistry and Physics, 23(24), 15507-15521.

Ghomsi, F. E. K., Mohamed, B., Raj, R. P., Bonaduce, A., Abiodun, B. J., Nagy, H., ... & Johannessen, O. M. (2024a). Exploring steric sea level variability in the Eastern Tropical Atlantic Ocean: a three-decade study (1993–2022). Scientific Reports, 14(1), 20458.

Ghomsi, F. E. K., Raj, R. P., Bonaduce, A., Halo, I., Nyberg, B., Cazenave, A., ... & Johannessen, O. M. (2024b). Sea level variability in Gulf of Guinea from satellite altimetry. Scientific Reports, 14(1), 4759.

Hardman-Mountford, N. J., & McGlade, J. M. (2002). 5 Variability of physical environmental processes in the gulf of guinea and implications for fisheries recruitment. An investigation using remotely sensed SST. In Large Marine Ecosystems (Vol. 11, pp. 49-xxviii). Elsevier.

Padi, M., Foli, B. A. K., Nyadjro, E. S., Owusu, K., & Wiafe, G. (2021). Extreme rainfall events over Accra, Ghana, in recent years. Remote Sensing in Earth Systems Sciences, 1-12.

Pujol, M. I., Faugère, Y., Taburet, G., Dupuy, S., Pelloquin, C., Ablain, M., & Picot, N. (2016). DUACS DT2014: the new multi-mission altimeter data set reprocessed over 20 years. Ocean Science, 12(5), 1067-1090.

Richter, I., Tokinaga, H., & Okumura, Y. M. (2022). The extraordinary equatorial Atlantic warming in late 2019. Geophysical Research Letters, 49(4), e2021GL095918.

Wiafe, G., Dovlo, E., & Agyekum, K. (2016). Comparative productivity and biomass yields of the Guinea Current LME. Environmental development, 17, 93-104.

Long term trends and spatial variability of surface hydrographic parameters around the broader Prince Edward Islands region.

T Toolsee[1], T Lamont[1,2,3,4]

[1] Marine Research Institute and Department of Oceanography, University of Cape Town, Cape Town, South Africa

[2] Department of Environment, Forestry and Fisheries (DEFF), Cape Town, South Africa

[3] Nansen–Tutu Centre for Marine Environmental Research, University of Cape Town, Cape Town, South Africa

[4] Bayworld Centre for Research and Education, Cape Town, South Africa

Abstract: The Prince Edward Islands (PEIs) Archipelago, positioned between the sub-Antarctic Front and the Antarctic Polar Front, are a critical location for the study of polar ecosystem responses to intrinsic climate variability and the impact of climate change on the Southern Ocean. We used 23 to 42 years of satellite and reanalysis data to determine the long-term trends and spatial variability of the Sea Surface Temperature (SST), wind forcing and surface circulation at the PEIs. All parameters showed long-term trends that were statistically insignificant or substantially weaker than observed intra- and interannual variations. Spatial correlations revealed that the PEIs experience substantial local modification of SST, winds, and currents, bounded by the fronts of the ACC. This further confirmed that the neighboring oceanography and surface wind speed variability around the PEIs differs from other regions of the Southern Ocean, most probably due to the frequent mesoscale instability such as eddies and frontal movement influencing the region. The impact of climate change on the PEIs ecosystem thus cannot be expected to be the same as the rest of the Southern Ocean.

1. Introduction

The Southern Ocean (SO) has experienced major physical changes in the past decades as a result of both anthropogenic and natural causes (Masson-Delmotte et al. 2021). These changes have been shown to vary regionally across the SO, causing major ecological changes to sub-Antarctic island regions (Ansorge et al. 2014, Rogers et al. 2020). Of particular interest to this study are the Prince Edward Islands (PEIs, Fig. 1), a South African archipelago located between the sub-Antarctic Front and the Antarctic Polar Front and seasonal home to many top predators of the SO (Ansorge & Lutjeharms, 2005, Bost et al. 2009).

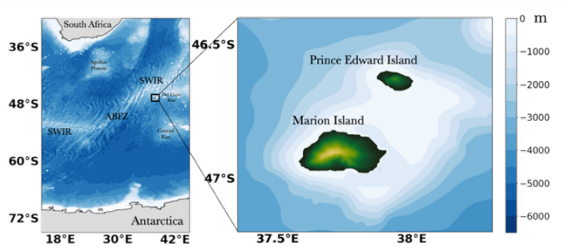

Figure 1: (Left) GEBCO bathymetry data showing the position of the Prince Edward Islands (within black box), eastward of the South-West Indian Ridge (SWIR) and downstream of the Andrew Bain Fracture Zone (ABFZ). (Right) Zoomed in 2° x 2° box within which data was averaged to analyse long-term trends. Image taken from Toolsee et al. 2021a)

It has been previously recorded that the PEIs ecosystem have undergone considerable changes due to climate change. A decline in the penguin population (Carpenter-Kling et al. 2020) and an increase in the albatross and seal populations (Hofmeyr et al. 2006) were recorded as a result of the long-term southward movement of the SAF (Gille, 2002, Fyfe & Saenko, 2006) which led to the simultaneous long-term decrease in phytoplankton blooms on the PEIs shelf (impacting the penguins), and closer proximity of breeding grounds for seals and albatross.

The oceanic conditions surrounding the islands thus strongly influence the biology of the islands (Ansorge et al. 2014), making it critical to investigate the long-term trends and the impact of climate change and variability on the surface ocean around the PEIs. Here, we used a combination of satellite and reanalysis data to investigate the long-term trends and spatial variability of the sea surface temperature (SST), surface wind speed and the surface currents around the PEIs. Further detailed results from this study have been published in Toolsee et al. (2022).

2. Data and Methods

SST data used in this study was obtained from an optimally interpolated SST product from the National Centers for the Environmental Information (NCEI) and produced by the Group for High Resolution Sea Surface Temperature (GHRSST). ERA5 Reanalysis wind speed data was obtained from the European Centre for Medium-Range Weather Forecasts (ECMWF). Surface Geostrophic and Ekman current was obtained from the multi-mission GlobCurrent v3.0. All data were obtained at a daily temporal resolution and were then averaged into monthly data. The spatial resolution of all the data is at a 0.25° x 0.25° resolution.

Each parameter was then averaged within a 2° x 2° area (Fig. 1) around the PEIs and their long-term trends were calculated for their respective periods (Table 1). The global map of the Pearson correlation between SST, wind speed and geostrophic current averaged within this 2° x 2° area and those parameters across the rest of the global ocean was calculated to investigate the spatial variability of the parameters (Fig. 2).

3. Results and Discussion

The long-term trends of SST, wind speed and Ekman current speed were all statistically insignificant (Table 1). Earlier studies conducted at the PEIs using *in situ* SST measured locally from 1949 to 1998 documented a statistically significant increase of up to 1.4 °C (Smith, 2002, Mélice et al. 2003, Rouault et al. 2005), and continuous warming of 1.54 °C was also observed over the 1949 to 2018 period (Shangheta, 2021). The coarse resolution of the GHRSST SST data (Martin et al. 2012) was an expected limitation in this study. However, the strong Pearson correlation coefficient ($r = 0.954$, $p < 0.001$) between the *in-situ* SST and the GHRSST SST provided good confidence in the GHRSST SST data. The shorter period (1982-2020) of GHRSST data compared to the much longer *in-situ* SST (1949-2018) could explain the discrepancy in the trends in SST at the PEIs.

Table 1: The long-term trends of each parameter with ** indicating those that are significant with a *p*-value less than 0.05.

Parameter	Data coverage	Trend
Sea Surface Temperature	1982 - 2020	0.0089 °C/decade
Wind Speed	1979 - 2020	0.0028 ms^{-1}/decade
Geostrophic Current Speed	1993 - 2016	0.0084 ms^{-1}/decade **
Ekman Current Speed	1993 - 2016	-0.0011 ms^{-1}/decade

Long-term changes, such as the strengthening and southward movement of the westerly wind belt have been recorded across the Southern Ocean (Thomas et al. 2015, Swart et al. 2018). Such long-term trends were not observed at the PEIs, indicating that the long-term impact of the westerly winds is not as apparent at the PEIs. This can be explained by the considerable intra-seasonal variability in the wind speed observed at the PEIs likely masks the long-term trends (Toolsee et al. 2022). The surface Ekman current speed, being strongly dependent on the wind speed, showed a similar lack of long-term trend.

The surface geostrophic current speed showed a very small yet statistically significant increase between 1993 and 2016 (0.0084 ms^{-1}/decade). The PEIs reside within the path of the Antarctic Circumpolar Current (ACC, Lamont et al. 2019, Toolsee et al. 2021b). Any changes experienced by the ACC, such as its southward movement, documented in some studies (Liau et al. 2017, Kim & Orsi, 2014) were thus expected to be reflected in the surface currents at the PEIs. The increase in geostrophic current speed could be a result of localised southward migration of the fronts of the ACC in the PEIs region (Asdar, 2019). Much shorter-term variations were, however, also observed in the geostrophic current (Toolsee et al. 2022), very likely moderating the long-term changes in the surface current at the PEIs.

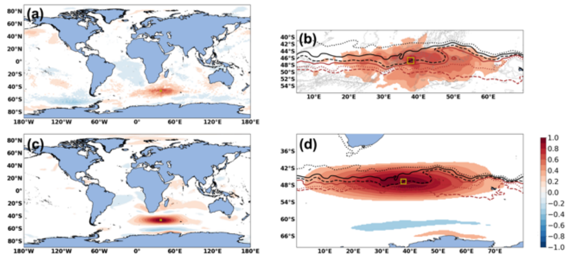

Figure 2: Spatial map of the significant Pearson correlation coefficient (p-value < 0.05) between the 2° x 2° averaged area around the PEIs and the rest of the global ocean for (a) GHRSST Sea Surface Temperature anomalies, and (c) ERA5 Wind speed anomalies. (b) and (d) are zoomed in maps around regions of strongest correlation (r > 0.3 & r < -0.3) around the PEIs.

To further understand why the lack of long-term changes at the PEIs did not match patterns observed over the rest of the Southern Ocean, a spatial correlation was conducted (Fig. 2). Both SST and wind speed showed strong positive correlations over a broader zonal area surrounding the PEIs bounded by the SAF and the APF (Fig. 2). This suggests that SST and wind speed variability at the PEIs are more strongly modified locally than by larger scale forcing such as climate modes or long term climate change (Toolsee et al. 2022). Substantial mesoscale variability originating from the ABFZ and the frontal meanders result in strong short-term variability. These local modifications, caused by substantial mesoscale variability and atmospheric low-pressure systems, create an environment with a low climate-to-noise ratio (Hawkins et al. 2020), explaining why long-term trends in the surface hydrography around the PEIs do not reflect the physical changes observed across the rest of the Southern Ocean.

References

Ansorge, I.J.; Durgadoo, J.V.; Treasure, A.M. Sentinels to climate change. The need for monitoring at South Africa's Subantarctic laboratory. South Afr. J. Sci. 2014, 110, 1–4.

Ansorge, I.J.; Lutjeharms, J.R.E. Direct observations of eddy turbulence at a ridge in the Southern Ocean. Geophys. Res. Lett. 2005, 32, 1–4.

Asdar, S. Climate Change Impact on Ecosystems of Prince Edward Islands: Role of Oceanic Mesoscale Processes. Ph.D. Thesis, University of Cape Town, Cape Town, South Africa, 2019, unpublished.

Bost, C.; Cotté, C.; Bailleul, F.; Cherel, Y.; Charrassin, J.; Guinet, C.; Ainley, D.; Weimerskirch, H. The importance of oceanographic fronts to marine birds and mammals of the southern oceans. J. Mar. Syst. 2009, 78, 363–376.

Carpenter-Kling, T.; Reisinger, R.R.; Orgeret, F.; Connan, M.; Stevens, K.L.; Ryan, P.G.; Makhado, A.; Pistorius, P.A. Foraging in a dynamic environment: Response of four sympatric sub-Antarctic albatross species to interannual environmental variability. Ecol. Evol. 2020, 10, 11277–11295.

Fyfe J. C. and Saenko O. A. Simulated changes in the extratropical Southern Hemisphere winds and currents. Geophys. Res. Lett., 2006, 33, L06701.

Gille S. T. Warming of the Southern Ocean since the 1950s. Science, 2002, 295, 1275–1277.

Hawkins, E.; Frame, D.; Harrington, L.; Joshi, M.; King, A.; Rojas, M.; Sutton, R. Observed Emergence of the Climate Change Signal: From the Familiar to the Unknown. Geophys. Res. Lett. 2020, 47, e2019GL086259.

Hofmeyr, G.J.G.; Bester, M.N.; Makhado, A.B.; Pistorius, P.A. Population changes in Subantarctic and Antarctic fur seals at Marion Island: Research article. S. Afr. J. Wildl. Res. 2006, 36, 55–68.

Kim, Y.S.; Orsi, A.H. On the Variability of Antarctic Circumpolar Current Fronts Inferred from 1992–2011 Altimetry*. J. Phys. Oceanogr. 2014, 44, 3054–3071.

Lamont, T.; van den Berg, M.A.; Tutt, G.C.O.; Ansorge, I.J. Impact of deep-ocean eddies and fronts on the shelf seas of a sub-Antarctic Archipelago: The Prince Edward Islands. Cont. Shelf Res. 2019, 177, 1–14.

Liau, J.-R.; Chao, B.F. Variation of Antarctic circumpolar current and its intensification in relation to the southern annular mode detected in the time-variable gravity signals by GRACE satellite. Earth Planets Space 2017, 69, 93.

Martin, M.; Dash, P.; Ignatov, A.; Banzon, V.; Beggs, H.; Brasnett, B.; Cayula, J.-F.; Cummings, J.; Donlon, C.; Gentemann, C.; et al. Group for High Resolution Sea Surface temperature (GHRSST) analysis fields inter-comparisons. Part 1: A GHRSST multi-product ensemble (GMPE). Deep Sea Res. Part II Top. Stud. Oceanogr. 2012, 77, 21–30.

Masson-Delmotte, V., Zhai, P., Pirani, A., Connors, S.L., Péan, C., Berger, S., Caud, N., Chen, Y., Goldfarb, L., Gomis, M.I. and Huang, M. Climate change 2021: the physical science basis. Contribution of working group I to the sixth assessment report of the intergovernmental panel on climate change, 2021, 2(1), p.2391.

Mélice, J.-L.; Lutjeharms, J.R.E.; Goosse, H.; Fichefet, T.; Reason, C.J.C. Evidence for the Antarctic circumpolar wave in the sub-Antarctic during the past 50 years. Geophys. Res. Lett. 2005, 32.

Rogers, A.; Frinault, B.; Barnes, D.; Bindoff, N.; Downie, R.; Ducklow, H.; Friedlaender, A.; Hart, T.; Hill, S.; Hofmann, E.; et al. Antarctic Futures: An Assessment of Climate-Driven Changes in Ecosystem Structure, Function, and Service Provisioning in the Southern Ocean. Annu. Rev. Mar. Sci. 2020, 12, 87–120.

Rouault, M.; Mélice, J.; Reason, C.J.C.; Lutjeharms, J.R.E. Climate variability at Marion Island, Southern Ocean, since 1960. J. Geophys. Res. Earth Surf. 2005, 110.

Shangheta, A.L. Long Term Climate Variability at the Prince Edward Islands in the Southern Ocean. Master's Thesis, University of Cape Town, Cape Town, South Africa, 2021.

Swart, N.C.; Gille, S.T.; Fyfe, J.C.; Gillett, N.P. Recent Southern Ocean warming and freshening driven by greenhouse gas emissions and ozone depletion. Nat. Geosci. 2018, 11, 836–841.

Thomas, J.L.; Waugh, D.W.; Gnanadesikan, A. Southern Hemisphere extratropical circulation: Recent trends and natural variability. Geophys. Res. Lett. 2015, 42, 5508–5515.

Toolsee, T(a) Interannual Variability and Long-Term Trends of Surface Hydrography around the Prince Edward Island Archipelago, Southern Ocean. Master's Thesis, University of Cape Town, Cape Town, South Africa, 2021, unpublished.

Toolsee, T.; Lamont, T.; Rouault, M.; Ansorge, I. (b) Characterising the seasonal cycle of wind forcing, surface circulation and temperature around the sub-Antarctic Prince Edward Islands. Afr. J. Mar. Sci. 2021, 43, 61–76.

Toolsee, T.; Lamont, T. Long-Term Trends and Interannual Variability of Wind Forcing, Surface Circulation, and Temperature around the Sub-Antarctic Prince Edward Islands. Remote Sens. 2022, 14, 1318.

Oceanographic variability assessed from observations and GLORYS reanalysis at the Prince Edward Islands, Southern Ocean

I. Halo[1,3], B.K. Soares[2], T. Lamont[1,2,3,4], C.S. Russo[1], M.A. van den Berg[1], G.C.O. Tutt[1]

[1] Oceans & Coasts Research, Department of Forestry Fisheries and the Environment, Cape Town, South Africa

[2] Department of Oceanography, University of Cape Town, Cape Town, South Africa

[3] Nansen-Tutu Centre for Marine Environmental Research, University of Cape Town, Cape Town, South Africa

[4] Bayworld Centre for Research and Education, Constantia, Cape Town, South Africa

Abstract: The Prince Edward Islands (PEI), comprising Marion and Prince Edward Islands, are home to various species which are supported by a sensitive and complex oceanic environment. Understanding the mechanisms that sustain this rich ecosystem is therefore imperative for both the ecological management of the PEIs, and for the possible prediction of future climate change-driven environmental impacts. The presence of a Taylor column has been suggested as the main driver supporting and maintaining the PEI ecosystem. However, the remote and hostile oceanic environment makes the collection of *in situ* data challenging, thus making it difficult to verify this hypothesis from *in situ* data collections. Therefore, a scaling analysis was performed using the GLORYS12v1 model reanalysis product. The results have shown that Taylor columns/Taylor cones, indeed occur at the PEIs.

1. Introduction

The Prince Edward Islands (PEIs) archipelago consists of Marion and Prince Edward Islands (Fig 1). The islands are positioned in the direct path of the eastward flowing Antarctic Circumpolar Current (ACC), between the northern (sub-Antarctic Front) and the southern (Antarctic Polar Front) boundaries of the Antarctic Polar Frontal Zone (APFZ) of the Southern Ocean (SO). The islands were declared a Marine Protected Area in 2013 due to the various ecosystems supported by the islands. The surrounding bathymetric features contribute to the high levels of mesoscale variability observed in the region (Sokolov and Rintoul, 2009; Toolsee et al. 2021).

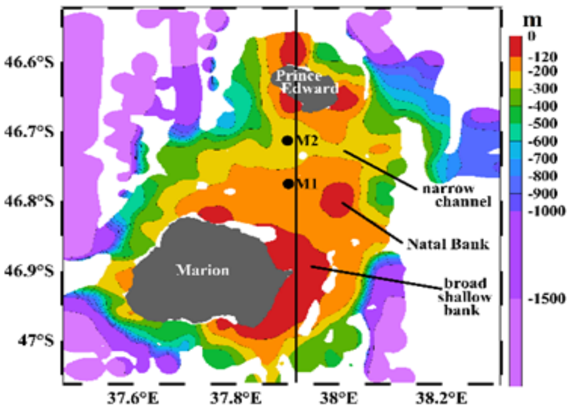

Figure 1: In situ bathymetry around the PEIs. The bold dots denote the positions of two hydrographic moorings, and the black line denotes the transect location used to produce Fig. 2. White shading indicates areas of no data.

The presence of a Taylor column (a persistent anticyclonic circulation) has been hypothesised as the main driver supporting and maintaining the PEI's diverse ecosystem (Perissinotto and Duncombe Rae, 1990; Lamont et al. 2019). However, the remote and hostile oceanic environment makes the collection of *in situ* data challenging, and limits the ability to investigate the above processes in detail from *in situ* data collections. Therefore, this study uses the Global Ocean Reanalysis product (GLORYS12v1) output to examine whether a Taylor column exists at the PEIs

2. Data and method

The GLORYS12v1 output used in this study was forced by atmospheric surface fields retrieved from the European Centre for Medium Range Weather Forecast (ECMWF) ERA-Interim reanalysis product. The model engine solves the hydrodynamic equations of motion in a c-grid. The configuration has a lateral spatial grid-resolution of ~8 km, and it has 50 vertical layers. The model is eddy-resolving, vested with high-performing data-assimilation schemes and a reduced order Kalman filter. The assimilation uptakes observational along-track sea-level anomalies from satellite altimetry, satellite-derived sea surface temperature (SST) from Advanced Very High Resolution Radiometers (AVHRR), and *in situ* hydrographic temperature and salinity profiles from CTDs and Argo floats. The outputs are daily, and span from 1993 to the present, distributed freely by the European Copernicus Marine Environment Monitoring Service (CMEMS; http://marine.copernicus.eu/).

3. Results

In 2021, moored observations (Fig. 1) indicated five localised cooling events, of which the June event could not be linked to mesoscale eddies or frontal interactions, suggesting the presence of a Taylor column over the PEI plateau. The days of the strongest surface cooling events were selected and investigated using GLORYS outputs through the upper 1000 m in the water column (Fig. 2). In addition, a scaling analysis was performed to investigate these events from 13 to 17 June. The calculated adimensional parameters, derived from the model output, are presented in Table 1. These include the Rossby number (Ro), which compares inertial and rotational circulation to describe instabilities of the flow, Burger number (B), describing how stratified the water column is, and Blocking parameter (Bl), which defines whether a Taylor column can be formed.

Table 1: Adimensional parameters, including Rossby Number (Ro), Burger Number (B) and Blocking Parameter (Bl), from 13 to 17 June 2021, averaged for the upper 100 m above the PEI plateau, between 45.75°S and 48.00°S, at a mean longitudinal position of 37.92°E.

	13 Jun	14 Jun	15 Jun	16 Jun	17 Jun
Ro	0.02	0.02	0.01	0.02	0.01
B	0.46	0.43	0.36	0.54	0.42
Bl	2.00	2.12	2.64	2.15	2.47

4. Discussion

For a Taylor column to form, each adimensional parameter must meet set thresholds (i.e. Ro < 2; B < 1, and Bl > 2) (Meredith et al., 2014). During the June 2021 cooling event, the daily calculated adimensional parameters satisfied each of the thresholds (Table 1). The calculated values indicated Ro << 1, implying a strong influence of the Earth's rotation on the flow dynamics. Values of B < 1 implied a nearly unstratified water column due to increased mixing, and values of Bl > 2 suggested the formation and persistence of a Taylor column. This allows us to infer that a Taylor column can indeed form over the PEI plateau.

Furthermore, during June 2021, daily zonal current speeds (Fig. 2) indicated westward flow (negative values), reflecting the anticyclonic circulation expected when a Taylor column is present. This westward flow was concentrated over the PEI plateau but did not always extend to the surface. This provides the first evidence that, instead of a Taylor column, a "Taylor cap", a.k.a. "Taylor cone" (Chapman and Haidvogel, 1992), may form predominantly over the PEI

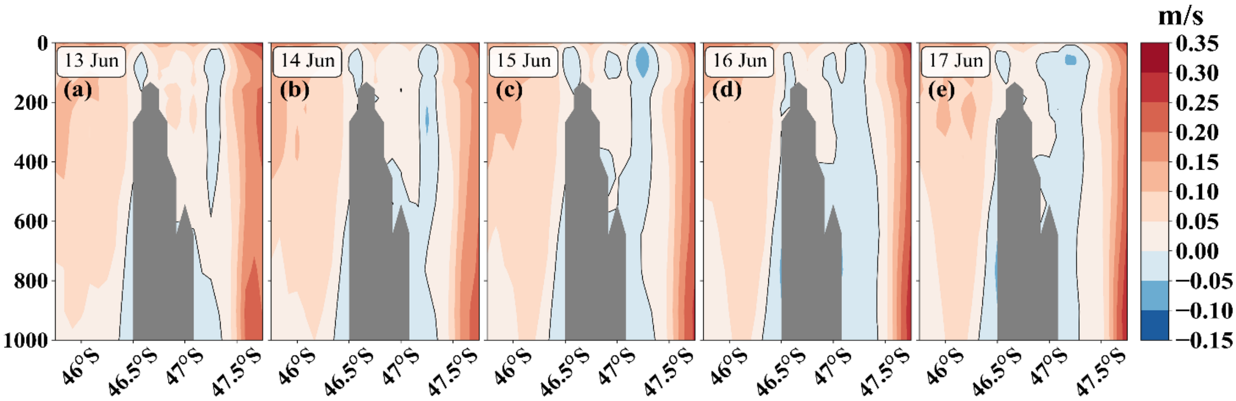

Figure 2: Daily GLORYS vertical sections, showing the zonal (east-west) current component (m s^{-1}) within the upper 1000 m of the water column between 13 and 17 June 2021, along 37.92°E, during the period of strongest cooling. Flow toward the east is positive, while westward flow is negative. Grey shading denotes the bathymetry of the PEI plateau between Prince Edward Island and Marion Island.

plateau. Compared to a Taylor column, a Taylor cap has a similar anticyclonic circulation but it does not present a surface expression. On occasion, this circulation may reach the surface, as on 15 June 2021 (Fig. 2), thus changing the Taylor cap into a Taylor column. This switching state may be the reason that researchers have thus far been unable to clearly prove the persistence of a Taylor column at the PEIs.

References

Sokolov., S, and S. R. Rintoul., 2009. Circumpolar structure and distribution of the Antarctic Circumpolar Current fronts: 1. Mean circumpolar paths. Journal of Geophysical Research: Oceans, 114(C11).

Toolsee, T., T. Lamont., M. Rouault, and I. Ansorge., 2021. Characterising the seasonal cycle of wind forcing, surface circulation and temperature around the sub-Antarctic Prince Edward Islands. African Journal of Marine Science, 43(1), pp.61-76.

, Oceans, 120, 547-562

Perissinotto., R, and C. D. Rae., 1990. Occurrence of anticyclonic eddies on the Prince Edward Plateau (Southern Ocean): effects on phytoplankton biomass and production. Deep Sea Research Part A. Oceanographic Research Papers, 37(5), pp.777-793.

Lamont, T., van den Berg, M.A., Tutt, G.C.O. and I. J. Ansorge., 2019. Impact of deep-ocean eddies and fronts on the shelf seas of a sub-Antarctic Archipelago: The Prince Edward Islands. Continental Shelf Research, 177, pp.1-14.

Chapman, D. C., and D. B. Haidvogel., 1992. Formation of Taylor caps over a tall isolated seamount in a stratified ocean. Geophysical & Astrophysical Fluid Dynamics, 64(1-4), pp.31-65.

Meredith, M. P., A. S. Meijers., A. C. Naveira Garabato., P. J. Brown., H. J. Venables., E. P. Abrahamsen., L. Jullion, and M-J. Messias., 2014. Circulation, retention, and mixing of waters within the Weddell-Scotia Confluence, Southern Ocean: The role of stratified Taylor columns, Journal of Geophysical Research

.

Zooplankton variability around the sub-Antarctic Prince Edward Islands and the influence of the environment.

Sarah A. du Preez[1], Tarron Lamont[1,2,3,4] and Jenny A. Huggett[2, 3, 5]

[1] Department of Oceanography, University of Cape Town, Cape Town, South Africa.

[2] Oceans & Coastal Research, Department of Forestry, Fisheries and the Environment, Cape Town, South Africa

[3] Bayworld Centre for Research and Education, Cape Town, South Africa

[4] Nansen-Tutu Centre for Marine Environmental Research, Department of Oceanography, University of Cape Town, South Africa

[5] Department of Biological Sciences, University of Cape Town, Cape Town, South Africa.

Oceanographic conditions around the sub-Antarctic Prince Edwards Islands (PEIs) are characterized by high mesoscale variability and cross-frontal mixing. Bongo nets (200µm) were used to sample the zooplankton community in the upper 200 m along routine monitoring transects during the 2018 and 2019 autumn cruises to re-supply the Marion research base. Zooplankton abundance and biovolume were assessed using a ZooScan with ZooProcess software, and images were validated using EcoTaxa. Temperature, salinity, and chlorophyll *a* were sampled *in situ* in 2018 only, but daily reanalysis and satellite data were used to identify positions of fronts and mesoscale features in both years. In 2018, 2 cyclonic eddies interacted with the PEIs and the southern branch of the sub-Antarctic Front (S-SAF) was located south of the archipelago. In contrast, the S-SAF was closer to the PEI shelf in 2019. Both years showed similar zooplankton abundances (2018: 527.84 ind.m^{-3}; 2019: 571.94 ind.m^{-3}), but the mean biovolume in 2018 (200.76 mm^{3}·m^{-3}) was significantly higher than in 2019 (74.72 mm^{3}·m^{-3}), suggesting a higher proportion of larger organisms in 2018. Copepods dominated zooplankton abundance (>90%) in both years, whereas the biovolume was largely made up of Chaetognaths (2018: 44.9%; 2019: 39.2%), Copepods (2018: 33.9%; 2019: 35.7%) and Euphausiids (2018: 14.0%; 2019: 6.3%). Peaks in zooplankton abundance and biovolume corresponded with elevated chlorophyll *a* (Chl a), but only biovolume was significantly correlated with Chl a. Our findings revealed the significant influence of mesoscale features like eddies and fronts on the spatial distribution and magnitude of zooplankton abundance and biovolume around the PEIs.

1. Introduction

Together Marion Island and Prince Edward Island form the Prince Edward Islands (PEIs), a sub-Antarctic archipelago located in the Indian sector of the Southern Ocean at approximately 46°50'S and 37°50'E (Ansorge et al. 2012). The islands are located within the Antarctic Polar Frontal Zone between two major fronts, namely the sub-Antarctic Front (SAF) and the Antarctic Polar Front (APF). As a result, this region is characterised by intense cross-frontal mixing and mesoscale oceanic variability (Durgadoo et al. 2010). The positions of the fronts relative to the PEIs have been shown to significantly alter the oceanographic conditions on the shelf (Pakhomov et al. 2000; Ansorge and Lutjeharms 2002).

The volcanic origins of the islands account for their steep rise from the surrounding complex bathymetry (Quilty 2007). The two islands are joined via a shallow shelf region between 40 to 200 m deep (Ansorge et al. 2012). Their presence disrupts the hydrographic flow of the region, resulting in localised upwelling and retention of nutrient-rich waters. This in turn supports the occurrence of the Island Mass Effect (locally enhanced chlorophyll *a* concentrations).

Zooplankton form an essential component of the region's food web, supporting an abundance of top predators (Ryan and Bester 2008) that make use of the islands seasonally. This study investigated the physical oceanographic conditions during cruises conducted in 2018 and 2019 and attempted to understand how oceanographic features influenced the abundance, biovolume and composition of the zooplankton community surrounding the PEIs.

2. Data and Methods

The *in situ* data used in this study were collected during the annual Marion Island relief voyages

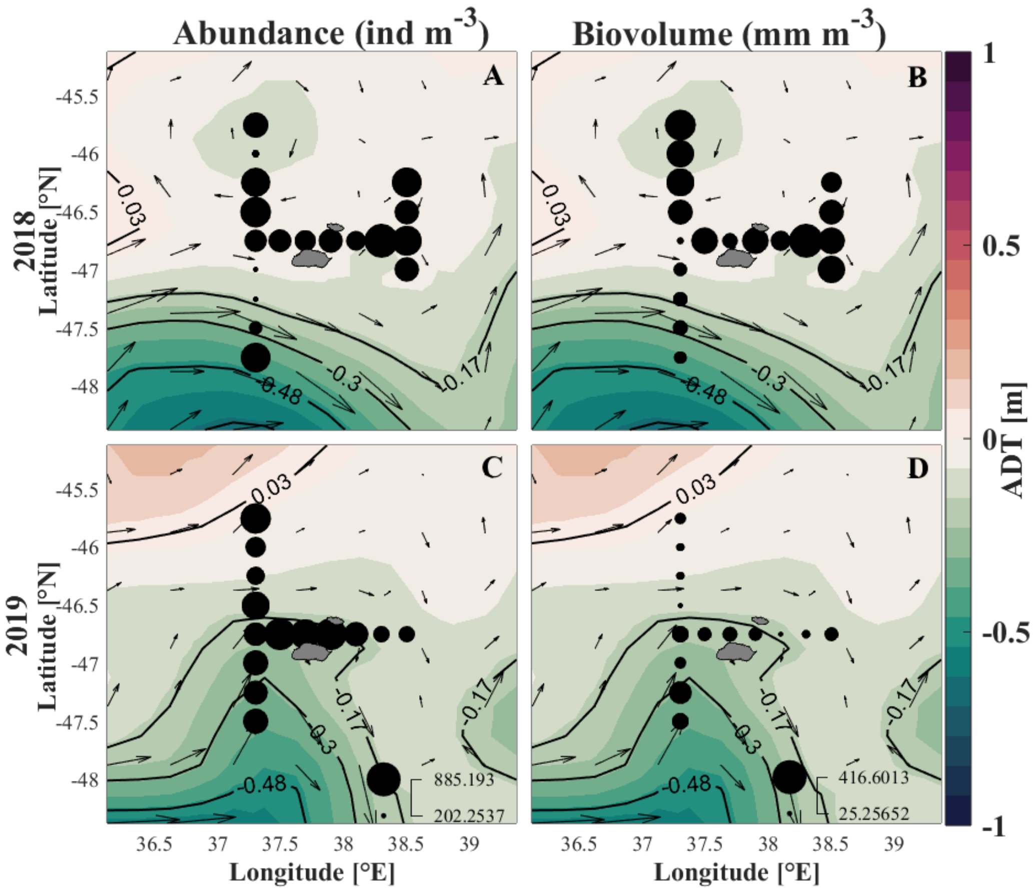

Figure 1. Mean daily Absolute Dynamic Topography (m) with overlaid geostrophic current vectors (arrows sizes depict strength of current in m s-1) for 23–28 April 2018 (A, B) and 24–27April 2019 (C, D). Black dots indicate sampling station positions, and bubble size indicates total zooplankton abundance (A, C) and biovolume (B, D) sampled at each station. Black contours indicate the positions of various branches of the SAF and APF (Middle-SAF: 0.03 m; Southern-SAF: -0.17 m; Northern-APF: -0.3 m; Middle-APF: -0.48 m; Southern-APF: -0.63 m)

in April of 2018 and 2019. Sampling was conducted along two established monitoring lines in both years, including an upstream transect, and an inter-island transect that passed between the islands (Fig. 1). An additional transect was sampled downstream of the islands in 2018. Zooplankton were sampled using a 200 µm Bongo net, hauled vertically through the upper 200 m. Zooplankton samples were imaged digitally using a ZooScan with ZooProcess software, and vignettes were imported into EcoTaxa for validation (Picheral et al. 2017). The data exported from EcoTaxa were converted to abundance (ind m^{-3}) and biovolume (mm^3 m^{-3}). Vertical profiles of temperature, salinity, and chlorophyll *a* (Chl a) were sampled using a Conductivity-Temperature-Depth (CTD) system in 2018 only, but daily reanalysis and satellite data were used to identify the positions of fronts and mesoscale features in both years. Applying Sokolov and Rintoul's (2009) definition, the northern, middle and southern branches of the SAF and APF were identified using Absolute Dynamic Topography. Statistical analysis was performed to investigate the relationship between the zooplankton abundance and biovolume and the average temperature, salinity and Chl a in the upper 200 m of the water column.

3. Results

The southern branch of the sub-Antarctic Front (S-SAF) was located south of the archipelago in 2018 (Fig. 1A, B). Two eddies interacted with the PEIs, including a larger cyclonic eddy southwest of PEIs, as well as a smaller cyclonic eddy to the northwest. The distance between the S-SAF and the PEI shelf, combined with the westward-flowing counter current associated with the southern limb of northwestern eddy, likely acted to reduce the current velocities within the region. This reduced flow, combined with the barrier imposed by the northward meander of the S-SAF downstream of the islands, likely promoted the retention of upwelled water, nutrients and biota around and on the PEI shelf. As a result, phytoplankton blooms were observed within the inter-island and downstream regions.

Elevated zooplankton abundances and biovolumes in 2018, corresponded with these regions of enhanced Chl a, but only biovolume showed a strong, statistically significant correlation ($r = 0.78$ $p < 0.001$; Fig. 2) with the mean Chl a. This relationship highlights the important influence of the Island Mass Effect on the zooplankton populations at the PEIs. Additionally, in 2018, the northwestern eddy exhibited elevated Chl a concentrations, high zooplankton biovolume and abundance (Fig. 1A, B), and a zooplankton community that was distinct from the surrounding region.

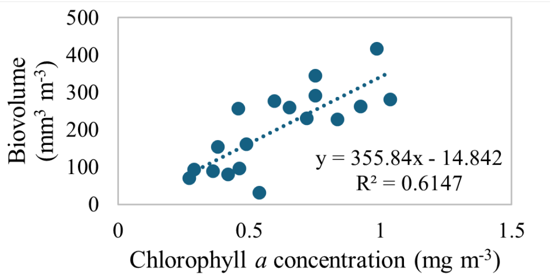

Figure 2. Linear relationship between the average chlorophyll *a* concentration (mg m^{-3}) in the upper 200 m of the water column and the corresponding zooplankton biovolume (mm^3 m^{-3}) in 2018.

In contrast, during 2019, the S-SAF extended northward in a frontal meander and interacted with the PEI shelf, resulting in enhanced current velocities, and the establishment of a flow-through system on the shelf. Under such conditions, we hypothesise that retention and primary production were likely inhibited, although due to the absence of CTD and Chl a data in 2019 we cannot confirm this.

Zooplankton abundances were similar during both cruises (2018: 528 ind.m^{-3}; 2019: 572 ind.m^{-3}). However, the average biovolume in 2018 (201 mm^3 m^{-3}; Fig. 1B) was 2.68 times larger than in 2019 (75 mm^3 m^{-3}; Fig. 1D). Size composition metrics derived from image analysis showed larger individuals in 2018 that may account for this. Copepods dominated the zooplankton abundance (> 90%) in both years, whereas the biovolume was largely accounted for by chaetognaths (2018: 44.9%; 2019: 39.2%), copepods (2018: 33.9%; 2019: 35.7%) and euphausiids (2018: 14.0%; 2019: 6.3%).

1. Discussion

The primary objective of this study was to develop a better understanding of the zooplankton community at the PEIs in terms of abundance, biovolume, and community composition. In addition, the study examined the influence of the physical ocean environment on the spatial and temporal variations of the zooplankton community. Improving our understanding of this is of vital importance, as zooplankton form an important component of the region's food web, and variations in their population may have cascading effects on the structure and function of the local ecosystem.

Our findings revealed the substantial influence of mesoscale features like eddies and fronts on the spatial distribution and magnitude of zooplankton abundance and biovolume around the PEIs. The SAF and APF exhibit a large degree of latitudinal variability near the PEIs (Hunt et al. 2001). Enhanced current velocities associated with these fronts have been shown to alter the hydrographic conditions on and around the PEI shelf from a retentive to a flow-through state, depending on their proximity to the islands (Perissinotto et al. 2000). We suggest this as a possible explanation for the differences observed in the zooplankton community between the 2018 and 2019 cruises. Due to the location of the S-SAF further away from the PEIs in 2018, more retentive conditions occurred at and around the islands. The retention of nutrient-rich waters downstream of the islands and enhanced water column stability likely supported primary productivity and thus promoted the Island Mass Effect (Perissinotto and Duncombe Rae 1990; Lamont et al. 2019). In contrast, during 2019, the proximity of the S-SAF to the PEI shelf resulted in a flow-through system that likely restricted retention and primary productivity.

In 2018, zooplankton abundance and biovolume appeared to correspond with the peaks in Chl a. However, only biovolume showed a strong, positive linear relationship with mean Chl a concentration (Fig. 2). This may be attributed to the relatively fast growth rate of zooplankton, and their ability to respond rapidly to an increased food supply, resulting in greater body weight and hence community biomass. This relationship indicates the importance of the Island Mass Effect in influencing zooplankton biovolume, with higher Chl a supporting larger organisms. This might explain why more larger organisms were present in 2018 compared to 2019.

Mesoscale eddies are an important mechanism for transporting plankton into the island ecosystem (Durgadoo et al. 2010). The northwestern cyclonic eddy exhibited elevated Chl a concentrations as well as a high zooplankton biovolume and abundance. Furthermore, it showed a unique community composition compared to the surrounding region, likely reflecting the transport of allochthonous zooplankton species into the region.

In light of the limited historical observations and investigations in the region, our findings have improved the understanding of the current composition and variability of the zooplankton community surrounding the PEIs. This provides a baseline against which we can monitor and evaluate future ecosystem responses that may occur as a result of climate change.

References

Ansorge IJ, Froneman PW, Durgadoo JV. 2012. The marine ecosystem of the subAntarctic, Prince Edward Islands. In: Cruzado A (ed.), *Marine Ecosystems*. InTech Press, Rijeka. pp. 61–76.

Ansorge IJ, Lutjeharms JRE. 2002. The hydrography and dynamics of the ocean environment of the Prince Edward Islands (Southern Ocean). *Journal of Marine Systems* 37: 107–127.

Durgadoo JV, Ansorge IJ, Lutjeharms JRE. 2010. Oceanographic observations of eddies impacting the Prince Edward Islands, South Africa. *Antarctic Science* 22:211–219.

Hunt BVP, Pakhomov EA, McQuaid CD. 2001. Short-term variation and long terms changes in the oceanographic environment and zooplankton community in the vicinity of a sub-Antarctic archipelago. *Marine Biology* 138: 369-381.

Lamont T, van den Berg MA, Tutt GCO, Ansorge IJ. 2019. Impact of deep-ocean eddies and fronts on the shelf seas of a sub-Antarctic Archipelago: The Prince Edward Islands. *Continental Shelf Research* 177: 1–14.

Pakhomov EA, Froneman PW. 2000. Composition and spatial variability of macroplankton and micronekton within the Antarctic Polar Frontal Zone of the Indian Ocean during austral autumn 1997. *Polar Biology* 23: 410–419.

Perissinotto R, Lutjeharms JRE, van Ballegooyen RC. 2000. Biological-physical interactions and pelagic productivity at the Prince Edward Islands, Southern Ocean. *Journal of Marine Systems* 24: 327–341.

Perissinotto R, Duncombe Rae CM. 1990. Occurrence of anticyclonic eddies on the Prince Edward Plateau (Southern Ocean): effects on phytoplankton biomass and production. *Deep Sea Research Part A* 37: 777-793.

Picheral M, Colin S, Irrison J-O. 2017. EcoTaxa, a Tool for the Taxonomic Classification of Images. Available at: http://ecotaxa.obs-vlfr.fr

Quilty PG. 2007. Origin and evolution of the sub-Antarctic islands: The foundation. *Papers and proceedings of the Royal Society of Tasmania 141*: 35–58.

Ryan PG, Bester MN. 2008. Pelagic predators. In: Chown SN, Froneman PW (eds.), The Prince Edward Archipelago: Land-sea interactions in a changing ecosystem. Stellenbosch. pp 121–164.

Sokolov S, Rintoul SR. 2009. Circumpolar structure and distribution of the Antarctic Circumpolar Current fronts: 1. Mean circumpolar paths. *Journal of Geophysical Research* 114: C11018.

Nansen-Tutu Centre, Department of Oceanography
University of Cape Town, Rondebosch, 7700, South Africa
https://www.nansen-tutu.uct.ac.za/

The Nansen-Tutu Centre has a remarkable team of students, post-doctoral fellows, research associates, staff, board members and collaborators.
This Annual Report 2023 celebrates the people behind the NTC with sincere thanks to their contributions.